Ph.D. DISSERTATION

A Study on the EM Wave Absorber for W-band Navigation Radars

By

Chang-Mook Choi

Under Supervision of Prof. Dong Il Kim

February 2008

Department of Radio Communication Engineering

in the Graduate School of the

Korea Maritime University

A Study on the EM Wave Absorber
for W-band Navigation Radars

by Chang-Mook Choi

Here is approved that this is the dissertation submitted in partial satisfaction of the requirements for degree of Doctor of Philosophy in Engineering in the Graduate School of the Korea Maritime University

Approved:

Prof. Se-Mo Chung

Prof. Min-Seok Kim

Prof. Kwang-Soob Ko

Prof. Kyeong-Sik Min

Prof. Dong Il Kim

Committee in charge

December 21, 2007

Contents

Nomenclature

d_n:	Thickness of n-th layer
$\overline{E}$:	Electric field vector
f :	Frequency
$\overline{H}$:	Magnetic field vector
I :	Current
k :	Wave number
ℓ :	Length of sample
S :	Absorption ability
V :	Voltage
Z or Z_{in} :	Input impedance
z or z_{in} :	Normalized input impedance
Z_c :	Characteristic impedance
z_c	Normalized characteristic impedance
Z_0 :	Impedance in free-space
α :	Attenuation constant
β :	Phase constant
Γ :	Reflection coefficient
γ :	Propagation constant
δ_s :	Skin depth of penetration
ε :	Permittivity
ε_0 :	Permittivity in free-space
ε_r :	Relative permittivity
η :	Wave impedance

λ : Wavelength

λ_c : Cutoff wavelength of the waveguide

λ_0 : Wavelength in free-space

μ : Permeability

μ_0 : Permeability in free-space

μ_r : Relative permeability

v_p : Phase velocity

σ : Conductivity

ω : Angular velocity

List of Tables

List of Figures

Abstract

A Study on the EM Wave Absorber
for W-band Navigation Radars

Chang-Mook Choi
Dept. of Radio Communication Engineering
Graduate School, Korea Maritime Univ.
Supervisor : Prof. Dong Il Kim, Ph.D

Since the removal of the selective-availability restriction, there still remains the concern that the global positioning system (GPS) may be rendered unusable by some form of interference or jamming. For this and other reasons, airborne vehicles generally rely on a combination of GPS and inertial navigation systems (INS). This combination is only effective for short periods once GPS becomes unavailable because residual errors and biases quickly integrate up into unacceptably large position errors.

Under these conditions, millimeter wave radar can be applied in a number of ways to improve the velocity-estimation accuracy by measuring the ground speed, or it can be used to produce high-resolution images that can be displayed for direct interpretation by the pilot or correlated with aerial photographs for navigation or guidance purposes.

Millimeter wave radars are superior to microwave and infrared-based radars in most applications, because millimeter wave radars offer better range resolution than lower frequency microwave radars and can penetrate fog, smoke, and other obscurants much better than infrared

radars.

However, radar systems suffer from two major problems, such as false images and system-to-system interference. False echoes cause driving hazards. These problems can be eliminated through the use of an electromagnetic (EM) wave absorber.

As is well known, EM wave absorbers can be broadly divided into three types from the viewpoint of material. One is a wave absorber using a conductive material, another is a wave absorber using a dielectric material, and the other is a wave absorber using a magnetic material.

In this dissertation, the EM wave absorbers are developed for W-band radars using Carbon as a conductive material, TiO_2 as a dielectric material, and Permalloy as a magnetic material with CPE as a binder.

First of all, the absorption ability of samples containing difference composition ratio of Carbon, TiO_2, and Permalloy with CPE is analyzed in frequency range of 65-110 GHz. It is known that the absorption ability of sample containing Carbon has a tendency to increase from 10 wt.% to 20 wt.% and decrease from 30 wt.% to 50 wt.%, the absorption ability of sample containing TiO_2 has a tendency to increase from 40 wt.% to 70 wt.% and decrease from 70 wt.% to 80 wt.%, and the absorption ability of sample containing Permalloy has a tendency to increase with increasing the composition ratio. As a result, the optimum composition ratios of Carbon, TiO_2, and Permalloy are about 20 wt.%, 70 wt.%, 70 wt.%, respectively.

To design an EM wave absorber in W-band, the material properties, such as complex relative permittivity and permeability, of samples are calculated from the S-parameter. Absorption abilities of the EM wave absorbers are simulated using the calculated complex relative permittivity and permeability by changing the thickness without changing the composition.

To verify design results, the EM wave absorbers are fabricated based on the simulated designs. The simulated and measured results agree very well. As a result, the EM wave absorbers which have absorption ability higher than 20 dB in W-band are developed. This result shows that altering the absorber thickness can control the absorption ability peak of composite material in frequency range of 65-110 GHz.

요 약

W-band 항행 레이더용 전파흡수체에 관한 연구

성 명 : 최 창 묵

학 교 : 한국해양대학교

학 과 : 전파공학과

지도교수 : 김 동 일

미국의 SA 정책이 해제된 이후, GPS 위성항법 시스템이 전파간섭이나 재밍에 의해 무력화 될 수 있기 때문에 항공기들은 GPS 위성항법 시스템과 관성항법 시스템의 복합시스템을 사용하고 있지만, 이 시스템은 잔여오차 및 바이어스가 큰 위치오차를 보상할 수 없기 때문에 단기간에만 유효한 특성이 있다.

따라서 이러한 조건들 때문에 밀리미터파 레이더가 대지속력을 측정하기 위해 정확도를 향상시키는 많은 방법으로 이용될 수도 있고, 조종사가 직접 식별할 수 있도록 전시하거나 또는 항해나 유도를 목적으로 공중사진과 연계시키는 고해상도의 이미지 생성을 위해 이용될 수도 있다.

밀리미터파 레이더는 마이크로파 레이더보다 파장이 짧기 때문에 비교적 높은 해상도를 제공하고, 적외선 레이더보다는 안개, 연기 등의 방해물을 보다 우수하게 투과하는 특성을 가지고 있기 때문에 밀리미터파 레이더들은 모든 적용분야에서 마이크로파와 적외선 레이더들보다 우수한 특성을 가지고 있다.

그러나 레이더 시스템은 허상과 시스템 간섭의 중요한 문제에 직면하고 있기 때문에 항행의 위험요소가 있을 수 있으며, 이러한 문제점들은 전파흡수체를 사용하여 제거할 수 있다.

전파흡수체는 재료의 관점에서 세가지 형태로 나누어 볼 수 있다. 첫 번째는 도전손실재료를 사용한 전파흡수체이며, 두 번째는 유전손실재료를 사용한 전파흡수체, 세 번째는 자성손실재료를 사용한 전파흡수체이다.

따라서 본 논문에서는 세가지 형태별 각각 도전손실재료는 카본, 유전손실재료는 이산화티탄, 자성손실재료는 퍼멀로이를 이용하여 W-band 레이더용 전파흡수체를 개발하였다.

먼저, 카본과 이산화티탄, 퍼멀로이를 지지재인 CPE와 조성비별 샘플을 제작하여 전파흡수능을 분석하였다. 카본을 이용한 전파흡수체는 함유량이 10 wt.%부터 20 wt.%까지는 전파흡수능이 향상되는 경향을 보이다가 30 wt.%부터 50 wt.%까지는 다시 감소하는 특성을 보였다. 이산화티탄을 이용한 전파흡수체는 함유량이 40 wt.%부터 70 wt.%까지는 전파흡수능이 향상되는 경향을 보이다가 다시 80 wt.%부터는 감소하는 특성을 보였다. 퍼멀로이를 이용한 전파흡수체는 함유량이 증가할수록 전파흡수능이 향상되는 특성을 보였다. 결과적으로 손실재료의 최적함유량은 각각 카본 20 wt.%, 이산화티탄 70 wt.%, 퍼멀로이 70 wt.%였다.

W-band에서 손실재료별 최적의 전파흡수체를 설계하기

위해 샘플로부터 재료정수인 복소비유전율과 복소비투자율을 계산하여 시뮬레이션을 하였다.

설계결과를 검증하기 위해 실제 전파흡수체를 설계에 의거 제작하여 전파흡수능을 비교 분석한 결과, 시뮬레이션 값과 실측 값이 잘 일치하였다. 결과적으로 W-band에서 20 dB 이상의 전파흡수능을 갖는 전파흡수체를 개발하였다. 또한 이 결과는 전파흡수체의 두께를 조정하여 65 GHz-110 GHz 범위 내에서 적용할 시스템의 사용 주파수에 맞는 전파흡수체를 개발할 수 있다.

Chapter 1
INTRODUCTION

The millimeter wave region of the electromagnetic spectrum corresponds to radio band frequencies of 30 GHz ($\lambda = 10\,mm$) to 300 GHz ($\lambda = 1\,mm$) and is sometimes called the Extremely High Frequency (EHF) range. Millimeter waves offer a solution to the increasing demand in frequency allocation due to the low-frequency-band saturation and the requirement for higher data rates. Moreover, a high directivity can be obtained with small antennas associated with small-sized circuits [1].

Millimeter wave radars are employed in a wide range of commercial, military and scientific applications for remote sensing, safety, and measurements [2]-[4]. Millimeter wave radars are superior to microwave and infrared-based radars in most applications. Millimeter wave radars offer better range resolution than lower frequency microwave radars, and can penetrate fog, smoke and other obscurants much better than infrared radars.

Since the removal of the selective-availability restriction, there still remains the concern that GPS may be rendered unusable by some form of interference or jamming. For this and other reasons, airborne vehicles generally rely on a combination of GPS and inertial navigation systems (INS) [5], [6]. This combination is only effective for short periods once GPS becomes unavailable because residual errors and biases quickly integrate up into unacceptably large position errors.

Under these conditions, millimeter wave radar can be applied in a number of ways to improve the velocity-estimation accuracy by measuring the ground speed, or it can be used to produce high-resolution images that can be displayed for direct interpretation by the pilot or correlated with aerial photographs for navigation or guidance purposes [3].

However, radar systems suffer from two major problems such as false images and system-to-system interference [7]. False echoes cause driving hazards. These problems can be eliminated through the use of an electromagnetic (EM) wave absorber [8], [9].

The initial purpose of EM wave absorber development was mainly the application to the anechoic chamber [10], [11]. A microwave oven is an example of the early application of wave absorbers. For EM wave leakage prevention from the door of a microwave oven, means for installing the EM wave absorptive material have been developed [12]. Later, the TV ghost created by a wave reflected from a high-rise building and the false image obtained by a ship's radar from a large bridge became problems. EM wave absorbers have been developed as countermeasures to these problems. Recently, because of the explosive increase in the usage of EM waves in wireless technologies such as wireless LAN [13]-[16], Electronic-Toll Collection (ETC) of the Dedicated Short-Range Communication (DSRC) system [15]-[18], Collision-Avoidance Radar [8], [9], [19], and suppression of noise from printed circuit board (PCB) [16], [20], EM wave absorbers are in huge demand and are extremely effective.

As is well known, EM wave absorbers can be broadly divided into three types from the viewpoint of material [12], [21], [22]. One is a wave absorber using a condictive material, another is a wave absorber using a dielectric material, and the other is a wave absorber using a magnetic material.

In general, Carbon black and Titanium dioxide are useful materials for EM wave absorption in V band and W band, and these EM wave absorption abilities have been investigated [23], [24]. Ferrite is a useful material for EM wave absorption in the frequency range of 1-20 GHz, and its EM wave absorption abilities have been investigated by many researchers [25]-[28]. However, EM wave absorbers using magnetic materials have not been reported in the V band and W band.

1.1 Dissertation Objective

We know that major problems can be eliminated through the use of an EM wave absorber. But, the EM wave absorber using three absorbing materials has not been investigated and developed in W-band of millimeter wave.

In this dissertation, the EM wave absorbers using Carbon black as a conductive material, TiO_2 as a dielectric material, and Permalloy as a magnetic material with chlorinated polyethylene (CPE) were designed and fabricated for W-band navigation radars.

First of all, the complex relative permittivity ($\varepsilon_r = \varepsilon_r^{'} - j\varepsilon_r^{''}$) and permeability ($\mu_r = \mu_r^{'} - j\mu_r^{''}$) of three-type absorbing materials are calculated from the S-parameter. The optimum composition ratios of absorbing materials were determined from absorption ability of various composite. The EM wave absorption abilities at different thicknesses are simulated using material properties of the EM wave absorbers, and the EM wave absorbers were fabricated based on the simulated design. The simulated and measured results agree very well.

As a result, the sheet-type absorbers were developed to eliminate false image and system-to-system interference of navigation radars in W-band.

1.2 Outline of Remaining Chapters

The remaining chapters proceed as follows.

Chapter 2 is devoted to a general discussion of navigation radar fundamental is presented. This includes history of radar development, radar system fundamental, millimeter wave radar, and contributions of EM wave absorber.

In chapter 3, theory of EM wave absorber is introduced briefly. This includes history of EM wave absorber, electromagnetic theory, loss mechanism, classification of EM wave absorber, and application of EM wave absorber.

In chapter 4, design of EM wave absorber is presented. This is the most important step to develop the EM wave absorber. This includes design theory of single-layer absorber and multi-layer absorber.

In chapter 5, the measurement of material properties is presented. In addition, manufacturing process of EM wave absorber is described in this chapter. An analysis of material properties of absorber samples is presented. The SEM photographs of samples are also presented.

In chapter 6, absorption ability of samples is presented. This includes measurement techniques of absorption ability, simulated absorption ability, and measured absorption ability. The EM wave absorber is fabricated based on the simulated design. A comparison of simulated and measured absorption ability of samples is presented.

Chapter 7 summarizes all results obtained in chapter 2 to chapter 6, and includes the further research topics or work to be investigated or supplemented.

Chapter 2
NAVIGATION RADAR FUNDAMENTAL

2.1 History of Radar Development

Radar did not come to the forefront as a useful sensor until World War Ⅱ, when tremendous strides were made in both the theory and practice of radar technology. The earliest account of the reflection of radio frequency waves from metallic and dielectric bodies was given by Hertz, who in 1886 used a 450 MHz spark-gap transmitter and receiver to test Maxwell's theories. The first detection of what might be called a military target by radar was achieved by Christian Hulsmeyer, a German engineer, who demonstrated a ship detection device to the German Navy in 1903. However, the range of the device was so limited that little interest was generated.

The earliest U.S. radar detection work was carried out by Taylor and Young of the Naval Research Laboratory (NRL). In late 1922 they used a continuous wave interference radar operating at 60 MHz to detect a wooden ship. The first radar detection of aircraft in the United States, also accomplished using a CW interference radar, was made in 1930 by Hyland of NRL.

Early radar work, both in the United States and abroad, often used a CW transmitter. These radars detected targets by sensing the modulation of the received signal caused by the Doppler shifted reflection from the target beating with the direct signal from the transmitter. Low transmitting frequencies were used because high-power transmitters were not available at the higher frequencies. These CW radars detected the presence of a target, but no range information could be extracted (making it doubtful if they should even be included in the class of objects whose name stands for “radio detection and ranging”). Also, at the low frequencies used, only coarse angular information was available. To allow range measurement, modulation of the signal waveform was required, and so pulsed systems were developed.

A pulsed radar operating at 28 MHz and using 5 μs pulses was developed at NRL and tested in early 1935. The tests were unsuccessful, but the radar was subsequently modified, and it detected its first target echo in 1936. Shortly after that, in late 1936, the U.S. Army Signal Corps tested its first pulsed radar. The Army also developed the first operational antiaircraft fire control radar in the United States, the SCR-268, which was fielded in 1938. It was an SCR-270, the long-range surveillance companion to the SCR-268, that detected Japanese aircraft at a range of over 130 mi as they approached Oahu, Hawaii, on the morning of December 7, 1941.

The British successfully demonstrated a pulsed radar at 12 MHz in 1935, obtaining detection ranges of more than 40 mi against a bomber aircraft. Both the United States and Britain were aware of the reduction of the physical size of equipment and angular resolution advantages available at higher frequencies, and groups in both countries were working at 200 MHz by the late 1930s.

The pivotal event allowing the practical development of microwave radar was the invention of the cavity magnetron by Randall and Boot in Britain. The magnetron is a self-excited crossedfield (i.e., the magnetic and electric fields are perpendicular) oscillator whose frequency of operation is determined by the dimensions of a regular series of holes and slots cut into a cylindrical anode structure surrounding a cylindrical cathode. The first cavity magnetron produced a peak pulse power of 100 kW at 3 GHz, a power level much greater than had previously been achieved at those frequencies. In late 1940, Britain and the United States began cooperative efforts in the radar area. The focal point for U.S. radar development efforts during World War Ⅱ was the Radiation Laboratory, established at MIT in November 1940. The initial staff of 40 had grown to about 4,000 by mid-1945, and their activities are documented in a 28 volume set of books (commonly known as the Rad Lab Series), Which even now, almost 50 years later, provides a valuable reference on radar fundamentals.

Improvements in radar technology have been enormous since World War Ⅱ. In the transmitter area, the development of the high-power traveling wave tube (TWT), millimeter-wave power tubes, solid-state microwave sources, and stable computer controlled oscillators have been important. In the receiver area, solid-state technology has improved mixers and allowed development of low-noise amplifiers. In the antenna area, large-scale phased arrays have become practical. In signal processing, as in every other area of radar, the advent of the small, fast digital computer has made practical radar techniques that could not otherwise have been considered.

It is interesting to note that the advent of “stealth” technology has somewhat reversed the historic trend in radar development toward the use of higher frequencies. Low cross section vehicles will generally show an RCS behavior proportional to the radar wavelength squared. This functional dependence, which is driven by the shaping that must be employed if very low RCS values are to be obtained, has understandably renewed interest in lower frequency radars [29].

2.2 Radar System Fundamentals

Radar is an acronym for Radio Detection and Ranging. Radar systems attempt to infer information about remotely located objects from reflections of deliberately generated electromagnetic waves at radio frequencies. Typically, a radar system operates in the environment depicted in Fig. 2.1 and the information sought is detection of the presence of target objects in the midst of clutter, recognition (classification) of targets, and estimation of target parameters such as range (distance from the radar antenna), bearing (azimuth and elevation), orientation, velocity, acceleration, or backscattering cross section (reflectivity) distribution [1].

Radar systems employ two basic types of energy transmission: pulse and continuous wave (CW). The pulsed radar transmits radio frequency energy in a series of short pulses separated by non-transmission intervals or rest time. Target echoes are processed during these non-transmission intervals, and range is determined based on the total travel time for the pulse/echo. In CW radar, on the other hands, the transmitter sends out a continuous signal. If a non-moving object is in the path of the transmitted wave train, the frequency of the reflected signal will be the same as the transmitted signal. If the object is moving, the frequency of the reflected signal will differ from that of the transmitted signal, and that difference can be used as an indicator of target motion. In CW transmission, either a movement of the radar or the target is necessary to produce an indication of target presence [30].

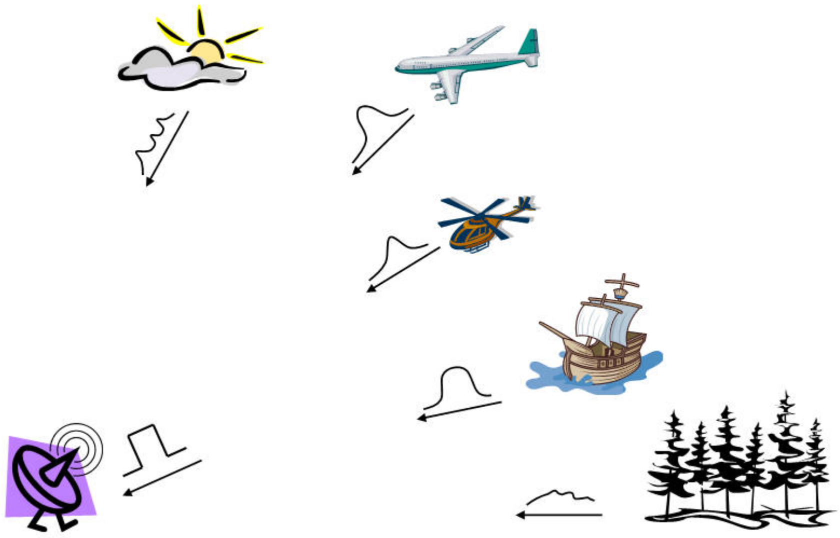

Fig. 2.1 Typical environment in which a radar needs to operate.

Navigation radar is used to provide the necessary data for piloting an aircraft from one position to another without any need for navigation information transmitted to the aircraft from a ground station. A self-contained aircraft navigation system utilizes a continuous-wave Doppler radar to measure the drift angle and true speed of the aircraft relative to Earth. The drift angle is the angle between the centerline (heading) of the aircraft and the horizontal direction (ground track). A navigation radar requires at least three noncoplanar beams to measure the vector velocity, that is, the speed and its direction, of the aircraft. Such a radar measures the vector velocity relative to the frame of reference of the antenna assembly.

This vector velocity can be converted to a horizontal reference on the ground by determining the direction of the vertical and the aircraft heading by some auxiliary means. Usually, the radar uses four beams that are initially disposed symmetrically about the aircraft axis, with two facing forward and two facing rearward. If the aircraft vector velocity is not in the direction of the aircraft heading, the two forward-facing beams will not read the same Doppler frequency. This Doppler difference can be fed in a servomechanism that will align the axes of the antennas with the ground track of the aircraft. The angular displacement of the antennas from the aircraft heading is the drift angle, and the magnitude of the Doppler frequency is a measure of the speed along the ground track. The uses of the two rearward beams are similar, but improve the accuracy considerably by reducing the errors caused by vertical motion of the aircraft and pitching movements of the antennas [1].

2.3 Millimeter Wave Radar

2.3.1 Characteristics of Millimeter Wave Radar

The millimeter wave region of the electromagnetic spectrum is usually considered to be the range of wavelengths from 10 millimeters to 1 millimeter. This means they are larger than infrared waves or x-rays, for example, but smaller than radio waves or microwaves. The millimeter wave region of the electromagnetic spectrum corresponds to radio band frequencies of 30 GHz to 300 GHz and is sometimes called the Extremely High Frequency (EHF) range. The millimeter wave domain is presented in Fig. 2.2.

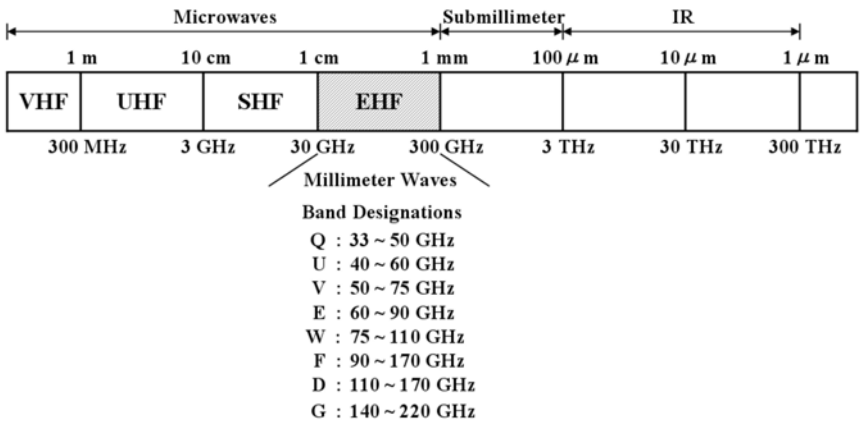

Fig. 2.2 The millimeter wave domain.

The high frequency of millimeters waves as well as their propagation characteristics (that is, the ways they change or interact with the atmosphere as they travel) makes them useful for a variety of applications including transmitting large amounts of computer data, cellular communications, and radar.

In microwave system, transmission loss is accounted for principally by the free space loss. However, in the millimeter wave bands additional loss factors come into play, such as gaseous and rain in the transmission medium.

Transmission losses occur when millimeter waves traveling through the atmosphere are absorbed by molecules of oxygen, water vapor and other gaseous atmospheric constituents. These losses are greater at certain frequencies, coinciding with the mechanical resonant frequencies of the gas molecules. Figure 2.3 shows the areas of peak absorption in the millimeter wave spectrum. It shows several peaks that occur due to absorption of the radio signal by water vapor (H_2O) and oxygen (O_2). At these frequencies, absorption results in high attenuation of the radio signal and, therefore, short propagation distance. For current technology the important absorption peaks occur at 24 and 60 GHz. The spectral regions between the absorption peaks provide windows where propagation can more readily occur. The transmission windows are at about 35 GHz, 94 GHz, 140 GHz and 220 GHz [31].

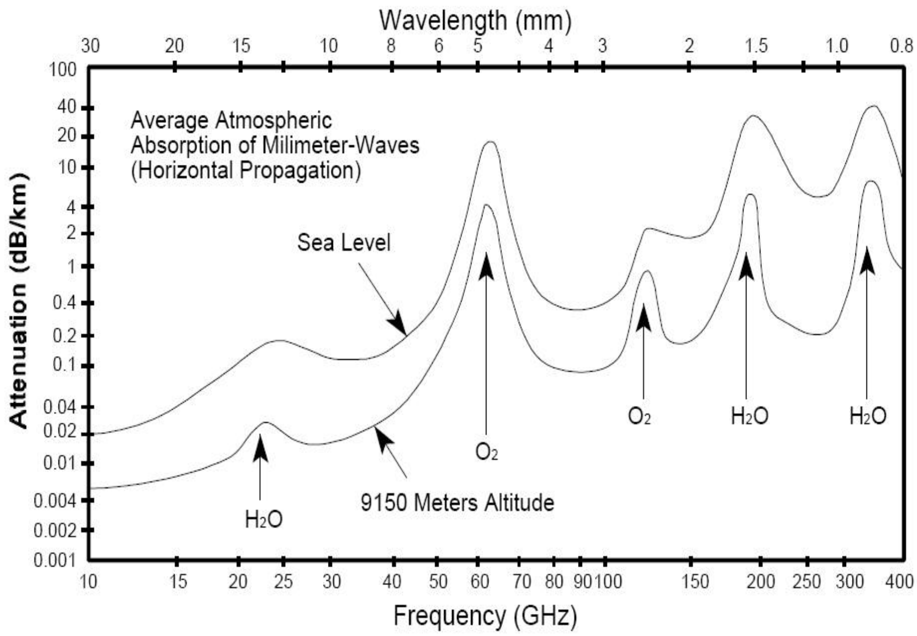

Fig. 2.3 Atmospheric absorption of millimeter waves.

One of the greatest and most important uses of millimeter waves is in transmitting large amounts of data. Every kind of wireless communication, such as the radio, cell phone, or satellite, uses specific range of wavelengths or frequencies. Their high frequency makes them a very efficient way of sending large amounts of data such as computer data, or many simultaneous television or voice channels.

Radar is another important use of millimeter waves, which takes advantage of another important property of millimeter wave propagation called beamwidth. Beamwidth is a measure of how a transmitted beam spreads out as it gets farther from its point of origin. In radar, it is desirable to have a beam that stays narrow, rather than fanning out. Small beamwidths are good in radar because they allow the radar to "see" small distant objects, much like a telescope. A carefully designed antenna allows microwaves to be focused into a narrow beam. Unfortunately, small beamwidths require large antenna sizes, which can make it difficult to design a good radar set. But for a given antenna size, the beamwidth can be made smaller by increasing the frequency, and so the antenna can be made smaller as well.

2.3.2 Applications

Millimeter wave radars are employed in a wide range of commercial, military and scientific applications for remote sensing, safety, and measurements. Millimeter wave sensors are superior to microwave and infrared-based sensors in most applications. Millimeter wave radars offer better range resolution than lower frequency microwave radars, and can penetrate fog, smoke and other obscurants much better than infrared sensors. Some of the most commonly employed millimeter wave radar subsystems show in Table 2.1 [32].

Table 2.1 Applications of millimeter wave radar.

Frequency	Type	Application and Comments
35 GHz	FMCW	Detection of intruders and moving vehicles, security, obstacle detection for robotic equipment, traffic monitoring and control
		Military seeker and sensor application for munitions and missiles
76 ~ 77 GHz	FMCW	Prototype radar for automobile collision warning, security and perimeter protection, robotic vision/ranging. Traffic monitoring/detection
	Multi-mode	Automobile Collision Warning and Autonomous Cruise Control
94 GHz	Pulsed	Missile Guidance and Collision Avoidance
	FMCW	Research radar for study of severe weather and clouds. Development and instrumentation radar. Military applications

2.4 Contributions of EM Wave Absorber

Today's modern warship has a wide variety of electronic systems on board. Navigational and target acquisitions radars, countermeasures systems, and a wide variety of communications equipment are all mounted on a large metal superstructure. This arrangement creates two major problems, such as false images from self-reflections and system-to-system interference. False images or ghosts are indirect radar returns resulting from specular reflections of radar energy off the ship's own superstructure. False echoes cause navigation hazards, and, if severe enough, can make radar navigation impossible. False returns to target acquisition and fire control systems can cause the system to "lock on" to the false images. These problems can be eliminated through the use of EM wave absorber.

Stealth is another important use of EM wave absorber. The radar cross section (RCS) of military aircrafts and other targets can be reduced by applying suitable EM wave absorber in their structures [33].

Chapter 3
THEORY OF EM WAVE ABSORBER

3.1 History

The start of the research on EM wave absorbers dates back to the mid-1930s. The first wave absorber was due to research in the 2 GHz band in Naamlooze Vennootschap Machinerieen in the Netherlands. The EM wave absorber reported in 1945 was for military purpose. It was used for protecting the periscope and snorkel of a submarine from search by radar as shown in Fig. 3.1. It consists of the structure that piled up “Wesch material” which is composed of composite rubber and carbonyl iron, a resistance sheet, and plastic. This absorber has been called a “Jauman absorber”. In the project organized by O. Halpen at the MIT Radiation Laboratory in the United States, an application-type absorber was developed. In the same project, a kind of resonant-type “Salisbury screen absorber” was developed which was made by putting a resistive sheet with a surface resistance value of 377Ω one-quarter wavelength away from a conductive plate. In 1953, a pyramidal absorber was developed by L. K. Neher. This absorber has been broadly used for anechoic chambers [10], [11].

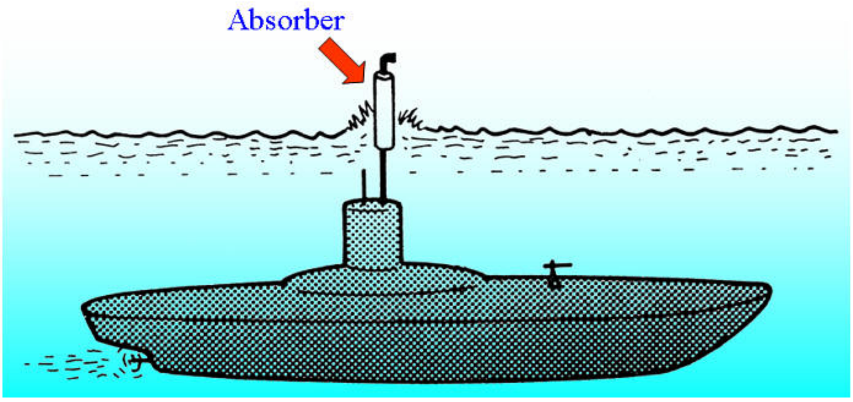

Fig. 3.1 The first wave absorber was used for protecting the periscope and snorkel of a submarine from search by radar.

In the late 1960's, Mr. R. E. Hiatt, Head of the Radiation Laboratory, University of Michigan, Ann Arbor, demonstrated significant absorber thickness reduction using magnetic ferrites as under layers. His work was sponsored by NASA. As they happened to be the days of satellite projects, the anechoic chambers had to be useful for making many types of measurements for multi-purposes. The 100 MHz to 400 MHz frequency resign was important for tracking and telemetry. It is known that at lower frequency it is more difficult to obtain high absorption ability. High permeability and high permittivity magnetic materials contribute for a high refraction index at low frequency regions and hence reduce the thickness of absorbers, This new development made it possible to obtain -40 dB return loss from 100 MHz to 1 GHz.

In the 1970's, the Japanese used magnetic ferrites to make EM wave absorbing paint and applied it on the outside wall of high buildings to reduce the ghost images on television screen. The Plessy company in UK, a renowned manufacturer of EM wave absorbers, developed a new generation of EM wave absorbers to satisfy the requirements of the British Navy including camouflage and minimizing electromagnetic interference (EMI).

All these efforts have resulted in the development of "Stealth Material" by several countries which will play a significant role in the development of Advanced Bomber and Fighter Aircrafts as well as the development of radar absorbing materials (RAM) of Naval Vessels. These developments have been achieved based on a synergistic approach. The reduction in the radar cross section (RCS) of a target has been obtained by a number of methods such as adjusting geometrical shapes to reduce the reflection at certain sensitive angles and applying the RAM onto the target surface [34].

3.2 Electromagnetic Theory

3.2.1 The Helmholtz Equation

In a source-free, linear, isotropic, homogeneous region, Maxwell's curl equations in phasor form are

$$\nabla \times \overline{E} = -j\omega\mu\overline{H} \tag{3.1}$$

$$\nabla \times \overline{H} = j\omega\varepsilon\overline{E} \tag{3.2}$$

And constitute two equations for the two unknowns, $\overline{E}$ and $\overline{H}$. As such, they can be solved for either $\overline{E}$ or $\overline{H}$. Thus, taking the curl of eq. (3.1) and using eq. (3.2) gives

$$\nabla \times \nabla \times \overline{E} = -j\omega\mu\nabla \times \overline{H} = \omega^2 \mu\varepsilon\overline{E} \tag{3.3}$$

Which is an equation for $\overline{E}$. This result can be simplified through the use of vector identity, $\nabla \times \nabla \times \overline{A} = \nabla(\nabla \cdot \overline{A}) - \nabla^2 \overline{A}$, which is valid for the rectangular components of an arbitrary vector $\overline{A}$.

Then,

$$\nabla^2 \overline{E} + \omega^2 \mu\varepsilon\overline{E} = 0 \tag{3.4}$$

since $\nabla \cdot \overline{E} = 0$ in a source-free region. Equation (3.4) is the wave equation, or Helmholtz equation, for $\overline{E}$. An identical equation for $\overline{H}$ can be derived in the same manner:

$$\nabla^2 \overline{H} + \omega^2 \mu\varepsilon\overline{H} = 0 \tag{3.5}$$

A constant $k = \omega\sqrt{\mu\varepsilon}$ is defined and called the wavenumber, or propagation constant, of the medium; its units are 1/m.

As a way of introducing wave behavior, we will next study the solutions to the above wave equations in their simplest forms, first for a lossless medium and then for a lossy medium.

3.2.2 Plane Waves in a Lossless Medium

In a lossless medium, ε and μ are real numbers, so *k* is real. A basic plane wave solution to the above wave equations can be found by considering an electric field with only an $\hat{x}$ component and uniform (no variation) in the x and y directions. Then, $\partial/\partial x = \partial/\partial y = 0$, and the Helmholtz equation of eq. (3.4) reduces to

$$\frac{\partial^2 E_x}{\partial z^2} + k^2 E_x = 0 \tag{3.6}$$

The two independent solutions to this equation are easily seen, by substitution, to be of the form

$$E_x(z) = E^+ e^{-jkz} + E^- e^{jkz} \tag{3.7}$$

where E^+ and E^- are arbitrary amplitude constants.

The above solution is for the time harmonic case at frequency ω. In the time domain, this result is written as

$$\mathcal{E}_x(z,t) = E^+ \cos(\omega t - kz) + E^- \cos(\omega t + kz) \tag{3.8}$$

where we have assumed that E^+ and E^- are real constants. Consider the first term in eq. (3.8). This term represents a wave traveling in the $+z$ direction, since, to maintain a fixed point on the wave $(\omega t - kz = \text{constant})$, one must move in the $+z$ direction as time increases. Similarly, the second term in eq. (3.8) represents a wave traveling in the negative z direction; hence the notation E^+ and E^- for these wave amplitudes. The velocity of the wave in this sense is called the phase velocity, because it is the velocity at which a fixed phase point on the wave travels, and it is given by

$$v_p = \frac{dz}{dt} = \frac{d}{dt}\left(\frac{\omega t - \text{constant}}{k}\right) = \frac{\omega}{k} = \frac{1}{\sqrt{\mu\varepsilon}} \tag{3.9}$$

In free-space, we have $v_p = 1/\sqrt{\mu_0\varepsilon_0} = c = 2.998 \times 10^8 m/\sec$, which is the speed of light.

The wavelength, λ, is defined as the distance between two successive maxima (or minima, or any other reference point) on the wave, at a fixed instant of time.

Then,

$$[\omega t - kz] - [\omega t - k(z + \lambda)] = 2\pi$$

so,

$$\lambda = \frac{2\pi}{k} = \frac{2\pi v_p}{\omega} = \frac{v_p}{f} \tag{3.10}$$

A complete specification of the plane wave electromagnetic field must include the magnetic field. In general, whenever $\overline{E}$ or $\overline{H}$ is known, the other field vector can be readily found by using one of Maxell's curl equations. Thus, applying eq. (3.1) to the electric field of eq. (3.7) gives $H_x = H_z = 0$ and

$$H_y = \frac{1}{\eta}[E^+ e^{-jkz} - E^- e^{jkz}] \tag{3.11}$$

where $\eta = \omega\mu/k = \sqrt{\mu/\varepsilon}$ is the wave impedance for the plane wave, defined as the ratio of the $\overline{E}$ and $\overline{H}$ field. For plane waves, this impedance is also the intrinsic impedance of the medium. In free-space we have $\eta_0 = \sqrt{\mu_0 / \varepsilon_0} = 377\,\Omega$. Note that the $\overline{E}$ and $\overline{H}$ vectors are orthogonal to each other and orthogonal to the direction of propagation $(\pm\hat{z})$; this is a characteristic of transverse electromagnetic (TEM) waves.

3.2.3 Plane waves in a general lossy medium

Now consider the effect of a lossy medium. If the medium is conductive, with a conductivity σ, Maxwell's curl equations can be written as

$$\nabla \times \overline{E} = -j\omega\mu\overline{H} \tag{3.12}$$

$$\nabla \times \overline{H} = j\omega\varepsilon\overline{E} + \sigma\overline{E} \tag{3.13}$$

The resulting wave equation for $\overline{E}$ then becomes

$$\nabla^2 \overline{E} + \omega^2 \mu\varepsilon(1 - j\frac{\sigma}{\omega\varepsilon})\overline{E} = 0 \tag{3.14}$$

where we see a similarity with eq. (3.4), the wave equation for $\overline{E}$ in the lossless case. The difference is that the wavenumber $k^2 = \omega^2\mu\varepsilon$ of eq. (3.4) is replaced by $\omega^2\mu\varepsilon[1 - j(\sigma/\omega\varepsilon)]$ in eq. (3.14). We then define a complex propagation constant for the medium as

$$\gamma = \alpha + j\beta = j\omega\sqrt{\mu\varepsilon}\sqrt{1 - j\frac{\sigma}{\omega\varepsilon}} \tag{3.15}$$

If we again assume an electric field with only an $\hat{x}$ component and uniform in x and y, the wave equation of eq. (3.14) reduces to

$$\frac{\partial^2 E_x}{\partial z^2} - \gamma^2 E_x = 0 \tag{3.16}$$

which has solutions

$$E_x(z) = E^+ e^{-\gamma z} + E^- e^{\gamma z} \tag{3.17}$$

The positive traveling wave then has a propagation factor of the form

$$e^{-\gamma z} = e^{-\alpha z} e^{-j\beta z}$$

which in the time domain is of the form

$$e^{-\alpha z}\cos(\omega t - \beta z)$$

We see that this represents a wave traveling in the $+z$ direction with a phase velocity $v_p = \omega/\beta$, a wavelength $\lambda = 2\pi/\beta$, and an exponential damping factor. The rate of decay with distance is given by the attenuation constant α. The negative traveling wave term of eq. (3.17) is similarly damped along the $-z$ axis. If the loss is removed, $\sigma = 0$, and we have $\gamma = jk$ and $\alpha = 0, \beta = k$.

Loss can also be treated through the use of a complex permittivity. From eq. (3.15) with $\sigma = 0$ but $\varepsilon = \varepsilon' - j\varepsilon''$ complex, we have that

$$\gamma = j\omega\sqrt{\mu\varepsilon} = jk = j\omega\sqrt{\mu\varepsilon^{'}(1 - j\tan\delta)} \qquad (3.18)$$

where $\tan\delta = \varepsilon^{''}/\varepsilon^{'}$ is the loss tangent of the material.

Next, the associated magnetic field can be calculated as

$$H_y = \frac{j}{\omega\mu}\frac{\partial E_x}{\partial z} = \frac{-j\gamma}{\omega\mu}(E^{+}e^{-\gamma z} - E^{-}e^{\gamma z}) \qquad (3.19)$$

As with the lossless case, a wave impedance can be defined to relate the electric and magnetic fields:

$$\eta = \frac{j\omega\mu}{\gamma} \qquad (3.20)$$

Then eq. (3.19) can be rewritten as

$$H_y = \frac{1}{\eta}(E^{+}e^{-\gamma z} - E^{-}e^{\gamma z}) \qquad (3.21)$$

Note that η is, in general, complex and reduces to the lossless case of $\eta = \sqrt{\mu/\varepsilon}$ when $\gamma = jk = j\omega\sqrt{\mu\varepsilon}$.

3.2.4 Plane Waves in a Good Conductor

Many problems of practical interest involve loss or attenuation due to good conductors. A good conductor is a special case of the preceding analysis, where the conductive current is much greater than the displacement current, which means $\sigma >> \omega\varepsilon$. Most metals can be categorized as good conductors. In terms of a complex ε, rather than conductivity, this condition is equivalent to $\varepsilon^{''} >> \varepsilon^{'}$. The propagation constant of eq. (3.15) can then be adequately approximated by ignoring the displacement current term, to give

$$\gamma = \alpha + j\beta \cong j\omega\sqrt{\mu\varepsilon}\sqrt{\frac{\sigma}{j\omega\varepsilon}} = (1+j)\sqrt{\frac{\omega\mu\sigma}{2}} \tag{3.22}$$

The skin depth, or characteristic depth of penetration, is defined as

$$\delta_s = \frac{1}{\alpha} = \sqrt{\frac{2}{\omega\mu\sigma}} \tag{3.23}$$

Then the amplitude of the field in the conductor decay by an amount $1/e$ or 36.8 %, after traveling a distance of one skin depth, since $e^{-\alpha z} = e^{-\alpha\delta_s} = e^{-1}$. At microwave frequencies, for a good conductor, this distance is very small. The practical importance of this result is that only a thin plating of a good conductor is necessary for low-loss microwave components [35].

3.3 Loss mechanism

The EM wave absorber has been defined as an object that can absorb incident EM waves and convert these into a Joule heat or which can cancel the phase of the incident wave [12].

Lossy materials attenuate electromagnetic waves that pass through them. This can be modeled with the refraction index, relative permittivity, or relative permeability which is all complex numbers. The imaginary component causes the loss in the material [33].

Physically, the absorbed power is converted into heat. In practical engineering applications where only the cumulative loss is of interest, the different loss mechanisms are combined into one set of normalised complex permittivity and permeability values ε_r and μ_r, given as

$$\varepsilon_r = \varepsilon_r^{'} - j\varepsilon_r^{''} \tag{3.24}$$

$$\mu_r = \mu_r^{'} - j\mu_r^{''} \tag{3.25}$$

In the above equations, the real parts showing the energy storage are denoted by single primes, and the complex parts showing the loss with double primes. If we specify the electric and magnetic loss tangents as

$$\tan\delta_e = \frac{\varepsilon_r^{''}}{\varepsilon_r^{'}} \tag{3.26}$$

$$\tan\delta_m = \frac{\mu_r^{''}}{\mu_r^{'}} \tag{3.27}$$

Equations (3.24) and (3.25) can be written in polar form as

$$\varepsilon_r = |\varepsilon_r| e^{j\delta_e} \tag{3.28}$$

$$\mu_r = |\mu_r| e^{j\delta_m} \tag{3.29}$$

The refraction index between free-space and a lossy material is

$$n = \frac{k}{k_0} = \sqrt{\mu_r \varepsilon_r} \tag{3.30}$$

where k and $k_0 = 2\pi f \sqrt{\mu_0 \varepsilon_0}$ are the wavenumbers in a lossy material and in free space, respectively. If $Z_0 = 120\pi$ is the free-space impedance, the charicteristic impedance of a material with $\varepsilon_r \neq 1$ and $\mu_r \neq 1$ can be defined as

$$Z_c = Z_0 \sqrt{\frac{\mu_r}{\varepsilon_r}} \tag{3.31}$$

For normal incidence, the reflection coefficient of the material interface is calculated as

$$\Gamma = \frac{Z_c - Z_0}{Z_c + Z_0} = \frac{Z_c / Z_0 - 1}{Z_c / Z_0 + 1} \tag{3.32}$$

In many practical applications, the dielectric absorbing material (with thickness *d*) has a metal backing, and its normalized input impedance (for normal incidence) can be shown to be

$$z_{in} = \sqrt{\frac{\mu_r}{\varepsilon_r}} \tanh(j \frac{2\pi}{\lambda} \sqrt{\varepsilon_r \mu_r} d) \tag{3.33}$$

In most cases we are only interested in absorption ability as shown in eq. (3.34).

$$S = -20\log_{10}|\Gamma| \qquad [dB] \tag{3.34}$$

However, the phase angle of Γ is important in some narrowband absorber applications where resonant energy cancellation is used.

The design of an EM wave absorber is a compromise between the front-face reflection coefficient and the loss per unit thickness. If high absorption ability is desired, then the material thickness will become large in wavelengths. In practice, multilayer structures are used to obtain the high loss and low reflection inside the EM wave absorber.

The level of absorption ability of the absorber is measured quantitatively using the reflection coefficient in decibels. Though a clear definition of what is a wave absorber has not been determined, the level of -20 dB in the reflection coefficient is considered that the EM wave absorber should be better than this limit indicates. This value of -20 dB corresponds to a 0.1 value of the reflection coefficient of the electric field and a 0.01 value of the reflection coefficient of electric power, as shown in Table 3.1. It means that 99% of the total EM wave energy to the absorber is absorbed.

Table 3.1. Reflection Coefficients in an EM wave absorber.

Reflection coefficient (dB)	Electric Field Reflection	Electric Power Reflection
0	1	1
-10	0.3	0.1
-20	0.1	0.01
-30	0.03	0.001

3.4 Classification of EM Wave Absorber

EM wave absorbers are normally classified from the viewpoint of constituent material, structural shape, frequency characteristics, and application, respectively.

3.4.1 Classification by Constituent Material

The classification from a constituent material viewpoint is as follows:

A. Conductive-Type Absorber

This type of absorber uses conductive materials such as carbon black, graphite nichrome, and chromium as a basic material. These materials are used in a usual plate-type absorber or a film form. The high-frequency current that flows on the surface of the conductive material is converted into Joule's heat, and the material can therefore absorb the EM wave.

B. Dielectric-Type Absorber

This is a EM wave absorber which is composed mainly of some of the above-mentioned carbon materials, mixing them into forming urethane, forming styrene, rubber materials, and so on. The matching characteristic depends on the frequency dispersion characteristic of the complex relative permittivity of the absorber.

C. Magnetic-Type Absorber

This is an EM wave absorber essentially formed of ferrite, for which sintering ferrite, rubber ferrite, plastic ferrite, and so on, are generally used. It can absorb the EM wave because it depends on the frequency dispersion characteristics of the complex relative permeability.

3.4.2 Classification by Structural Shape

EM wave absorbers are also classified on the basis of two structural shapes: one based on number of layers constituting the wave absorber and the other based on appearance.

A. Classification by Number of Layers

① Single-Layer Type Absorber

The absorber that is composed of only a single layer or single material is called a single-layer absorber. Generally, a conductive plate is attached to the back of this absorber. A type example of this type is the ferrite wave absorber.

② Double-Layer Type Absorber

The absorber is composed of two different absorptive materials. This arrangement is chosen to obtain broadband absorption characteristics and to improve them.

③ Multilayer Type Absorber

Generally, the absorber will more than three layers is called a multilayer wave absorber. In this case, the different layers are composed of absorbers with different material constants. When constituting a multilayer absorber, one can realize an absorber with broadband frequency characteristics.

B. Classification by Appearance

① Plane-Type Absorber

The plane-type absorber has the shape of a plane surface in the incident plane of the EM wave, as shown in Fig. 3.2(a). Usually, this is a ferrite absorber.

② Sawtooth-Type Absorber

This wave absorber has the shape of a sawtooth in the incident plane of the EM wave, as shown in Fig. 3.2(c). This offers a means to realize a broadband absorber, as does the next type of absorber.

③ Pyramidal-Type Absorber

This absorber has a broadband frequency characteristic because the absorber had the structure of pyramidal taper in the incident plane of the EM wave, as shown in Fig. 3.2(f). A typical absorber of this kind is made of foam polyurethane rubber containing carbon powder.

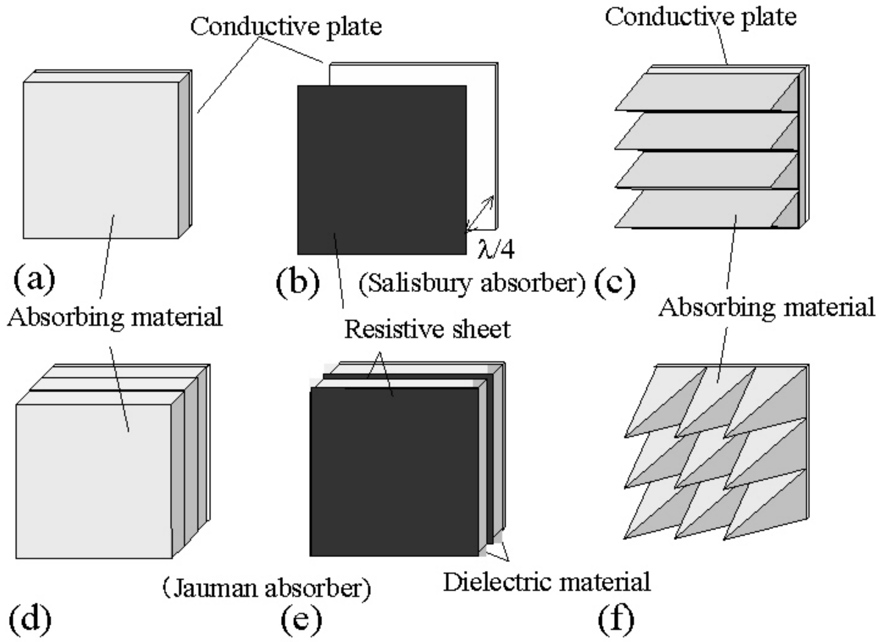

Fig. 3.2 Classification by appearance.

3.5 Application of EM Wave Absorber

The initial purpose of the EM wave absorber development was mainly the application to the anechoic chamber. A microwave oven is an example of the early application of wave absorbers. For EM wave leakage prevention from the door of a microwave oven, means for installing the EM wave absorptive material have been developed.

Later, the TV ghost created by a wave reflected from a high-rise building and the false image obtained by a ship’s radar from a large bridge became problems. EM wave absorbers have been developed as countermeasures to these problems.

Recently, because of the explosive increase in the usage of EM waves in wireless technologies such as wireless LAN, Electronic-Toll Collection (ETC) of the Dedicated Short-Range Communication (DSRC) system, Collision-Avoidance Radar, and suppression of noise from printed circuit board (PCB), EM wave absorbers are in huge demand and are extremely effective.

3.5.1 The EM Wave Absorber for an Anechoic Chamber

An important application of absorbers is in construction of anechoic chambers. Using today's state-of-the-art absorbers and chamber designs, "free-space" with regard to amplitude and phase uniformity can be simulated to a very high degree. It is not uncommon at high microwave frequencies to be able to create a chamber test volume (quiet zone) in which the level of reflections from all regions is greater than 60 dB below the level of the incident signal. Chambers are customarily used to frequencies as low as 30 MHz and as high as 100 GHz. The lower frequency limit requires pyramidal absorbers, having thickness as great as 15 feet (4.6 m). Most chambers use a mix of absorber thickness and types in various regions in order to achieve optimum performance and low cost [36].

Figure 3.3 shows an EM wave absorber which is used in anechoic chamber applications.

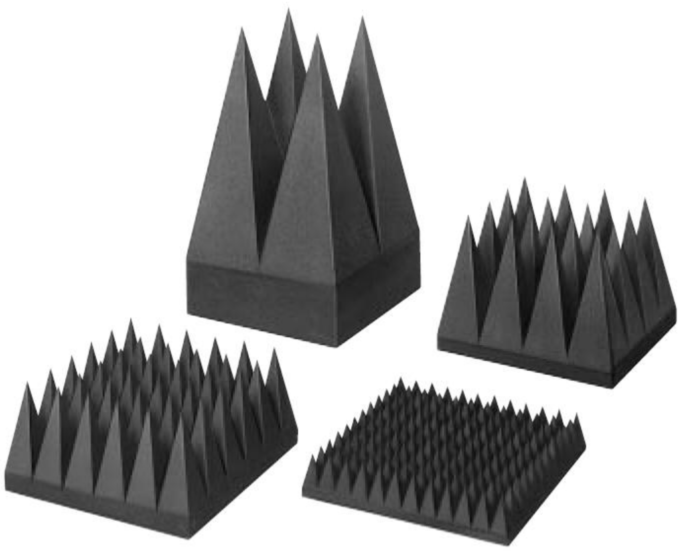

Fig. 3.3 The EM wave absorbers which are used in anechoic chamber are pyramidal absorbers.

3.5.2 The EM wave absorber for preventing TV ghost

Recently, the TV ghost created by a wave reflected from a high-rise building became serious social problems. EM wave absorbers have been developed as countermeasures to these problems. Sintered ferrite absorber is used to suppress TV ghost images caused by TV signal reflections from skyscrapers. Figure 3.4 shows EM environment of TV ghost generating.

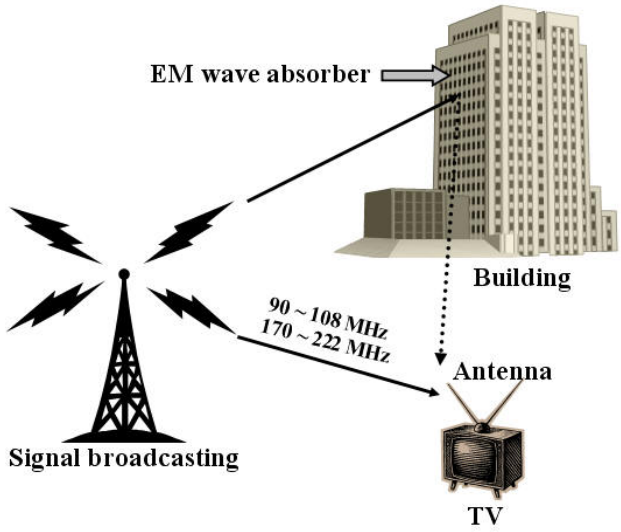

Fig. 3.4 EM environment of TV ghost generating.

3.5.3 The EM wave absorber for preventing a radar ghost

All radar systems create two major problems, such as false images and system-to-system interference. These problems can be eliminated through the use of the EM wave absorber. Especially, these type Absorbers are frequently used to reduce radiation from nearby reflecting objects or surfaces that can cause spurious radar signals. In the case of an airborne radar, for example, absorber may be used to cover a bulkhead behind the antenna, the base of the radome, and parts of the antenna mechanism. In a ship' radar, absorber may be used to cover a nearby bulkhead or portions of a mast and front face of a large bridge [10]. In a collision-avoidance radar of ITS, absorber may be used to cover the guard rails on both sides of the road or the inner walls of tunnels for preventing false operation of the radar [19].

Figure 3.5 shows EM environments to generate ghost in the cases of navigation radar and collision-avoidance radar.

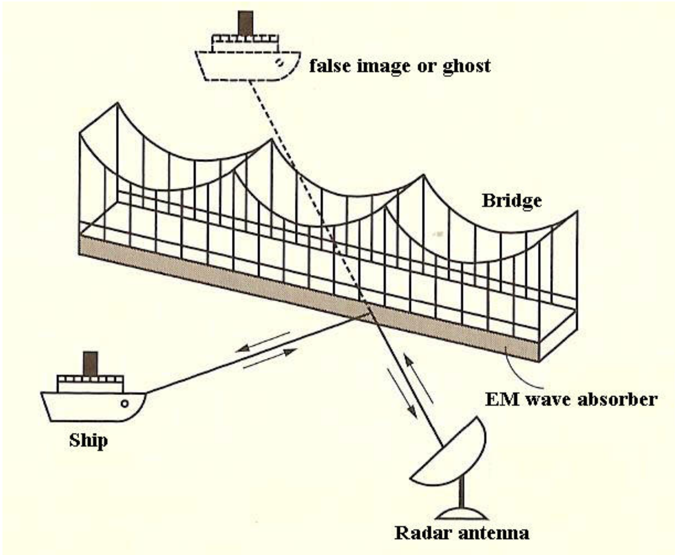

(a) Navigation radar in a ship

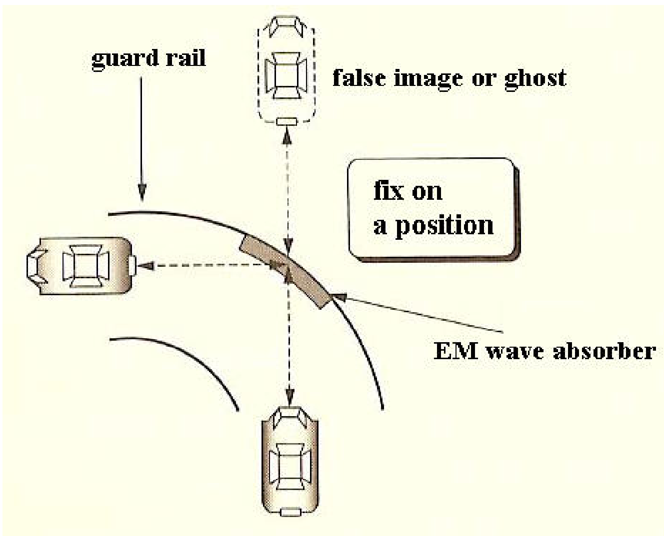

(b) Collision-avoidance radar in a car

Fig. 3.5 EM environments of radar ghost generating.

3.5.4 The EM Wave Absorber for Wireless LAN

Indoor wave absorbers for improving the EM environment in wireless LAN may not necessarily possess the ability of environmental endurance like outdoor devices, but they require cheaper, easy construction, and the guarantee of performance under changing humidity conditions. This type absorber has been made using building materials such as plasterboard, and constructed in multilayer structures. Hence the absorber can meet the wireless LAN demands at both 2.4 GHz and 5.2 GHz. Figure 3.6 shows EM environment in wireless LAN [15], [16].

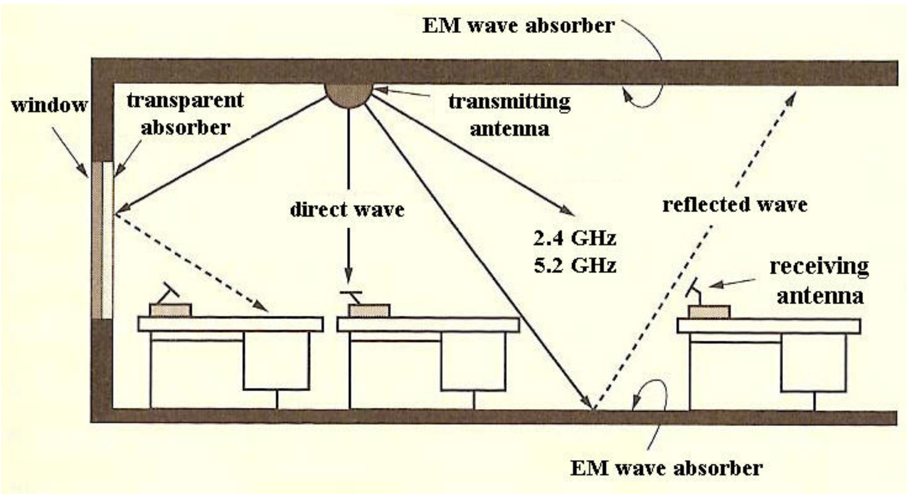

Fig. 3.6 EM environment in wireless LAN.

3.5.5 The EM Wave Absorber for ETC System

These type absorbers for outdoor applications, such as ETC and DSRC systems, require environmental endurance properties, as well as transparent and wide-angle characteristics (20 dB is required for the absorption rate from 0 to 55 degrees) at 5.8 GHz. To satisfy these demands, Indium Tin Oxide (ITO) film, Acryl Carbonated (AC) and glass plates in multilayer structures are used in the fabrication of wave absorbers [15], [16]. Figure 3.7 shows EM environment in ETC system.

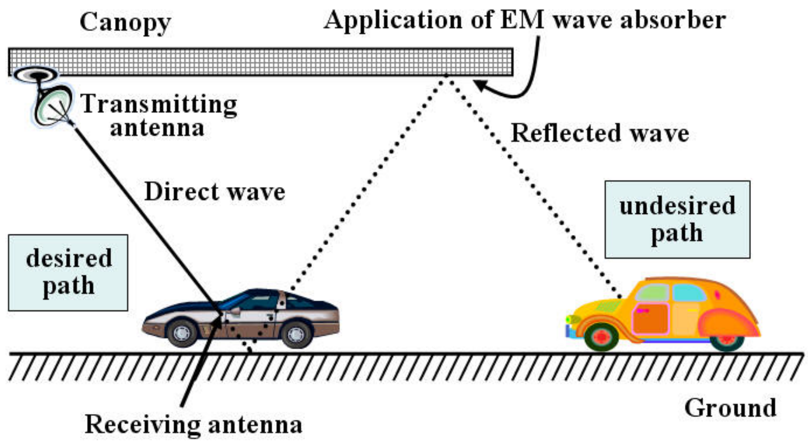

Fig. 3.7 EM environment in ETC system.

3.5.6 The EM Wave Absorber for Suppression of Noise from PCB

This type absorber for protecting against noise from printed circuit boards (PCB) have been required because the circuit speeds have been accelerated and packaging density has greatly been increased. [16].

To meet existing EMC regulations, an EM wave absorber sheet could be placed over the ICs as a measure to reduce electromagnetic emissions, wrapped around flexibly, or used to cover the whole PCB. Since an EM absorber sheet can also reduce case resonance, the approach of covering the inside of the case with EM wave absorber sheet could also be considered. An EM wave absorber sheet could also be attached inside the RF block shield to resolve the problem of internal interference. Furthermore, for SAR reduction in cellular phones, SAR levels can be reduced by mounting an EM wave absorber in an appropriate location within the telephone [37].

Figure 3.8 shows that the EM wave absorbers are frequently used to reduce EM emissions from PCB.

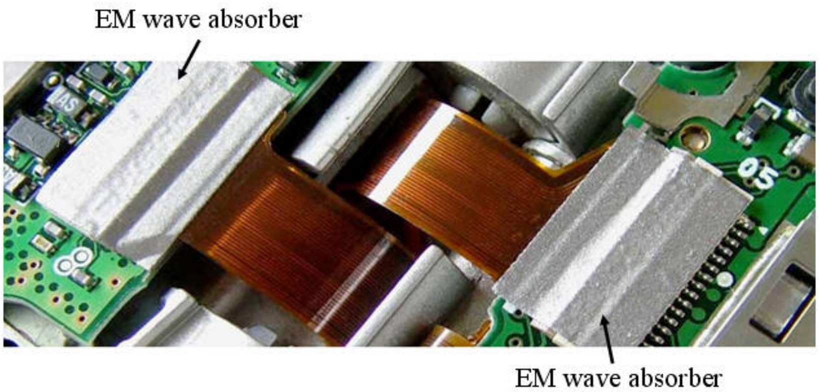

Fig. 3.8 The EM wave absorbers are frequently used to reduce EM emissions from PCB.

Chapter 4
DESIGN OF EM WAVE ABSORBER

4.1 Introduction

For the EM wave absorber made of a conductor-backed single layer as shown in Fig. 4.1, the absorption ability S can be obtained from the equivalent circuit as follows [22], [23]:

$$S = -20\log_{10}\left|\frac{z-1}{z+1}\right| \quad [dB] \tag{4.1}$$

here, z is the normalized input impedance.

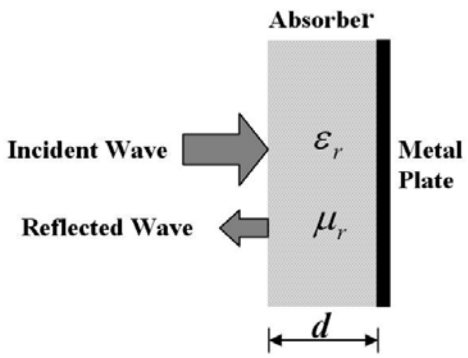

Fig. 4.1 The EM wave absorber

From the measured values of z, the frequency characteristics of material properties are calculated in terms of the following expression:

$$z = \sqrt{\frac{\mu_r}{\varepsilon_r}} \tanh(j\frac{2\pi}{\lambda}\sqrt{\varepsilon_r \mu_r}d) \quad (4.2)$$

where λ is the wavelength, d is the thickness of the sample, μ_r is the complex relative permeability, and ε_r is the complex relative permittivity. The reflectionless condition for normal incidence of an electromagnetic wave is given by

$$\sqrt{\frac{\mu_r}{\varepsilon_r}} \tanh(j\frac{2\pi}{\lambda}\sqrt{\varepsilon_r \mu_r}d) = 1 \quad (4.3)$$

If the EM wave absorber is designed in a rectangular waveguide as shown in Fig. 4.2, TE_{10} mode is the only propagating mode in waveguide region [38], and the normalized input impedance is expressed as [22]

$$z = \mu_r \sqrt{\frac{1-(\lambda/2a)^2}{\varepsilon_r \mu_r - (\lambda/2a)^2}} \tanh\left(j\frac{2\pi}{\lambda}\sqrt{\varepsilon_r \mu_r - (\lambda/2a)^2}\,d\right) \quad (4.4)$$

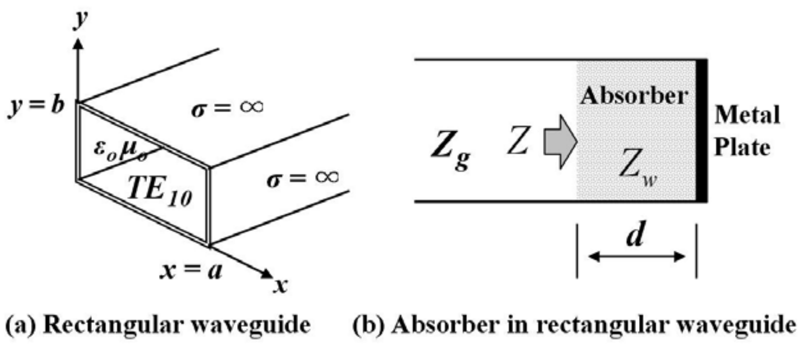

Fig. 4.2 Absorber in rectangular waveguide

where a is the x-direction length in the rectangular waveguide. The reflectionless condition for normal incidence of an electromagnetic wave is given by

$$\mu_r \sqrt{\frac{1-(\lambda/2a)^2}{\varepsilon_r\mu_r-(\lambda/2a)^2}} \tanh\left(j\frac{2\pi}{\lambda}\sqrt{\varepsilon_r\mu_r-(\lambda/2a)^2}\, d\right)=1 \tag{4.5}$$

Hence, if eq. (4.5) is solved, the relationship between the material properties (complex relative permittivity and permeability) and the sample thickness can be simulated. Further, it is possible to use eq. (4.1) for confirmation of the absorption abilities.

4.2 Single-layer Absorber

First, let us derive the expression of the reflection coefficient when a plane TE wave makes an oblique incidence with a single-layer absorber with thickness *d*. The coordinate system is defined as shown in Fig. 4.3. In usual wave absorbers, medium Ⅰ is considered a vacuum while medium Ⅱ is composed of homogeneous absorptive material backed with a metal plate. As shown in Fig. 4.3, the incident wave, forming an incident angle θ_i with the z axis, is reflected by a metal plate, while the outgoing of transmitted wave and the reflected wave coexist in medium Ⅱ. The following expressions are derived from Maxwell's equations [12].

The derivation is done here for TE waves, while it can be done similarly for TM waves.

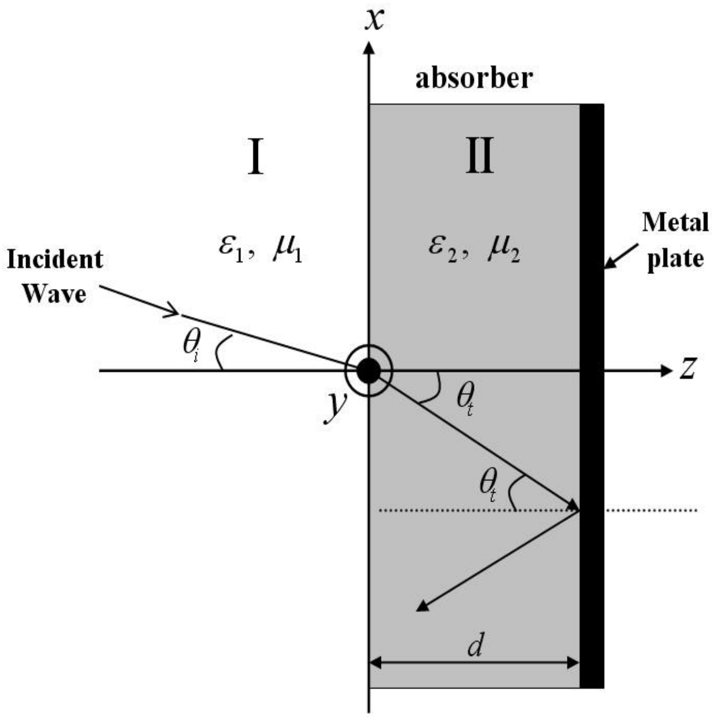

Fig. 4.3 Coordinate system for analysis of EM wave.

In TE waves, the electric and magnetic fields in each medium that satisfy the wave equation derived from Maxwell's equations are expressed as follows.

A. Medium Ⅰ:

$$E_{y1} = Ae^{[-j\gamma_1(z\cos\theta_i - x\sin\theta_i)]} + Be^{[j\gamma_1(z\cos\theta_r + x\sin\theta_r)]} \tag{4.6}$$

$$H_{x1} = -\frac{A\cos\theta_i}{Z_{c1}}e^{[-j\gamma_1(z\cos\theta_i - x\sin\theta_i)]} + \frac{B\cos\theta_r}{Z_{c1}}e^{[j\gamma_1(z\cos\theta_r + x\sin\theta_r)]} \tag{4.7}$$

B. Medium Ⅱ:

$$E_{y2} = Ce^{[-j\gamma_2(z\cos\theta_i^{'} - x\sin\theta_i^{'})]} + De^{[j\gamma_2(z\cos\theta_r^{'} + x\sin\theta_r^{'})]} \quad (4.8)$$

$$H_{x2} = -\frac{C\cos\theta_i^{'}}{Z_{c2}}e^{[-j\gamma_2(z\cos\theta_i^{'} - x\sin\theta_i^{'})]} + \frac{D\cos\theta_r^{'}}{Z_{c2}}e^{[j\gamma_2(z\cos\theta_r^{'} + x\sin\theta_r^{'})]} \quad (4.9)$$

Where $\theta_i^{'}$ and $\theta_r^{'}$ designate the mean incident angle and reflected angle at the surface of a metal plate in medium Ⅱ, reflectively, satisfying the relation $\theta_i^{'} = \theta_r^{'} = \theta_t$. We are imposing the following boundary conditions to expressions:

In $z = 0$,

$$E_{y1}\big|_{z=0} = E_{y2}\big|_{z=0} \quad (4.10)$$

$$H_{x1}\big|_{z=0} = H_{x2}\big|_{z=0} \quad (4.11)$$

In $z = d$,

$$E_{y2}\big|_{z=d} = 0 \quad (4.12)$$

Then we obtain the expression of the reflection coefficient:

$$\Gamma = \frac{z_{TE} - 1/\cos\theta_t}{z_{TE} + 1/\cos\theta_i} \qquad (4.13)$$

where

$$z_{TE} = \frac{\mu_{r2}}{\sqrt{\varepsilon_{r2}\mu_{r2} - \sin^2\theta_i}} \tanh\left(j\frac{2\pi}{\lambda}\sqrt{\varepsilon_{r2}\mu_{r2} - \sin^2\theta_i}\, d \right) \qquad (4.14)$$

And where ε_r and μ_r are the complex relative permittivity and permeability, respectively. The reflection coefficient $\Gamma = B/A$. In the course of this derivation, Snell's law has been used:

$$\frac{\sin\theta_t}{\sin\theta_i} = \frac{\gamma_1}{\gamma_2} \qquad (4.15)$$

In the case of normal incidence of the TE wave, we can obtain the reflection coefficient by putting $\theta_i = 0$. Then,

$$z = \sqrt{\frac{\mu_{r2}}{\varepsilon_{r2}}} \tanh\left(j\frac{2\pi}{\lambda}\sqrt{\varepsilon_{r2}\mu_{r2}}\, d \right) \qquad (4.16)$$

$$\Gamma = \frac{z-1}{z+1} \qquad (4.17)$$

Similarly, we can derive the reflection coefficient from a TM wave:

$$\Gamma = \frac{z_{TM} - \cos\theta_i}{z_{TM} + \cos\theta_i} \tag{4.18}$$

where

$$z_{TM} = \frac{\sqrt{\varepsilon_{r2}\mu_{r2} - \sin^2\theta_i}}{\varepsilon_{r2}} \tanh\left(j\frac{2\pi}{\lambda}\sqrt{\varepsilon_{r2}\mu_{r2} - \sin^2\theta_i}\, d \right) \tag{4.19}$$

4.3 Multi-layer absorber

4.3.1 Normal Incident Case

Next, let us consider how to derive the reflection coefficient of an absorber composed of different layers of material with different constants and different thicknesses for each layer. Figure 4.4 illustrates the configuration of the multi-layer absorber. Generally, this type absorber can exhibit broadband absorption ability or broadband matching characteristic. In Fig. 4.4, the incident wave propagates from the left side to the right and goes into the absorber with normal incidence.

In the *n*-th layer, the characteristic impedance and propagation constant are denoted by Z_{cn}, and γ_n, respectively. These expressions are given as follows:

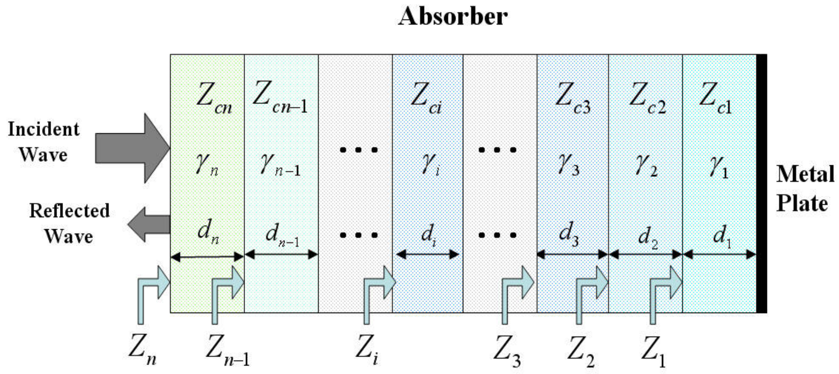

Fig. 4.4 Configuration of multi-layer absorber

$$Z_{cn} = Z_0\sqrt{\frac{\mu_{rn}}{\varepsilon_{rn}}} = Z_0\sqrt{\frac{\mu_{rn}^{'} - j\mu_{rn}^{''}}{\varepsilon_{rn}^{'} - j\varepsilon_{rn}^{''}}} \tag{4.20}$$

$$\gamma_n = j\frac{2\pi}{\lambda}\sqrt{\varepsilon_{rn}\mu_{rn}} = j\frac{2\pi}{\lambda}\sqrt{(\varepsilon_{rn}^{'} - j\varepsilon_{rn}^{''})(\mu_{rn}^{'} - j\mu_{rn}^{''})} \tag{4.21}$$

where ε_{rn} and μ_{rn} are the complex relative permittivity and permeability, respectively. The reflection coefficient in this case can be calculated from the following expression when the value of the input impedance Z_n at the front plane is obtained:

$$\Gamma = \frac{Z_n - Z_0}{Z_n + Z_0} \tag{4.22}$$

where $Z_0 = 120\pi$ ohms. Now, the value of Z_n is calculated using the input impedance Z_{n-1} in the n-1-th layer, where Z_{n-1} is expressed as the recurrence formula. To derive the recurrence formula Z_{n-1}, let us consider the expression of the input impedance Z_1 when looking into first layer at front face of metal plate. The expression Z_1 is denoted by the expression

$$Z_1 = Z_{C1} \tanh \gamma_1 d_1 = Z_{C1} \tanh\left(j \frac{2\pi}{\lambda} \sqrt{\varepsilon_{r1}\mu_{r1}} d_1 \right) \tag{4.23}$$

Since the input impedance looking into the *i*-1-th layer is denoted by Z_{i-1}, Z_i is expressed by the following recurrence formula using the characteristic impedance Z_{ci} in the *i*-th layer:

$$Z_i = Z_{ci} \frac{Z_{i-1} + Z_{ci} \tanh \gamma_i d_i}{Z_{ci} + Z_{i-1} \tanh \gamma_i d_i} \tag{4.24}$$

Note that this recurrence formula should be calculated from the side of a terminal metal plate. Then, calculating Z_i successively from the input impedance Z_1 looking into the first layer, we can obtain the value of Z_n. Hence, the reflection coefficient Γ is obtained by substituting the free-space impedance Z_0 and Z_n in eq. (4.22).

4.3.2 Oblique Incident Case

The recurrence formula (4.24) can be used also when the plane wave with an incident angle θ is obliquely transmitted to the multi-layer type absorber. However, the equations which calculate the characteristic impedance Z_{cn}, propagation constant γ_n, and reflection coefficient Γ of the *n*-th layer differ from the previous case, such as the following equations, depending on the TE wave or TM wave:

A. TE wave:

$$Z_{cn} = \frac{Z_0 \mu_{rn}}{\sqrt{\varepsilon_{rn}\mu_{rn} - \sin^2\theta}} \tag{4.25}$$

$$\gamma_n = j\frac{2\pi}{\lambda}\sqrt{\varepsilon_{rn}\mu_{rn} - \sin^2\theta} \tag{4.26}$$

$$\Gamma = \frac{Z_1 - Z_0/\cos\theta}{Z_1 + Z_0/\cos\theta} \tag{4.27}$$

B. TM wave:

$$Z_{cn} = \frac{Z_0\sqrt{\varepsilon_{rn}\mu_{rn} - \sin^2\theta}}{\varepsilon_{rn}} \tag{4.28}$$

$$\gamma_n = j\frac{2\pi}{\lambda}\sqrt{\varepsilon_{rn}\mu_{rn} - \sin^2\theta} \tag{4.29}$$

$$\Gamma = \frac{Z_1 - Z_0\cos\theta}{Z_1 + Z_0\cos\theta} \tag{4.30}$$

The reflection coefficient can be calculated from eqs. (4.27) and (4.30) if the recurrence formula (4.24) is calculated using the values of Z_{cn} and γ_n in each layer and if the input impedance Z_1 which looks into the absorber plane in the first layer is obtained.

Chapter 5
MATERIAL PROPERTIES

5.1 Introduction

The measurement of material properties is well-established in papers of Y. Naito and O. Hashimoto [21], [22]. Techniques have been developed to extract permittivity and permeability of materials from dc up to infrared frequency, but for a given situation, the preferred measurement technique is highly dependent on the frequency range of interest, the state of the material (i.e., solid, liquid, or gaseous), sample shape and size, the actual value and nature of its measurable property, and the accuracy desired [39].

Measurement techniques can be classified as narrowband and wideband. Narrowband techniques are characterized by measurements made at a small number of discrete frequencies at which the sample perturbs the resonance of a confined or open cavity. The observed change in the frequency and resonance width is related to the real and imaginary parts of the permittivity. Resonator methods determine loss very accurately and, therefore, yield the most accurate information about the imaginary part of the permittivity of low-loss samples. In wideband method, sample measurements are available over a frequency range limited only by the waveguide selected or the measuring instrument's frequency-generation and detection abilities. Wideband methods are required for a multitude of applications. Due to its relative simplicity, the transmission line method is presently a widely used wideband method technique [40].

The transmission line methods are also classified as one-port method and two-port method. One-port method is a reflection measurement which is taken on two short-circuited samples of lengths ℓ and 2ℓ. Two-port method is a technique that require both reflection and transmission measurements.

The waveguide sample holder has the advantage that the rectangular shape makes the sample easy to form. However, the frequency coverage is restricted by the high pass characteristic of the waveguide. The coaxial fixture provides wide frequency coverage, although it is much more difficult to form the sample into the appropriate shape so that the sample completely fills the area between the inner and outer conductor in the beadless air line structure [41].

5.2 Measurement Techniques of Material Properties

5.2.1 One Port Method

In the one-port method, reflection measurements are taken on two short-circuited samples of lengths ℓ and $n\ell$, where n is any integer >1. Integer n is small for lossy samples and large for low-loss samples. Thus, this technique encompasses a wider range of material characteristics than previous methods, which rely on a single sample length.

One-port method as shown in Fig. 5.1 requires reflection measurements only on short circuits with samples of lengths ℓ or 2ℓ.

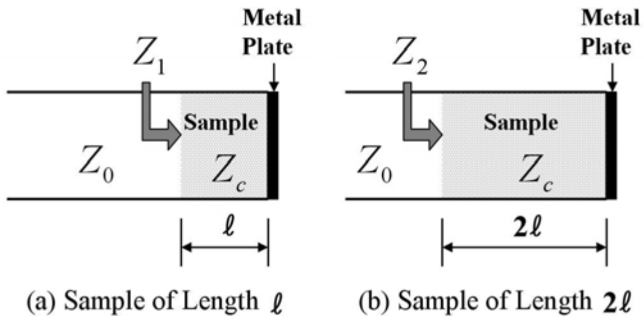

Fig. 5.1 One-port method using short circuits with samples of lengths ℓ or 2ℓ.

Within the region of sample, the characteristic impedance normalized to Z_0 and propagation constant are obtained as follows:

$$z_c = \sqrt{\frac{\mu_r}{\varepsilon_r}} \tag{5.1}$$

$$\gamma = j\frac{2\pi}{\lambda}\sqrt{\varepsilon_r \mu_r} \tag{5.2}$$

where, ε_r and μ_r are the complex relative permittivity and permeability, respectively, of sample.

From eqs. (5.1) and (5.2), the complex relative permittivity and permeability can be written:

$$\varepsilon_r = -j\frac{\lambda}{2\pi}\frac{\gamma}{z_c} \tag{5.3}$$

$$\mu_r = -j\frac{\lambda}{2\pi} z_c \gamma \tag{5.4}$$

In Fig. 5.1, z_1 and z_2 are the input impedances normalized to Z_0, corresponding to sample lengths ℓ or 2ℓ, respectively, as follows:

$$z_1 = z_c \tanh \gamma \ell \tag{5.5}$$

$$z_2 = z_c \tanh \gamma 2\ell \tag{5.6}$$

From characteristics of tanh, eq. (5.6) can be written as

$$z_2 = \frac{2z_2}{1+\tanh^2 \gamma \ell} \tag{5.7}$$

Using eqs. (5.6) and (5.7) then gives

$$\tanh \gamma \ell = \sqrt{\frac{2z_1 - z_2}{z_2}} \tag{5.8}$$

and

$$\gamma = \frac{1}{\ell} \tanh^{-1} \sqrt{\frac{2z_1 - z_2}{z_2}} \tag{5.9}$$

From eqs. (5.5) and (5.8), the normalized characteristic impedance z_c is obtained as follow:

$$z_c = z_1 \sqrt{\frac{z_2}{2z_1 - z_2}} \tag{5.10}$$

Using eqs. (5.9) and (5.10) in eqs. (5.3) or (5.4), respectively, the normalized characteristic impedance and propagation constant allow us to solve for the complex relative permittivity and permeability

5.2.2 Two Port Method

The original idea for computation of complex permittivity and permeability from S-parameter data was suggested by Nicolson and Ross for their time domain measurement of dielectric materials. In the ideal case, consider the sample material installed in 50-ohm(Z_0) air line as shown in Fig. 5.2.

Assuming no source and load mismatched, then eq. (5.11) through eq. (5.16) describe the electromagnetic relationships in each region of Fig. 5.2.

In $\ell \le 0$,

$$V_1 = V_1^+ e^{-j\gamma_0 \ell} + V_1^- e^{j\gamma_0 \ell} \tag{5.11}$$

$$I_1 = \frac{1}{Z_0}(V_1^+ e^{-j\gamma_0 \ell} - V_1^- e^{j\gamma_0 \ell}) \tag{5.12}$$

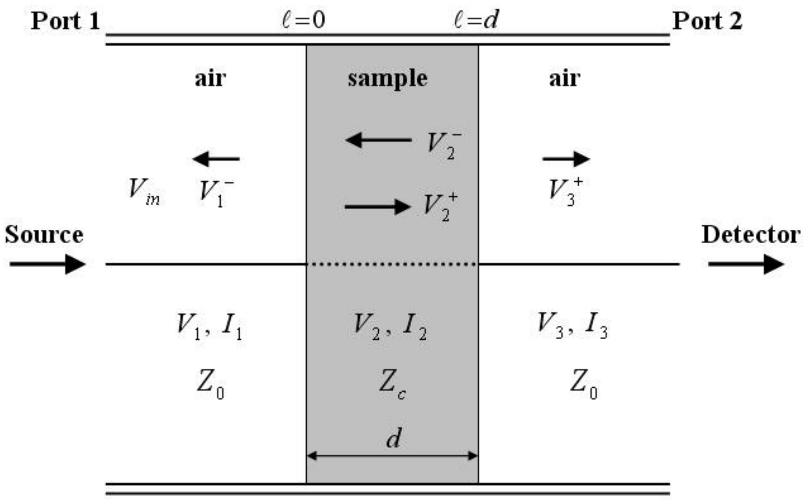

Fig. 5.2 Two-port method using air line with filled material

In $0 \le \ell \le d$,

$$V_2 = V_2^+ e^{-j\gamma\ell} + V_2^- e^{j\gamma\ell} \tag{5.13}$$

$$I_2 = \frac{1}{Z_c}(V_2^+ e^{-j\gamma\ell} - V_2^- e^{j\gamma\ell}) \tag{5.14}$$

In $\ell \ge d$,

$$V_3 = V_3^+ e^{-j\gamma_0(\ell-d)} \tag{5.15}$$

$$I_1 = \frac{1}{Z_0}(V_3^+ e^{-j\gamma_0(\ell-d)}) \tag{5.16}$$

The boundary conditions for Fig. 5.2 are:

$$
\begin{aligned}
V_1 &= V_2 \quad && at \quad \ell = 0 \\
I_1 &= I_2 \quad && at \quad \ell = 0 \\
V_2 &= V_3 \quad && at \quad \ell = d \\
I_2 &= I_3 \quad && at \quad \ell = d
\end{aligned} \tag{5.17}
$$

From eq. (5.11) through eq. (5.17), the reflection coefficient Γ and transmission coefficient T can be written:

$$\Gamma = K \pm \sqrt{K^2 - 1} \tag{5.18}$$

where,

$$K = \frac{\{S_{11}^2(\omega) - S_{21}^2(\omega)\} + 1}{2S_{11}(\omega)}$$

$$T = \frac{\{S_{11}(\omega) + S_{21}(\omega)\} - \Gamma}{1 - \{S_{11}(\omega) + S_{21}(\omega)\}\Gamma} \tag{5.19}$$

When the length of materials is infinite $(\ell = \infty)$, the reflection coefficient Γ between Z_0 and Z_c is obtained as follow:

$$\Gamma = \frac{Z_c - Z_0}{Z_c + Z_0} = \frac{\sqrt{\mu_r / \varepsilon_r} - 1}{\sqrt{\mu_r / \varepsilon_r} + 1} \tag{5.20}$$

The transmission coefficient T in the materials of finite length can be written:

$$T = e^{-j\omega\sqrt{\mu\varepsilon}d} = e^{-j\frac{\omega}{c}\sqrt{\mu_r\varepsilon_r}d} \tag{5.21}$$

From eqs. (5.20) and (5.21) we can define X and Y as follows:

$$\frac{\mu_r}{\varepsilon_r} = \left(\frac{1+\Gamma}{1-\Gamma}\right)^2 = X \tag{5.22}$$

$$\mu_r\varepsilon_r = -\left\{\frac{c}{\omega d}\ln\left(\frac{1}{T}\right)\right\}^2 = Y \tag{5.23}$$

then,

$$\mu_r = \sqrt{XY} \tag{5.24}$$

$$\varepsilon_r = \sqrt{\frac{Y}{X}} \tag{5.25}$$

For measurements using the waveguide sample holder, the eqs. (5.22) and (5.23) can be written as follows:

$$\frac{1}{\Lambda^2} = \left(\frac{\varepsilon_r\mu_r}{\lambda_0^2} - \frac{1}{\lambda_c^2}\right) = \left\{\frac{1}{2\pi d}\ln\left(\frac{1}{T}\right)\right\}^2 \tag{5.26}$$

where,

$$\mathrm{Re}\left(\frac{1}{\Lambda}\right) = \frac{1}{\lambda_g} \tag{5.27}$$

$$\mu_r = \frac{1+\Gamma}{\Lambda(1-\Gamma)\sqrt{\dfrac{1}{\lambda_0^2} - \dfrac{1}{\lambda_c^2}}} \tag{5.28}$$

$$\varepsilon_r = \frac{\left(\dfrac{1}{\Lambda^2} + \dfrac{1}{\lambda_c^2}\right)\lambda_0^2}{\mu_r} \tag{5.29}$$

where, λ_0 and λ_c are free-space wavelength and cutoff wavelength of the waveguide, respectively.

Equations (5.28) and (5.29) are also applicable to measurements using the coaxial sample holder, where $\lambda_c = \infty$.

5.3 Manufacturing Process of Absorber

We fabricated some samples in different composition ratio of absorbing materials such as Carbon Black, TiO_2, and Permalloy with chlorinated polyethylene (CPE) as shown in Table 5.1. Absorbing materials were mixed with the binder of CPE, and the sheet-type absorber was fabricated by using an open roller. The open roller's surface temperature was uniform during sample preparation because the surface temperature affects the EM wave properties of sheet type absorbers [42]. The manufacturing process of absorber is shown in Fig. 5.3. Figure 5.4 shows a photo of absorber samples containing Carbon, TiO_2, and Permalloy with CPE.

Table 5.1 Composition ratios of absorbing materials with a binder.

Type	Material	Binder	Composition ratio
Conductive material	Carbon Black	CPE	Carbon : CPE = 10 : 90 wt.%
			Carbon : CPE = 20 : 80 wt.%
			Carbon : CPE = 30 : 70 wt.%
			Carbon : CPE = 40 : 60 wt.%
			Carbon : CPE = 50 : 50 wt.%
Dielectric material	TiO_2	CPE	TiO_2 : CPE = 40 : 60 wt.%
			TiO_2 : CPE = 50 : 50 wt.%
			TiO_2 : CPE = 60 : 40 wt.%
			TiO_2 : CPE = 70 : 30 wt.%
			TiO_2 : CPE = 80 : 20 wt.%
Magnetic material	Permalloy	CPE	Permalloy : CPE = 40 : 60 wt.%
			Permalloy : CPE = 50 : 50 wt.%
			Permalloy : CPE = 60 : 40 wt.%
			Permalloy : CPE = 70 : 30 wt.%

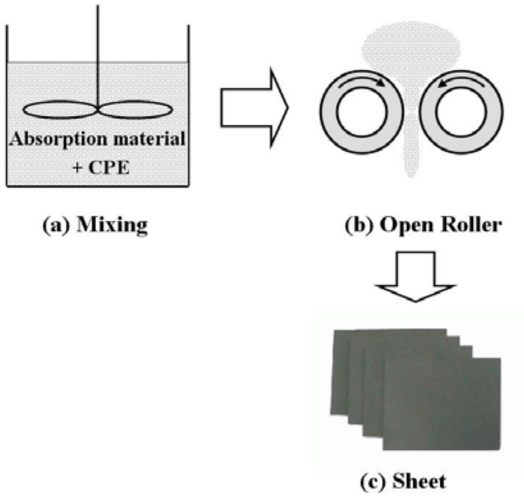

Fig. 5.3 Manufacturing process of absorber

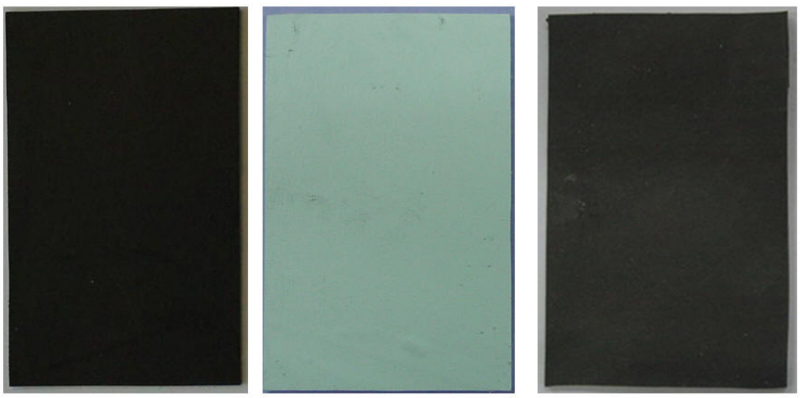

Fig. 5.4 A photo of absorber samples containing Carbon, TiO2, and Permalloy with CPE.

5.4 Measured Material Properties

One-port method which is taken on two short-circuited samples of lengths ℓ and 2ℓ is used to measure material properties such as the complex relative permittivity and permeability. Reflection coefficient of the samples can be obtained from S_{11} after critical calibration of an ANRITSU ME 78080A broadband vector network analyzer.

The measurement system is shown in Fig. 5.5. Figure 5.6 presents a photo of absorber, jig, and sample. The dimensions of the samples for measurement of the complex relative permittivity and permeability were 2.54×1.27×1.5 mm and 2.54×1.27×3 mm.

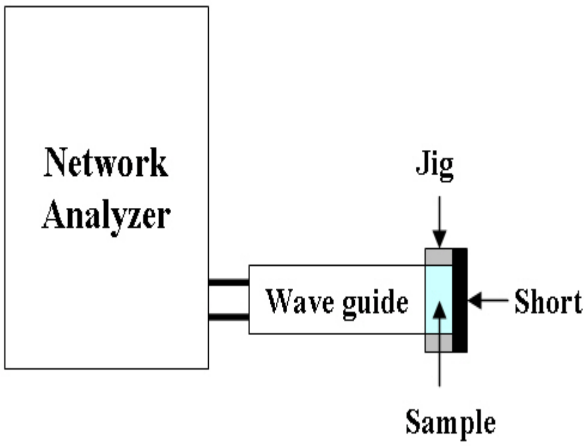

Fig. 5.5 Measurement system.

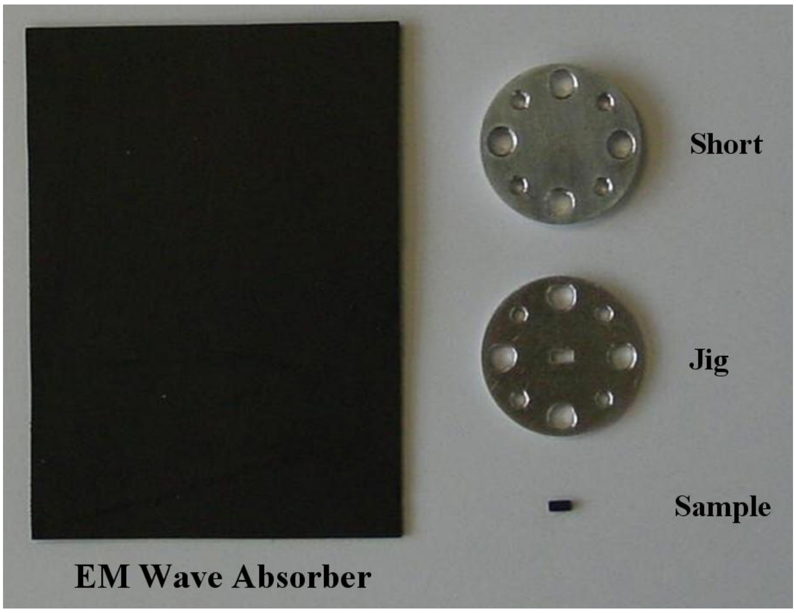

Fig. 5.6 A photo of the absorber, test jig, and sample.

5.4.1 Samples Using Carbon

The complex relative permittivity of samples containing different composition ratios of Carbon and CPE is calculated in the frequency range of 65-110 GHz by using measured S-parameters.

Figures 5.7 - 5.11 present plots of the real and imaginary parts of permittivity as a function of frequency for samples. As the frequency increases, the real parts of permittivity decrease, but the imaginary parts of permittivity show nearly constant.

The EM wave absorption ability of dielectric materials is related with the dielectric loss tangent, $\tan\delta_e = \varepsilon_r'' / \varepsilon_r'$, and the dielectric loss is strong for $\tan\delta_e \geq 1$. In Figs. 5.7 – 5.11, the samples containing 20 wt.% and 30 wt.% Carbon have a large dielectric loss tangent.

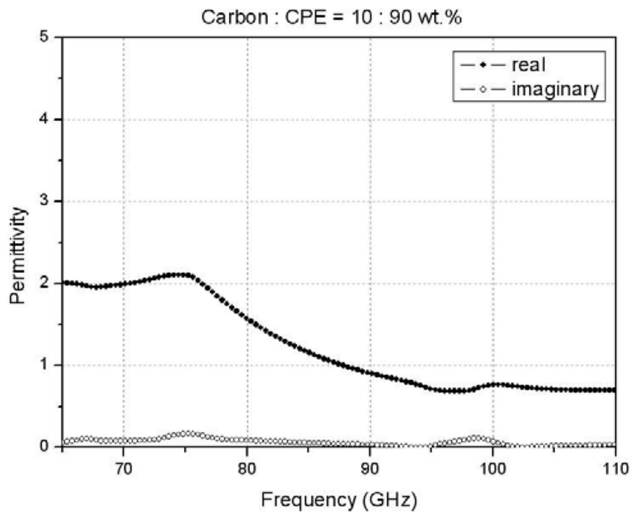

Fig. 5.7 Frequency dependence on complex relative permittivity of the sample containing Carbon:CPE=10:90 wt.%.

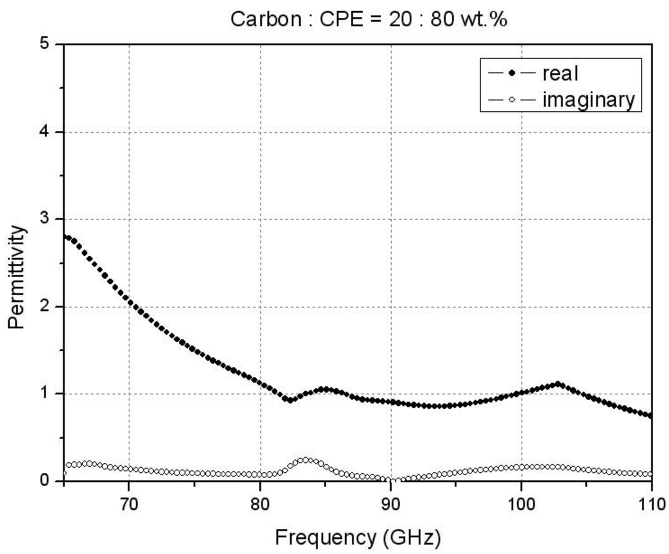

Fig. 5.8 Frequency dependence on complex relative permittivity of the sample containing Carbon:CPE=20:80 wt.%.

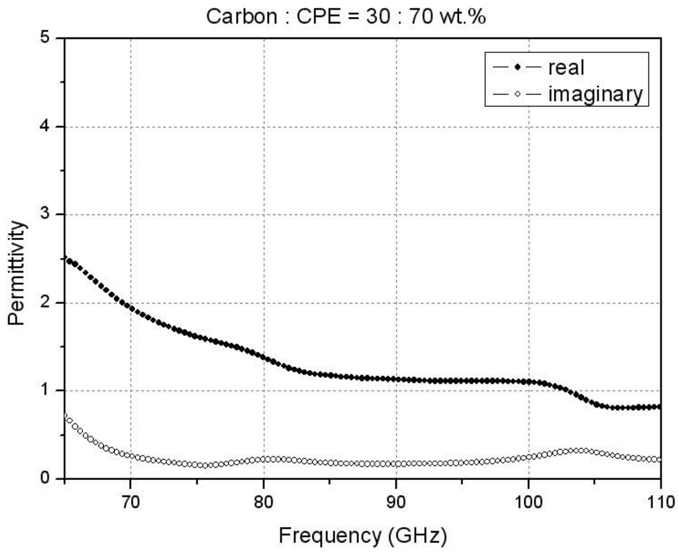

Fig. 5.9 Frequency dependence on complex relative permittivity of the sample containing Carbon:CPE=30:70 wt.%.

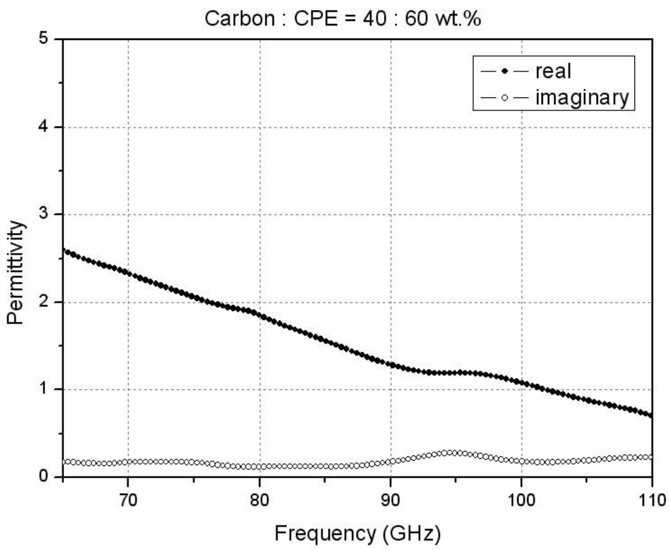

Fig. 5.10 Frequency dependence on complex relative permittivity of the sample containing Carbon:CPE=40:60 wt.%.

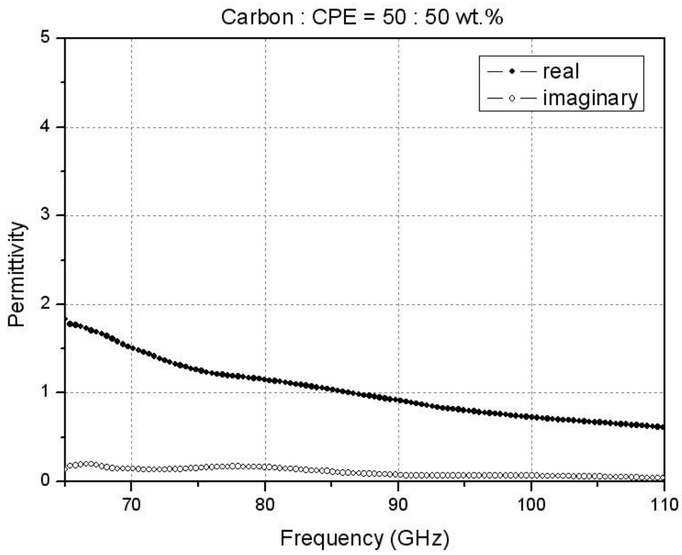

Fig. 5.11 Frequency dependence on complex relative permittivity of the sample containing Carbon:CPE=50:50 wt.%.

5.4.2 Samples Using TiO_2

The complex relative permittivity of samples containing different composition ratios of TiO_2 and CPE is calculated in the frequency range of 65-110 GHz by using measured S-parameters.

Figures 5.12 - 5.16 present plots of the real and imaginary parts of permittivity as a function of frequency for samples. As the frequency increases, the real parts of permittivity decrease. The sample containing TiO_2 : CPE = 70 : 30 wt.% has a maximum value in the imaginary part of permittivity.

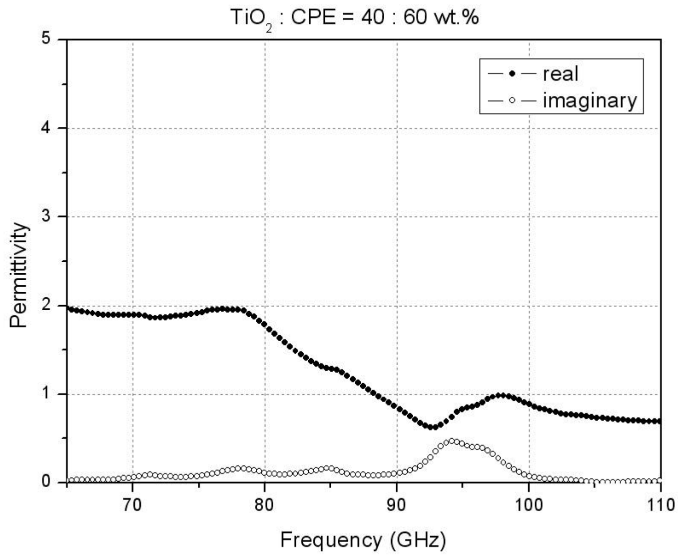

Fig. 5.12 Frequency dependence on complex relative permittivity of the sample containing TiO_2:CPE=40:60 wt.%.

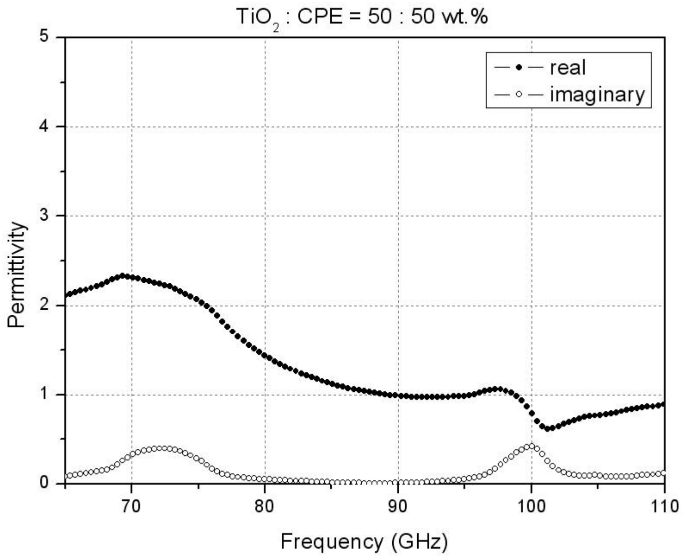

Fig. 5.13 Frequency dependence on complex relative permittivity of the sample containing TiO_2:CPE=50:50 wt.%.

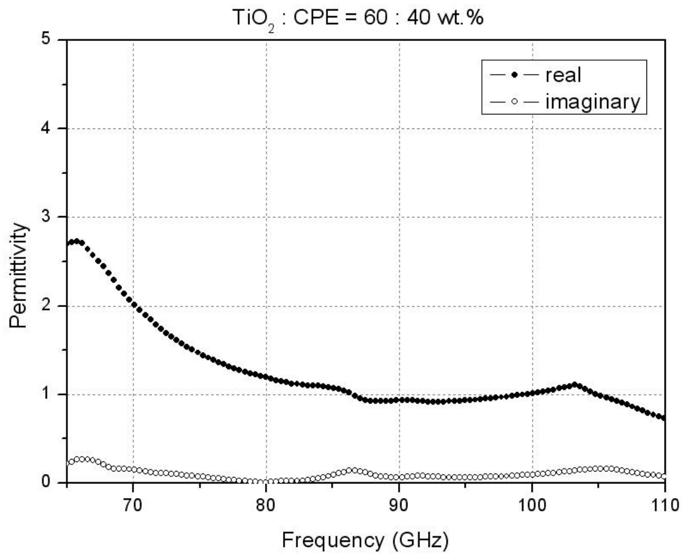

Fig. 5.14 Frequency dependence on complex relative permittivity of the sample containing TiO_2:CPE=60:40 wt.%.

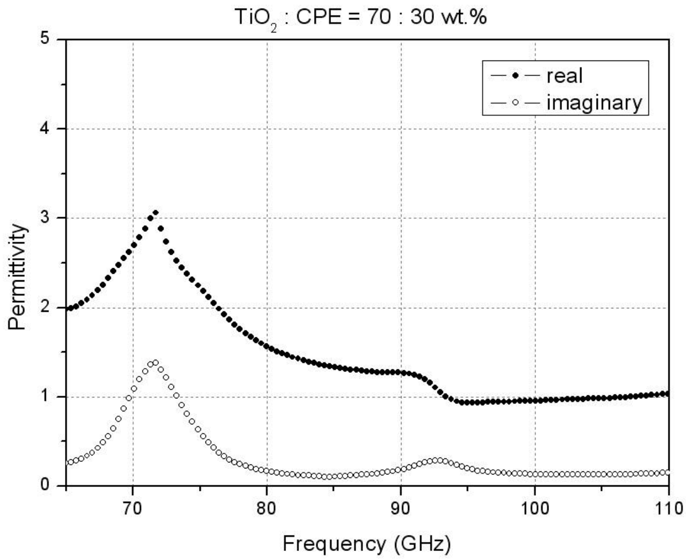

Fig. 5.15 Frequency dependence on complex relative permittivity of the sample containing TiO_2:CPE=70:30 wt.%.

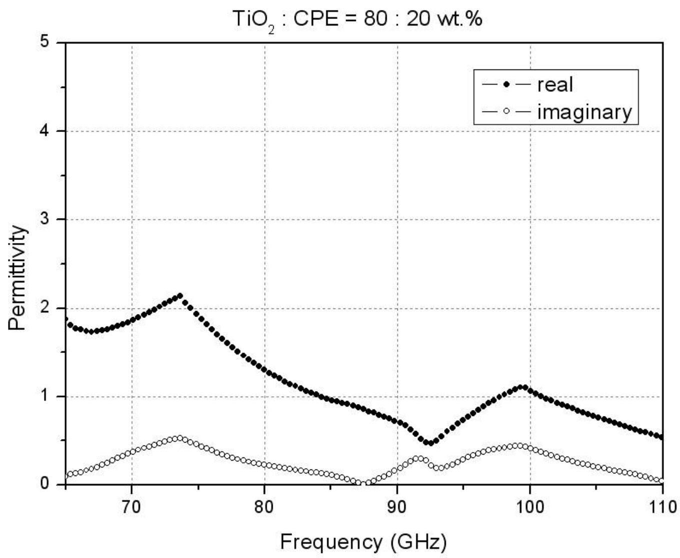

Fig. 5.16 Frequency dependence on complex relative permittivity of the sample containing TiO_2:CPE=80:20 wt.%.

5.4.3 Samples Using Permalloy

The complex relative permittivity and permeability of samples containing different composition ratios of Permalloy and CPE is calculated in the frequency range of 65-110 GHz by using measured S-parameters.

Figures 5.17 - 5.24 present plots of the real and imaginary parts of permittivity and permeability, respectively, as a function of frequency for samples. As the frequency increases, the real parts and imaginary parts of permittivity decrease, but the real and imaginary parts of permeability show nearly constant, less than 1, in frequency range for 65 – 110 GHz. The high frequency permittivity of samples decreases due to the eddy current loss induced by EM waves.

As is well known, magnetic properties no longer contribute much to performance at higher frequencies. However, Permalloy has a very low conductivity, and the EM properties of CPE such as a binder are considered at a frequency higher than 40 GHz. Therefore, these samples are based on the dielectric or conductor loss.

The sample containing Permalloy : CPE = 70 : 30 wt.% has a maximum value in the imaginary part of permittivity and permeability.

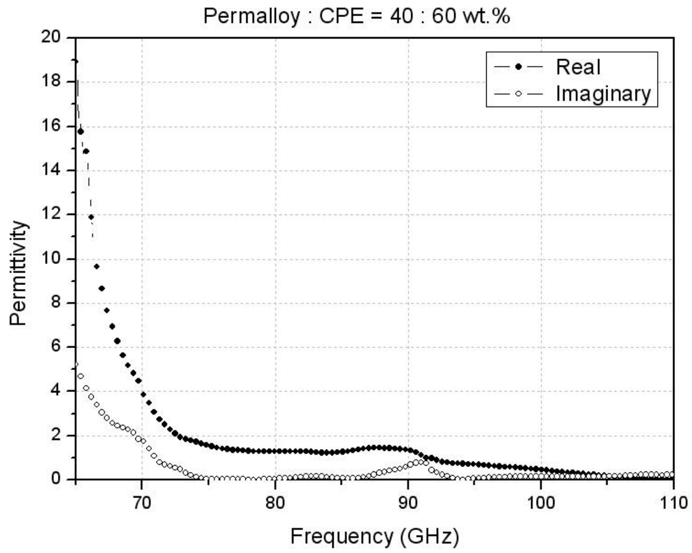

Fig. 5.17 Frequency dependence on complex relative permittivity of the sample containing Permalloy:CPE=40:60 wt.%.

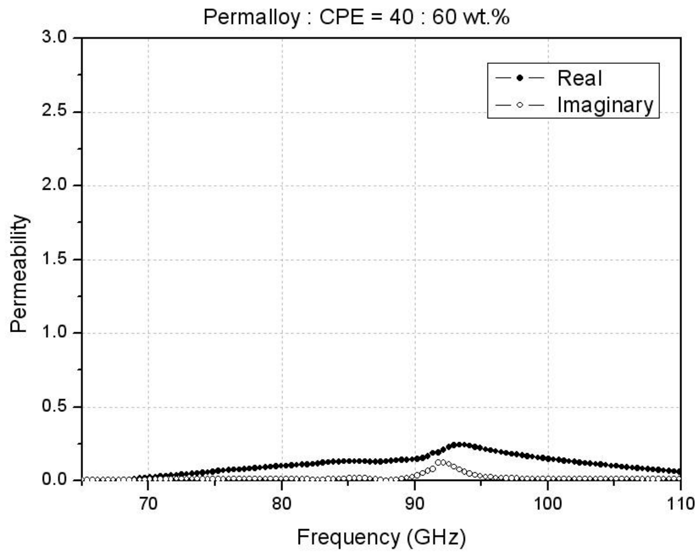

Fig. 5.18 Frequency dependence on complex relative permeability of the sample containing Permalloy:CPE=40:60 wt.%.

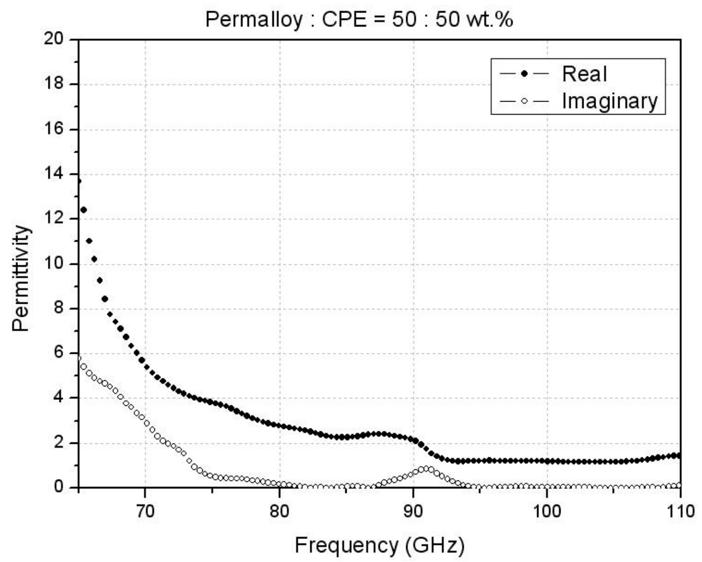

Fig. 5.19 Frequency dependence on complex relative permittivity of the sample containing Permalloy:CPE=50:50 wt.%.

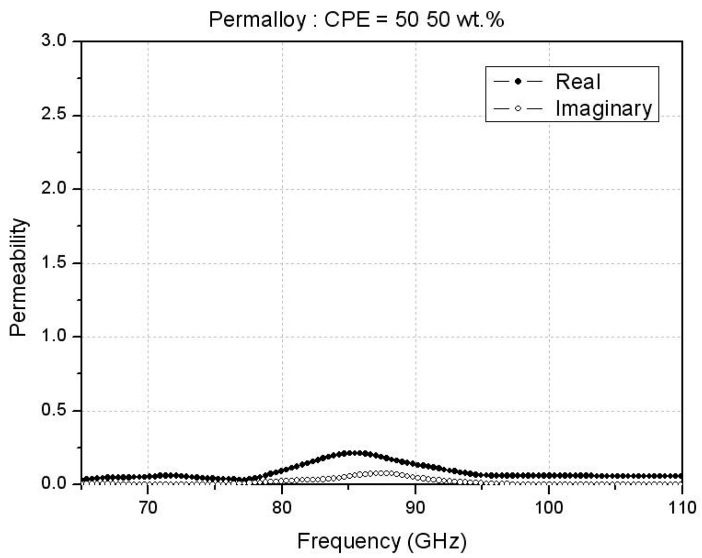

Fig. 5.20 Frequency dependence on complex relative permeability of the sample containing Permalloy:CPE=50:50 wt.%.

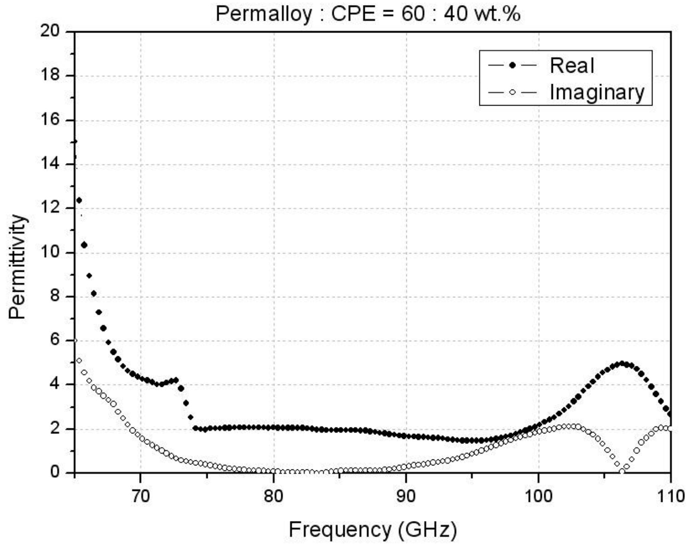

Fig. 5.21 Frequency dependence on complex relative permittivity of the sample containing Permalloy:CPE=60:40 wt.%.

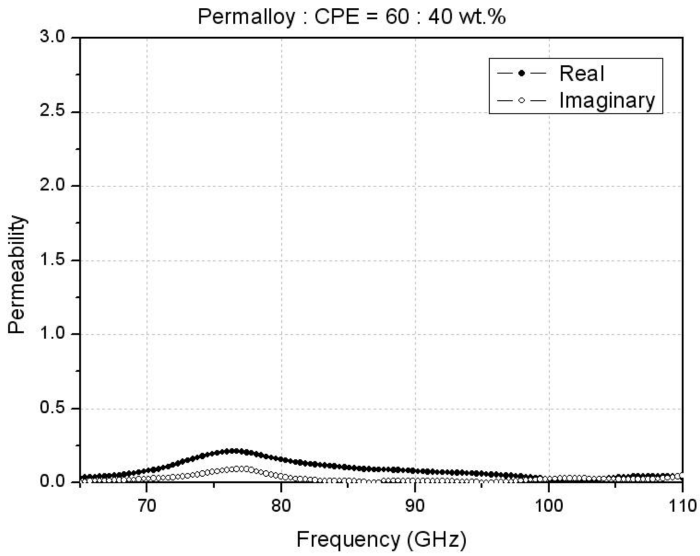

Fig. 5.22 Frequency dependence on complex relative permeability of the sample containing Permalloy:CPE=60:40 wt.%.

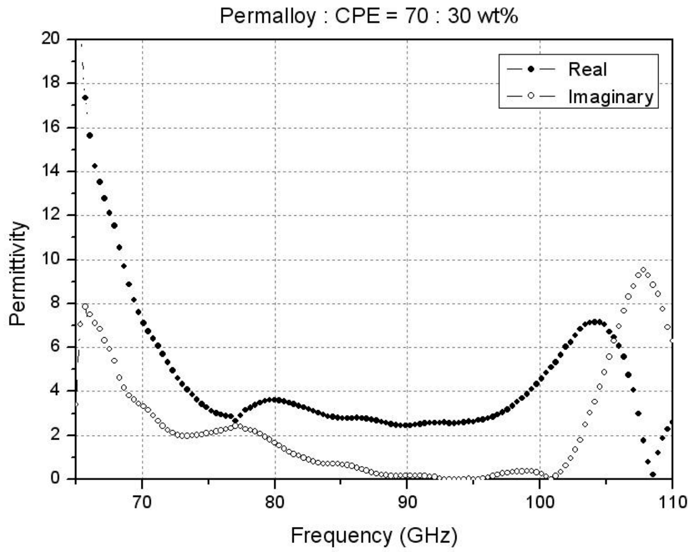

Fig. 5.23 Frequency dependence on complex relative permittivity of the sample containing Permalloy:CPE=70:30 wt.%.

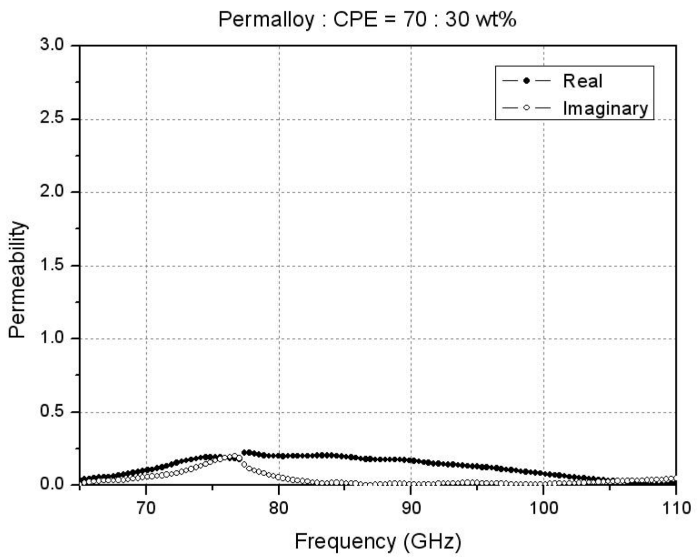

Fig. 5.24 Frequency dependence on complex relative permeability of the sample containing Permalloy:CPE=70:30 wt.%.

5.5 SEM Photographs

5.5.1 Samples Using Carbon

The scanning electron microscope (SEM) photographs of samples containing Carbon Black with CPE are presented in Fig. 5.25, and shows that all carbon particles were mixed with the binder and that the number air holes decreased with increasing composition ratio.

5.5.2 Samples Using TiO_2

The SEM photographs of samples containing TiO_2 with CPE are presented in Fig. 5.26, and shows that all TiO_2 particles were mixed with the binder and that the number air holes decreased with increasing composition ratio.

5.5.3 Samples Using Permalloy

The SEM photographs of samples containing Permalloy with CPE are presented in Fig. 5.27, and shows that all Permalloy particles were mixed with the binder and that the number air holes decreased with increasing composition ratio.

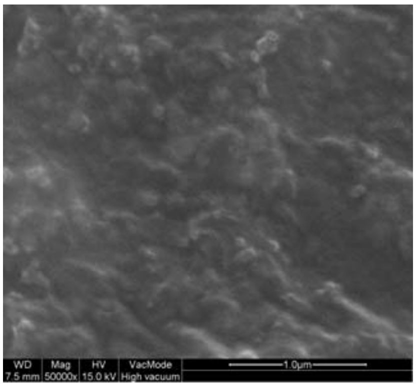

(a) Carbon : CPE = 10 : 90 wt.%

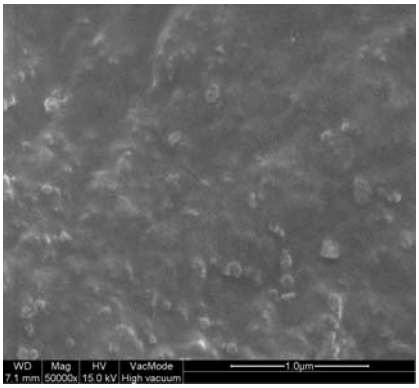

(b) Carbon : CPE = 20 : 80 wt.%

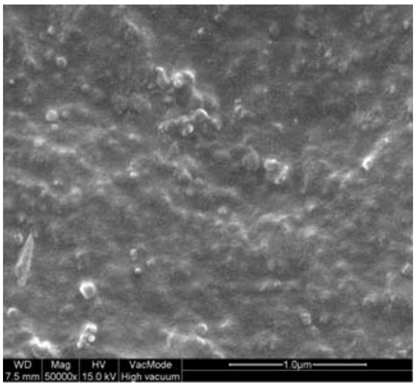

(c) Carbon : CPE = 30 : 70 wt.%

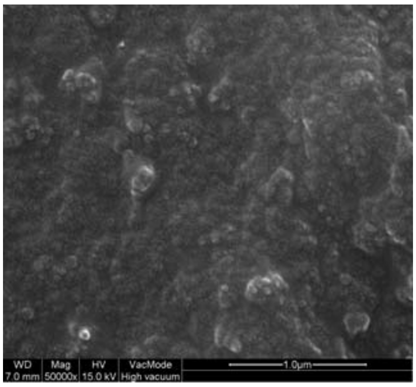

(d) Carbon : CPE = 40 : 60 wt.%

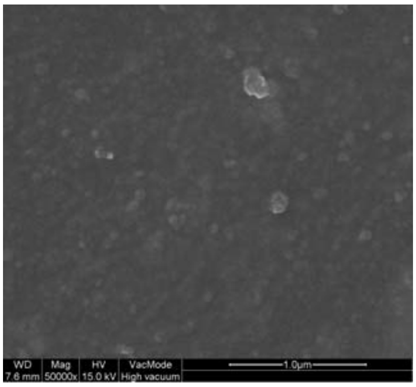

(e) Carbon : CPE = 50 : 50 wt.%

Fig. 5.25 The SEM photographs of samples containing different composition ratios of Carbon with CPE.

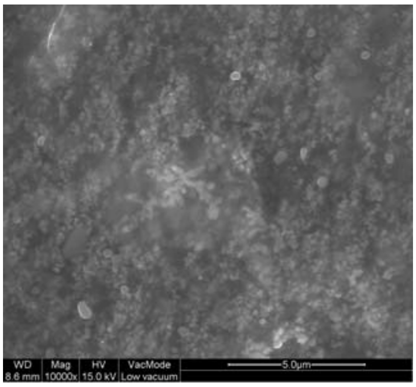

(a) TiO_2 : CPE = 40 : 60 wt.%

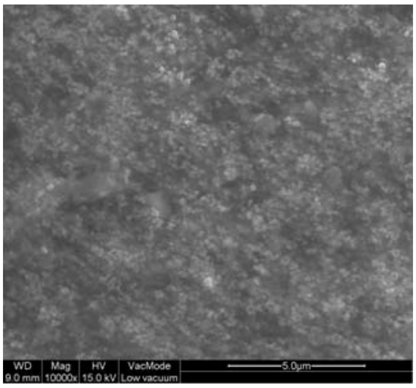

(b) TiO_2 : CPE = 50 : 50 wt.%

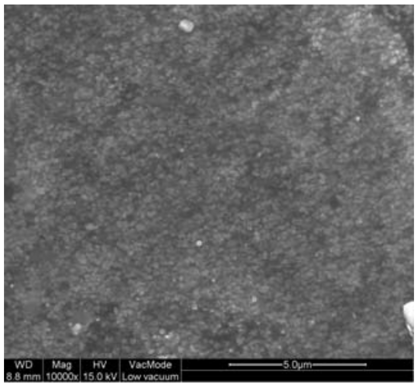

(c) TiO_2 : CPE = 60 : 40 wt.%

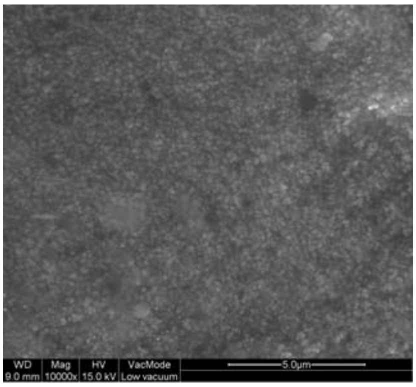

(d) TiO_2 : CPE = 70 : 30 wt.%

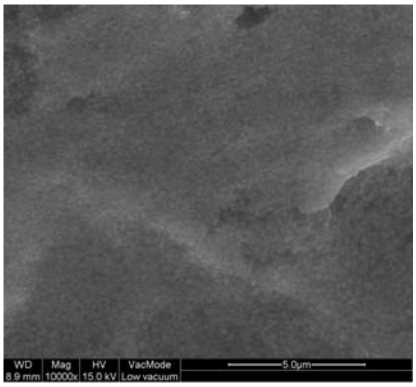

(e) TiO_2 : CPE = 80 : 20 wt.%

Fig. 5.26 The SEM photographs of samples containing different composition ratios of TiO_2 with CPE.

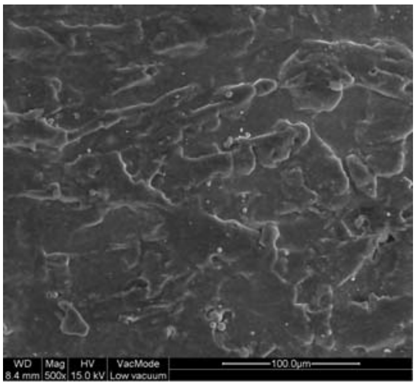

(a) Permalloy : CPE = 40 : 60 wt.%

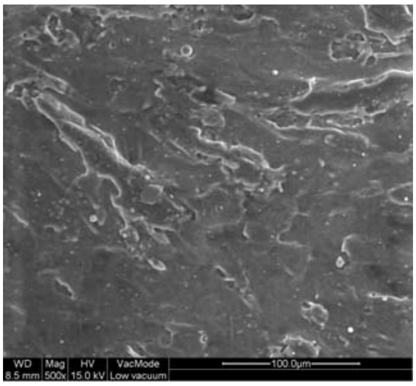

(b) Permalloy : CPE = 50 : 50 wt.%

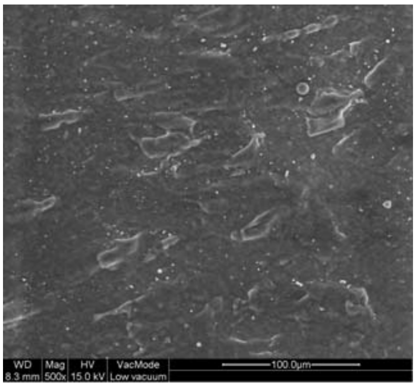

(c) Permalloy : CPE = 60 : 40 wt.%

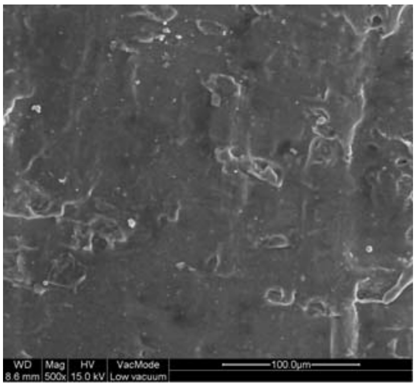

(b) Permalloy : CPE = 70 : 30 wt.%

Fig. 5.27 The SEM photographs of samples containing different composition ratios of Permalloy with CPE.

Chapter 6
ABSORPTION ABILITY

6.1 Introduction

In development of EM wave absorber, it is very important to evaluating absorption ability of absorber sample. The evaluation methods will be discussed in this chapter. The evaluation methods of absorption ability are usually used two-type methods. One is the transmission line method and the other is the free space method.

The transmission line methods are also compact enough to fit on a laboratory bench, which makes them convenient to use and easy to operate. But, because the construction of most finished absorber products is ill-suited for insertion into small coaxial lines or waveguides, the free space methods are used as a nondestructive evaluation. And the free space methods are closely simulated as free space conditions. The transmission line methods and the free space methods are described in Section 6.2 and 6.3, respectively. And Section 6.4 and 6.5 show the simulated absorption ability and measured absorption ability, respectively, of the fabricated absorbers.

In this research, the rectangular waveguide as a transmission line method is used for evaluating the fabricated absorbers.

6.2 Measurement Techniques of Absorption Ability

6.2.1 Transmission Line Method

The transmission line is a basic device used to measure the electromagnetic properties of materials because the theory of wave propagation within the line is well understood and RF energy is confined within the system. A sample holder, a short section of transmission line, is loaded with a test sample machined to fit the line, and the reflection of RF energy from it, or the transmission of RF energy through it, or both, are measured as shown in Fig. 6.1.

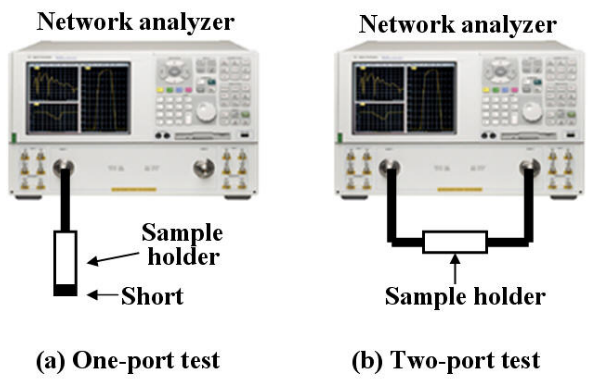

Fig. 6.1 S-parameter test set containing sample holder

The coaxial line (a TEM transmission line) is more convenient to use than the rectangular waveguide if the frequencies of interest cover more than an octave. This is because waves propagating in the coaxial line do not suffer the cutoff phenomenon. The coaxial line is usually used in the frequency range from 50 MHz to 10 GHz. The rectangular waveguide is often used between 10 GHz and 100 GHz. The coaxial line demands a washer-shaped test specimen whereas the test specimen needed for the rectangular waveguide is simply a slab, as illustrated in Fig. 6.2. The samples may be as thick as can be conveniently handled and measured, but in many cases they are machined to a thickness of $\lambda/8$ to minimize the possibility of generating undesired modes within the sample.

The samples should be fabricated to fit snugly within the sample holder, making good contact with all conducting surface, which sometimes complicates the design of the sample holder. Good contact is generally assured if the samples fit snugly in the holder without deformation, sometimes a difficult requirement to satisfy when the test material is soft or rubbery.

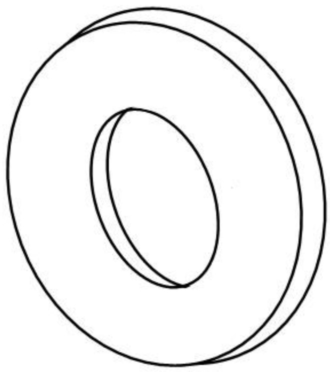

(a) A sample for coaxial

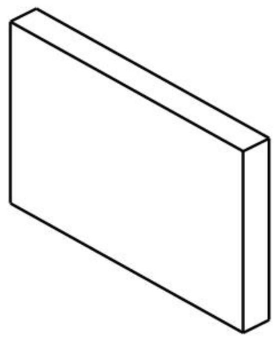

(b) A sample for rectangular waveguide

Fig. 6.2 Test samples for sample holder such as coaxial and rectangular waveguide.

6.2.2 Free Space Method

In contrast to the measurement of intrinsic material properties, the evaluation of absorbers for quality control or product development demands fewer measurements and less manipulation of test data and can often be accomplished with less sophisticated equipment. In the interest of economy, moreover, the nondestructive evaluation is required. And even if absorber samples can be sacrificed for the fabrication of test specimens for transmission line testing, the construction of most finished absorber products is ill-suited for insertion into small coaxial lines or waveguides. Therefore, the relative simplicity of free-space testing is attractive.

Usually, two free-space methods for absorber testing are the NRL arch method and the RCS method. Although these are labeled free-space methods, the label refers only to the fact that the test panel is not installed in a waveguide or transmission line.

NRL arch method has been developed at the Massachusetts Institute of Technology in the 1940s. The arch is a model of simplicity. As shown in Fig. 6.3, it is vertical semicircular framework, often made of plywood, which allows a pair of small horns to be aimed at a test panel at a constant distance. The horns are mounted in carriages that can be clamped anywhere along the arch, making it possible to measure samples at virtually any desired bistatic angle. The two horns cannot be brought any closer than the width of one horn aperture, making pure monostatic measurements impossible. Nevertheless, the residual bistatic angle was small enough in most cases that the test results were very good indications of monostatic absorber performance.

Because the arch antennas are situated at best a few feet from the test sample, the phase fronts incident on, it are spherical. To evaluate absorber samples under the more realistic conditions, measurement is used for the flatter phase fronts available in compact ranges or conventional RCS ranges. As shown in Fig. 6.4, this method of mounting the sample is easy to implement, and it exposes both the absorber-covered front face and the bare rear face of the backing plate to the radar once in every revolution for the support column. As such, the measurement is self-calibrating, because the specular echo seen from the back side becomes the reference by which the specular echo from the front side may be compared. The test panel used in the RCS method of absorber evaluations should probably be at least 5λ along a side at the lowest frequency used in the measurements but no larger than 25λ at the highest frequency. In the RCS method, by contrast, free-space conditions are closely simulated.

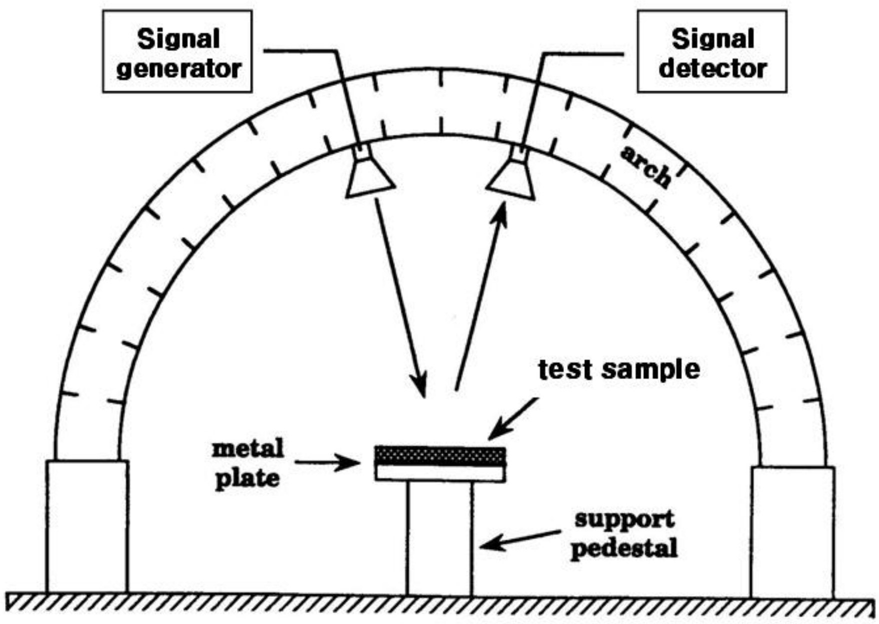

Fig. 6.3 The classic NRL arch.

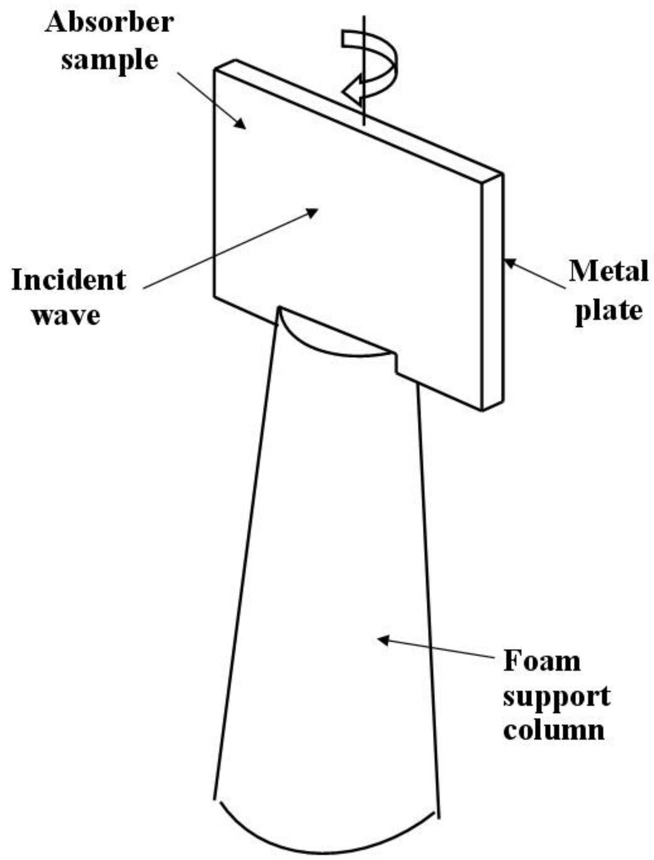

Fig. 6.4 The test panel used in the RCS method.

6.3 Simulated Absorption Ability

6.3.1 Absorber Using Carbon

Figure 6.5 shows the composition ratio dependence on the measured reflection coefficient as a function of frequency. It is shown that the absorption ability has a tendency to increase from 10 wt.% to 20 wt.% and decrease from 30 wt.% to 50 wt.% of Carbon. Moreover, note that the maximum absorption ability of sample containing Carbon 10 wt.% is about 2.8 dB at 103 GHz, the maximum absorption ability of sample containing Carbon 20 wt.% is about 11 dB at 82 GHz, the maximum absorption ability of sample containing carbon 30 wt.% is about 12.5 dB at 109 GHz, the maximum absorption ability of sample containing Carbon 40 wt.% is about 9.5 dB at 104 GHz, and the maximum absorption ability of sample containing Carbon 50 wt.% is about 5.5 dB at 85 GHz. As a result, the optimum composition ratio of Carbon is about 20 wt.% or 30 wt.%.

Absorption abilities of the EM wave absorbers are simulated using the measured complex relative permittivity by changing the thickness without changing the composition. The optimized result of sample containing Carbon:CPE=20:80 wt.% has a thickness of 2 mm and absorption ability higher than 20 dB in frequency range of 76-77 GHz as shown in Fig. 6.6. The optimized result of sample containing Carbon:CPE=30:70 wt.% has a thickness of 0.7 mm and absorption ability higher than 22 dB at 94 GHz as shown in Fig. 6.7.

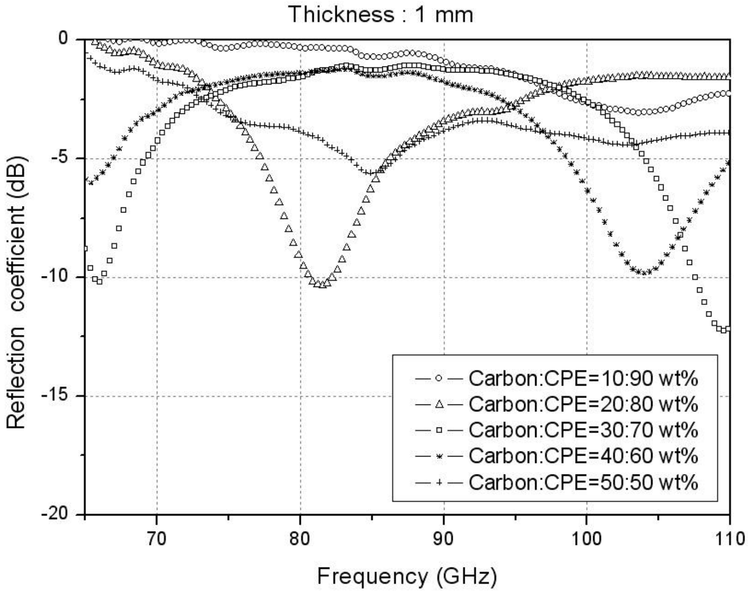

Fig. 6.5 Reflection coefficients of 1 mm samples with different composition ratios of Carbon and CPE.

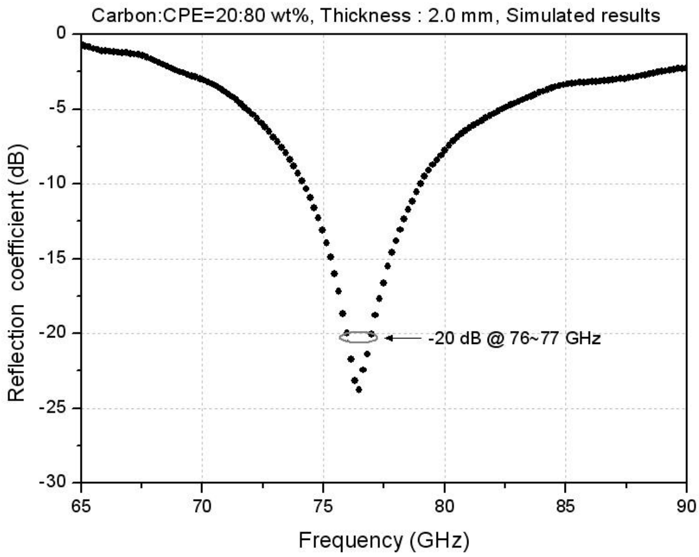

Fig. 6.6 Simulated reflection coefficient of 2 mm sample containing Carbon:CPE=20:80 wt.% in frequency range of 76-77 GHz.

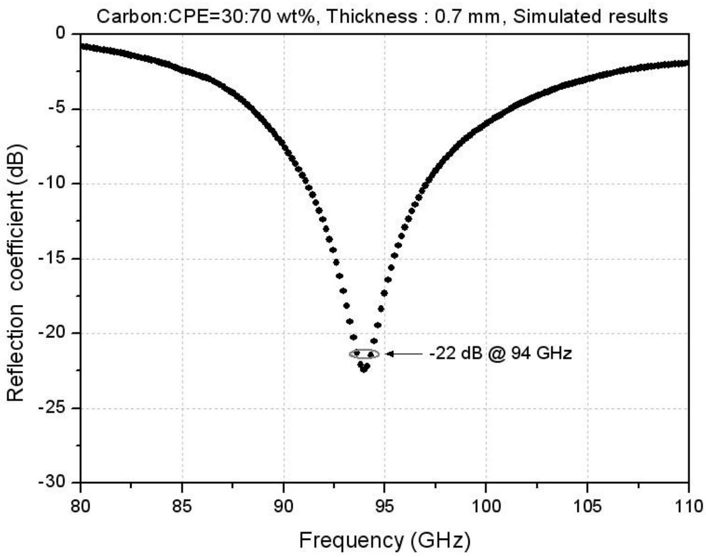

Fig. 6.7 Simulated reflection coefficient of 0.7 mm sample containing Carbon:CPE=30:70 wt.% at 94 GHz.

6.3.2 Absorber Using TiO_2

Figure 6.8 shows the composition ratio dependence on the measured reflection coefficient as a function of frequency. It is shown that the absorption ability has a tendency to increase from 40 wt.% to 70 wt.% and decrease from 70 wt.% to 80 wt.% of TiO_2. Moreover, note that the maximum absorption ability of sample containing TiO_2 40 wt.% is about 3 dB at 79 GHz, the maximum absorption ability of sample containing TiO_2 50 wt.% is about 7 dB at 108 GHz, the maximum absorption ability of sample containing TiO_2 60 wt.% is about 11 dB at 65 GHz, the maximum absorption ability of sample containing TiO_2 70 wt.% is about 32 dB at 87 GHz, and the maximum absorption ability of sample containing TiO_2 80 wt.% is about 12 dB at 72 GHz. As a result, the optimum composition ratio of TiO_2 is about 70 wt.%.

Absorption abilities of the EM wave absorbers are simulated using the measured complex relative permittivity by changing the thickness without changing the composition. The optimized result of sample containing TiO_2:CPE=70:30 wt.% has a thickness of 1.85 mm and absorption ability higher than 20 dB in frequency range of 76-77 GHz as shown in Fig. 6.9. The optimized result of sample containing TiO_2:CPE=70:30 wt.% has a thickness of 1.45 mm and absorption ability higher than 25 dB at 94 GHz as shown in Fig. 6.10.

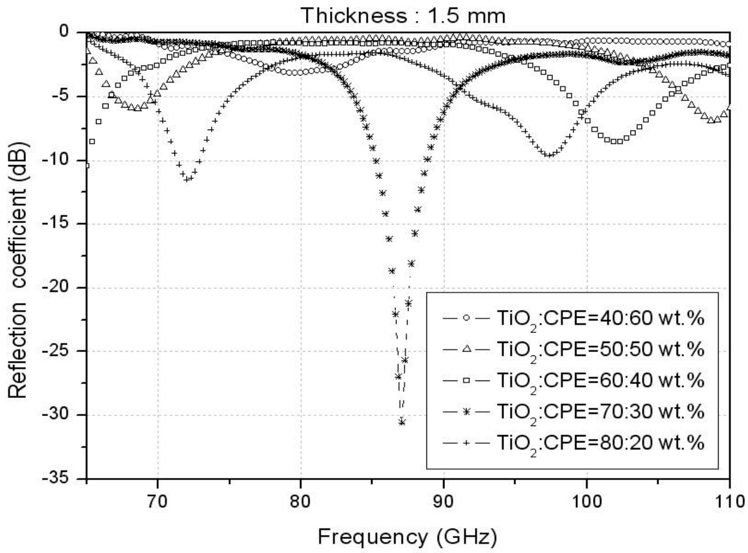

Fig. 6.8 Reflection coefficients of 1.5 mm samples with different composition ratios of TiO_2 and CPE.

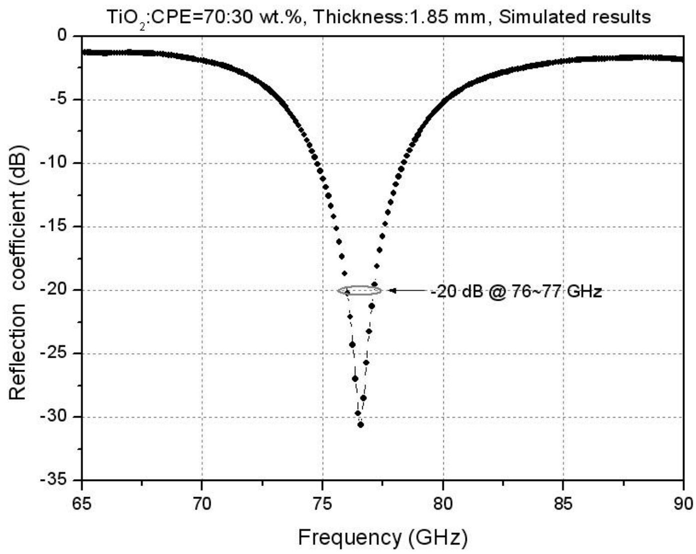

Fig. 6.9 Simulated reflection coefficient of 1.85 mm sample containing TiO_2:CPE=70:30 wt.% in frequency range of 76-77 GHz

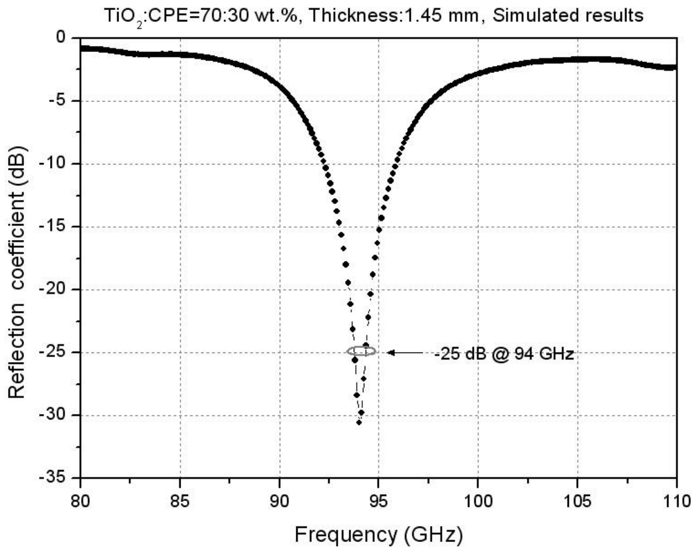

Fig. 6.10 Simulated reflection coefficient of 1.45 mm sample containing TiO_2:CPE=70:30 wt.% at 94 GHz.

6.3.3 Absorber Using Permalloy

Figure 6.8 shows the composition ratio dependence on the measured reflection coefficient as a function of frequency. It is shown that the absorption ability has a tendency to increase with increasing the composition ratio of Permalloy. Moreover, note that the maximum absorption ability of sample containing Permalloy 40 wt.% is about 4.5 dB at 92 GHz, the maximum absorption ability of sample containing Permalloy 50 wt.% is about 10 dB at 76 GHz, the maximum absorption ability of sample containing Permalloy 60 wt.% is about 16 dB at 74.5 GHz, and the maximum absorption ability of sample containing Permalloy 70 wt.% is about 25 dB at 74.5 GHz. As a result, the optimum composition ratio of Permalloy is about 70 wt.%.

Absorption abilities of the EM wave absorbers are simulated using the measured complex relative permittivity and permeability by changing the thickness without changing the composition. The optimized result of sample containing Permalloy:CPE=70:30 wt.% has a thickness of 1.4 mm and absorption ability higher than 22 dB in frequency range of 76-77 GHz as shown in Fig. 6.12. The optimized result of sample containing Permalloy:CPE=70:30 wt.% has a thickness of 1.15 mm and absorption ability higher than 20 dB at 94 GHz as shown in Fig. 6.13.

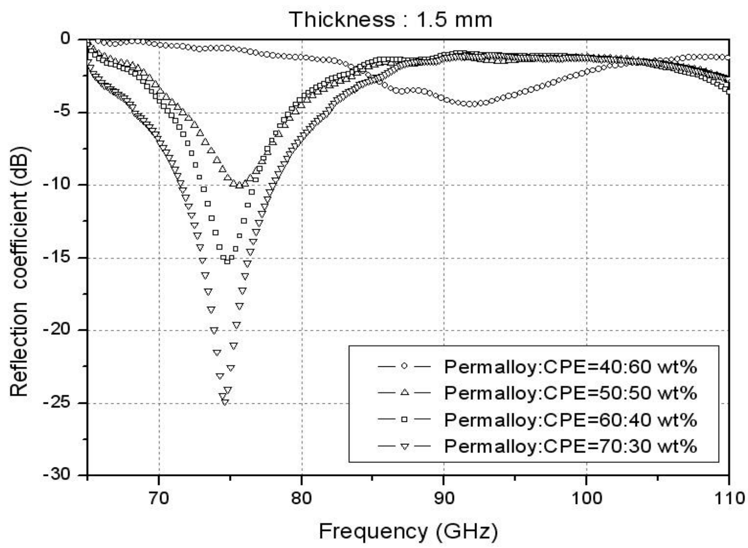

Fig. 6.11 Reflection coefficients of 1.5 mm samples with different composition ratios of Permalloy and CPE.

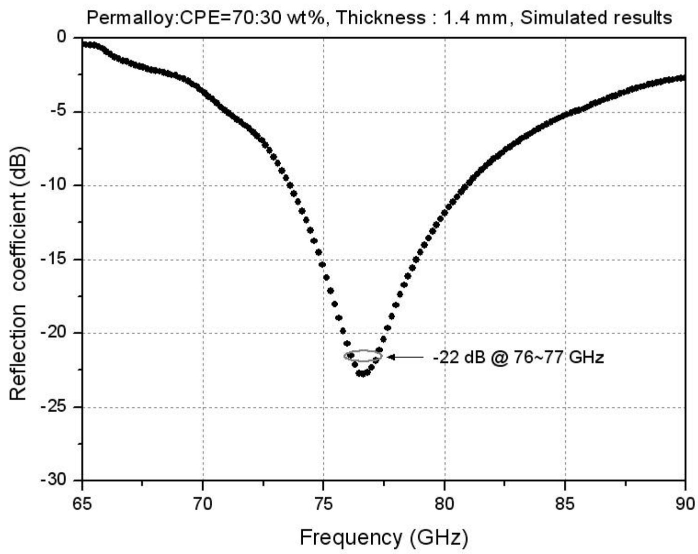

Fig. 6.12 Simulated reflection coefficient of 1.4 mm sample containing Permalloy:CPE=70:30 wt.% in frequency range of 76-77 GHz

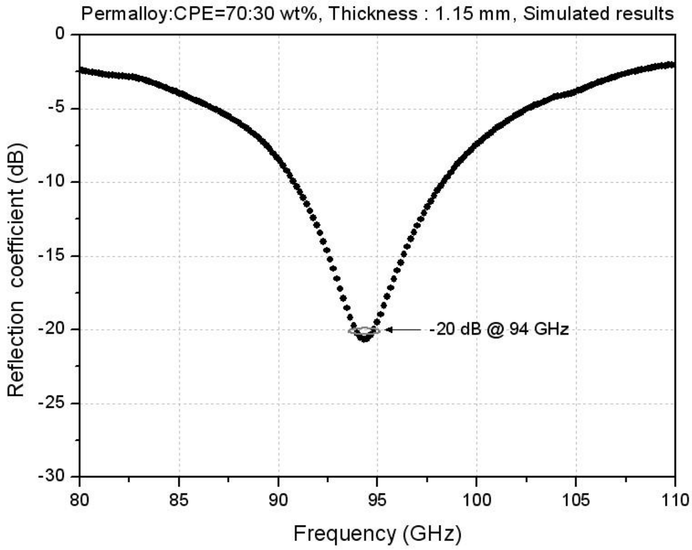

Fig. 6.13 Simulated reflection coefficient of 1.15 mm sample containing Permalloy:CPE=70:30 wt.% at 94 GHz.

6.4 Measured Absorption Ability

6.4.1 Absorber Using Carbon

Figures 6.14-6.17 plot the reflection coefficients of samples containing difference composition ratio of Carbon with changing thickness. The absorption ability has a tendency to increase from 10 wt.% to 20 wt.% and decrease from 30 wt.% to 50 wt.% of Carbon. As a result, the absorption ability of the sample containing Carbon:CPE= 20:80 wt.% has a maximum value in frequency range of 65-110 GHz.

The EM wave absorbers were fabricated based on the simulated designs. The fabricated EM wave absorber containing Carbon:CPE= 20:80 wt.% has a thickness of 2 mm and absorption ability higher than 20 dB in frequency range of 76-77 GHz as shown in Fig. 6.19. The fabricated EM wave absorber containing Carbon:CPE=30:70 wt.% has a thickness of 0.7 mm and absorption ability higher than 24 dB at 94 GHz as shown in Fig. 6.20. The simulated and measured results agree very well as shown in Figs. 6.19 and 6.20.

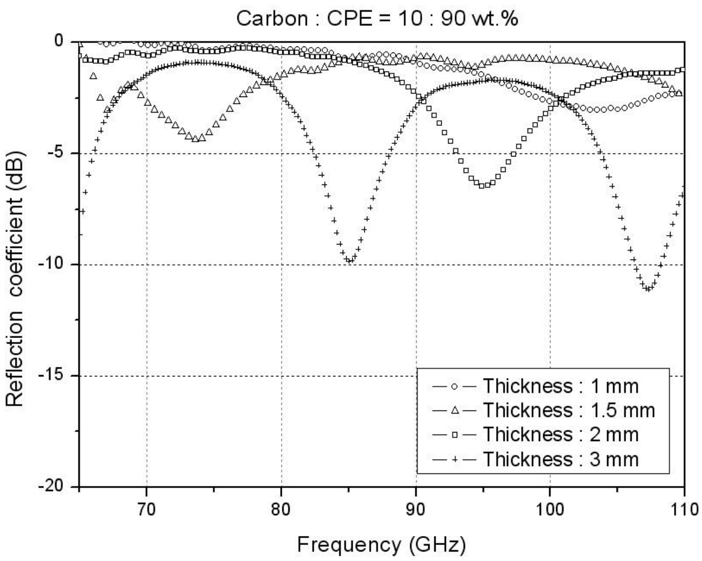

Fig. 6.14 Reflection coefficients of samples containing Carbon:CPE=10:90 wt.% at several thicknesses.

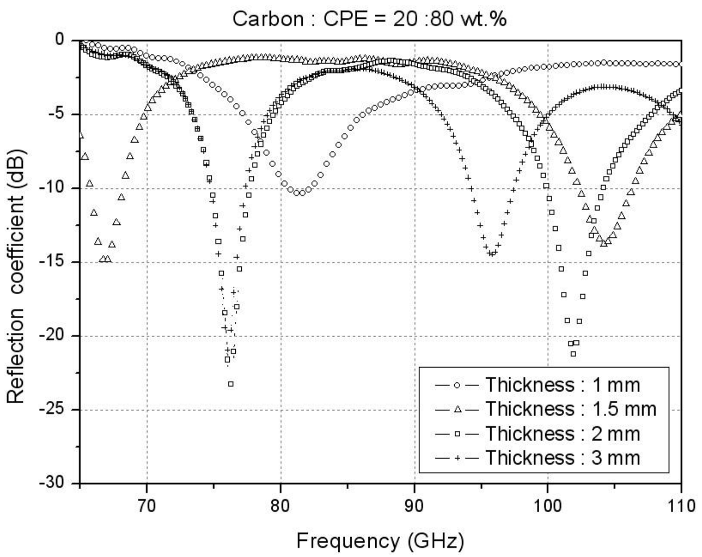

Fig. 6.15 Reflection coefficients of samples containing Carbon:CPE=20:80 wt.% at several thicknesses.

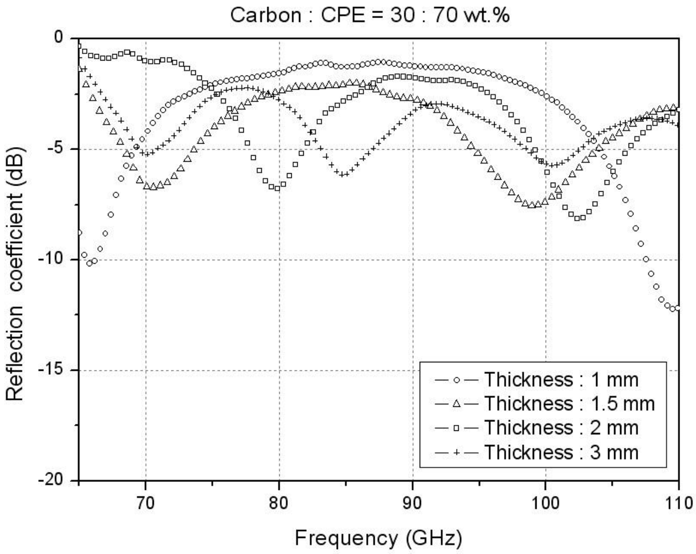

Fig. 6.16 Reflection coefficients of samples containing Carbon:CPE=30:70 wt.% at several thicknesses.

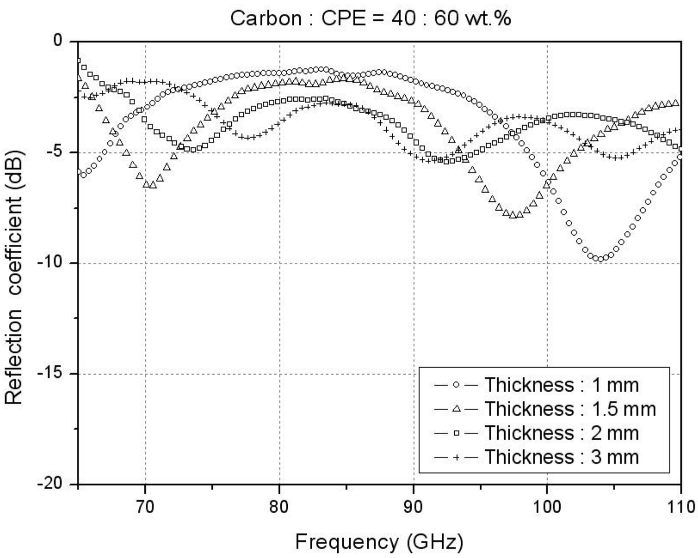

Fig. 6.17 Reflection coefficients of samples containing Carbon:CPE=40:60 wt.% at several thicknesses.

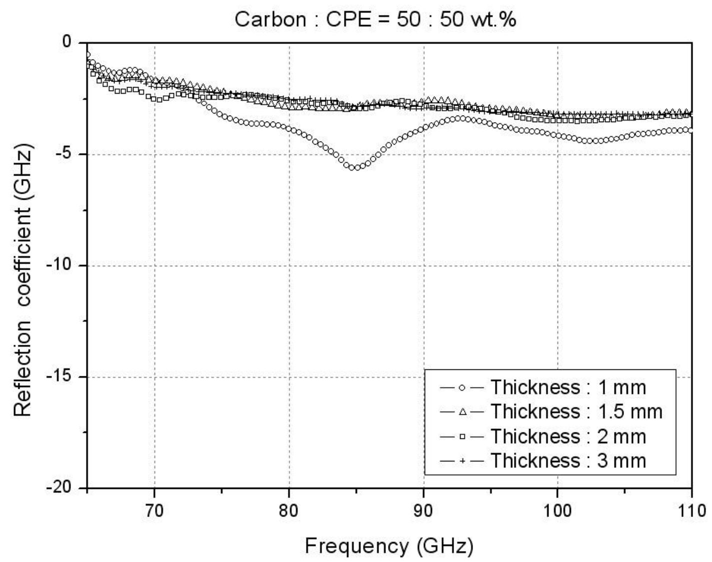

Fig. 6.18 Reflection coefficients of samples containing Carbon:CPE=50:50 wt.% at several thicknesses.

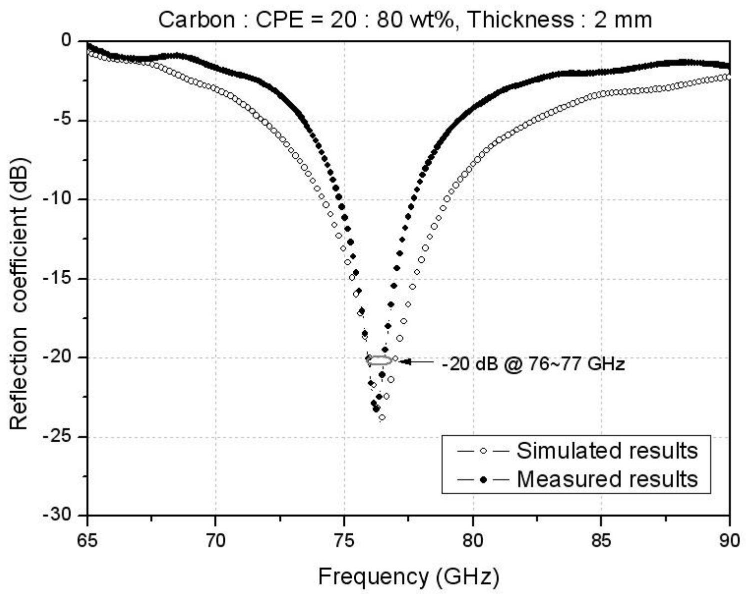

Fig. 6.19 Simulated and measured reflection coefficients of 2 mm sample containing Carbon:CPE=20:80 wt.% in frequency range of 76-77 GHz

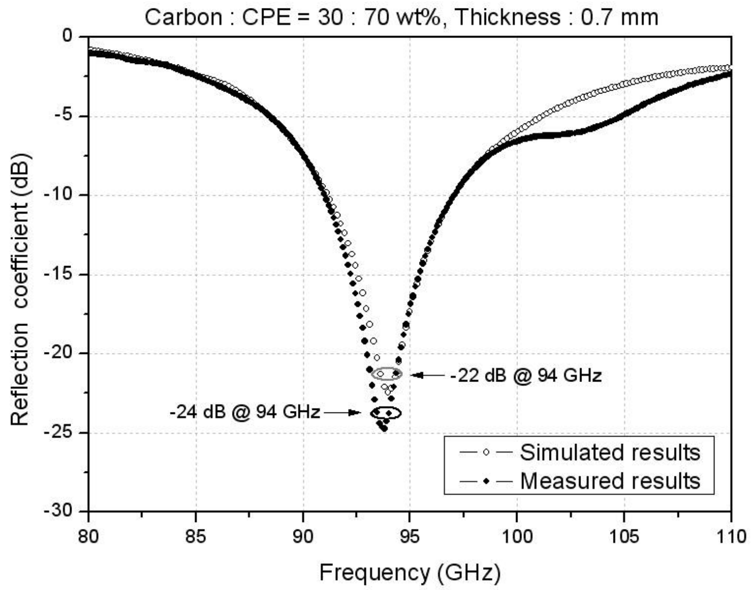

Fig. 6.20 Simulated and measured reflection coefficients of 0.7 mm sample containing Carbon:CPE=30:70 wt.% at 94 GHz

6.4.2 Absorber Using TiO_2

Figures 6.21-6.25 plot the reflection coefficients of samples containing difference composition ratio of TiO_2 with changing thickness. The absorption ability has a tendency to increase from 40 wt.% to 70 wt.% and decrease from 70 wt.% to 80 wt.% of TiO_2. As a result, the absorption ability of the sample containing TiO_2:CPE= 70:30 wt.% has a maximum value in frequency range of 65-110 GHz.

The EM wave absorbers were fabricated based on the simulated designs. The fabricated EM wave absorber containing TiO_2:CPE= 70:30 wt.% has a thickness of 1.85 mm and absorption ability higher than 20 dB in frequency range of 76-77 GHz as shown in Fig. 6.26. The fabricated EM wave absorber containing TiO_2:CPE=70:30 wt.% has a thickness of 1.45 mm and absorption ability higher than 17 dB at 94 GHz as shown in Fig. 6.27. The simulated and measured results agree very well as shown in Figs. 6.26 and 6.27.

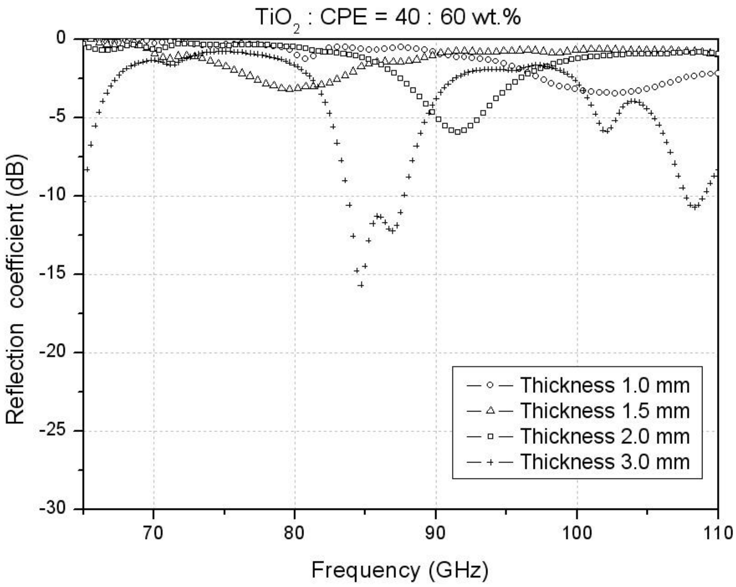

Fig. 6.21 Reflection coefficients of samples containing TiO_2:CPE=40:60 wt.% at several thicknesses.

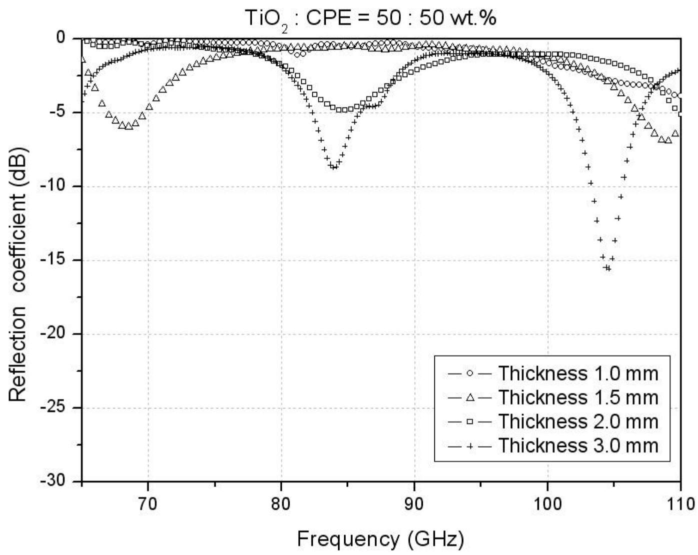

Fig. 6.22 Reflection coefficients of samples containing TiO_2:CPE=50:50 wt.% at several thicknesses.

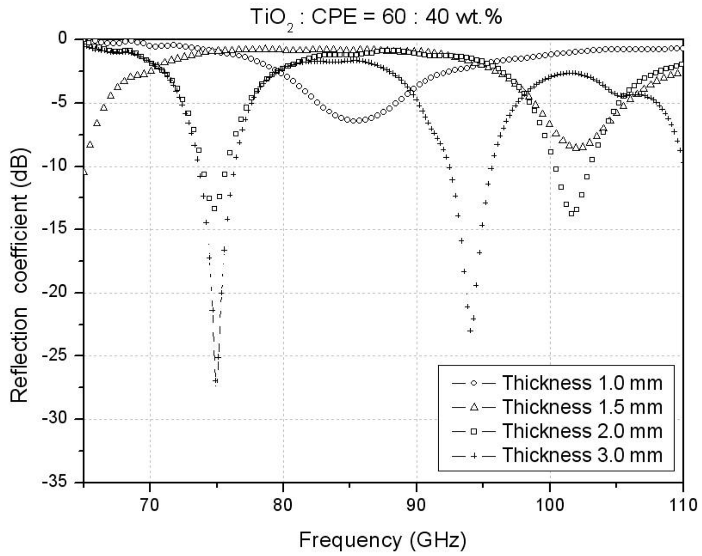

Fig. 6.23 Reflection coefficients of samples containing TiO_2:CPE=60:40 wt.% at several thicknesses.

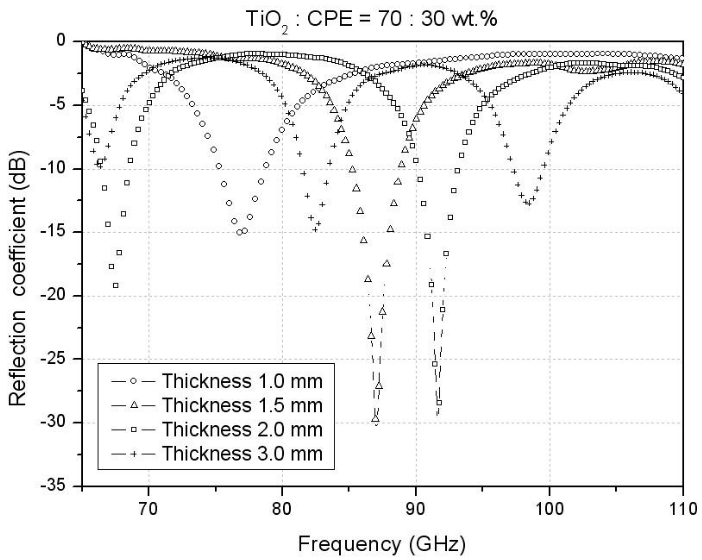

Fig. 6.24 Reflection coefficients of samples containing TiO_2:CPE=70:30 wt.% at several thicknesses.

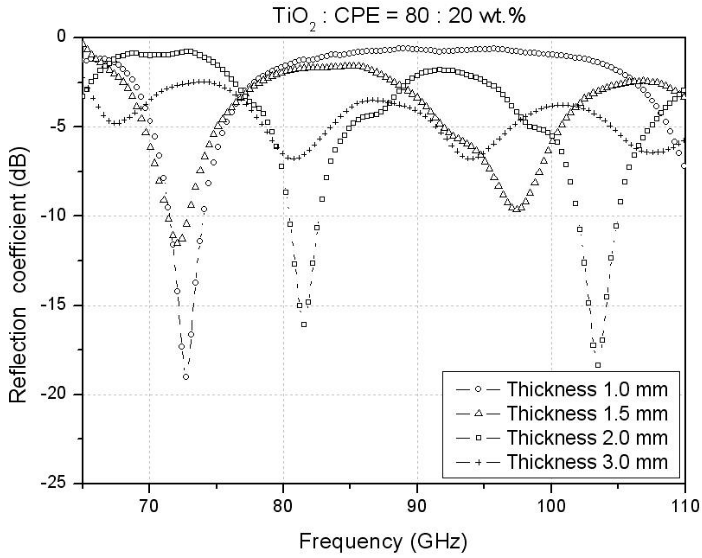

Fig. 6.25 Reflection coefficients of samples containing TiO_2:CPE=80:20 wt.% at several thicknesses.

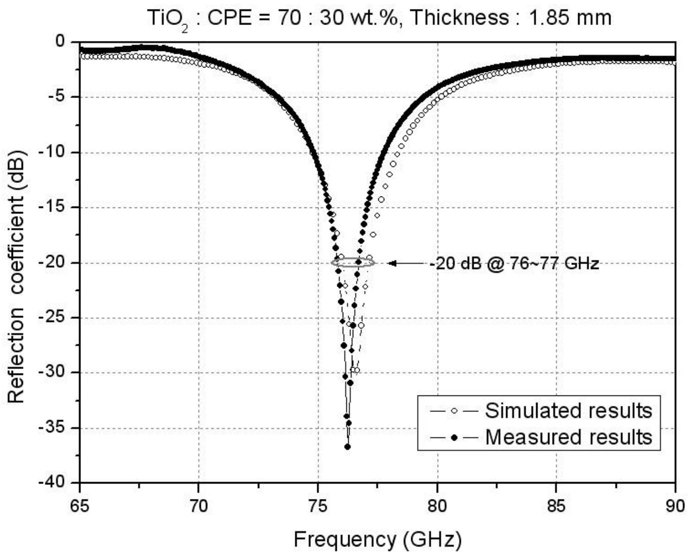

Fig. 6.26 Simulated and measured reflection coefficients of 1.85 mm sample containing TiO_2:CPE=70:30 wt.% in frequency range of 76-77 GHz

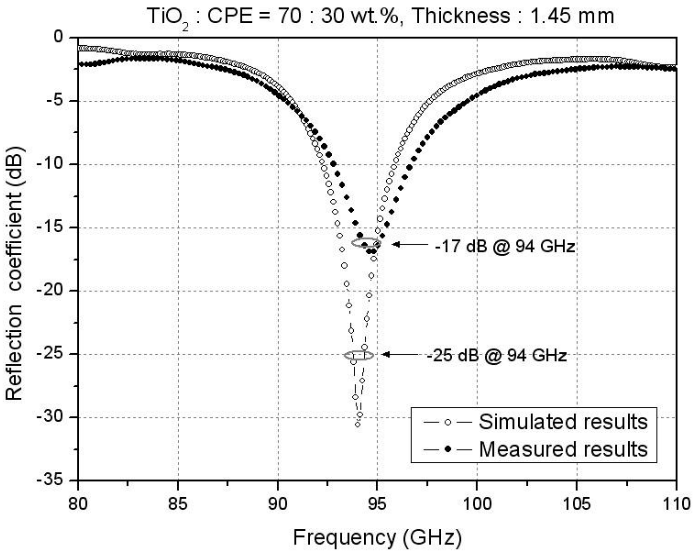

Fig. 6.27 Simulated and measured reflection coefficients of 1.45 mm sample containing TiO_2:CPE=70:30 wt.% at 94 GHz

6.4.3 Absorber Using Permalloy

Figures 6.28-6.31 plot the reflection coefficients of samples containing difference composition ratio of Permalloy with changing thickness. The absorption ability has a tendency to increase with increasing the composition ratio of Permalloy. As a result, the absorption ability of the sample containing Permalloy:CPE=70:30 wt.% has a maximum value in frequency range of 65-110 GHz.

The EM wave absorbers were fabricated based on the simulated designs. The fabricated EM wave absorber containing Permalloy:CPE =70:30 wt.% has a thickness of 1.4 mm and absorption ability higher than 18 dB in frequency range of 76-77 GHz as shown in Fig. 6.32. The fabricated EM wave absorber containing Permalloy:CPE=70:30 wt.% has a thickness of 1.15 mm and absorption ability higher than 18 dB at 94 GHz as shown in Fig. 6.33. The simulated and measured results agree very well as shown in Figs. 6.32 and 6.33.

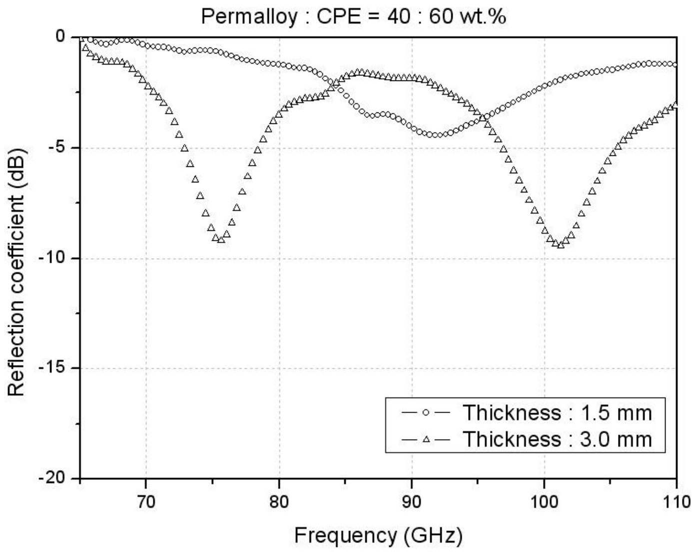

Fig. 6.28 Reflection coefficients of samples containing Permalloy:CPE=40:60 wt.% at several thicknesses.

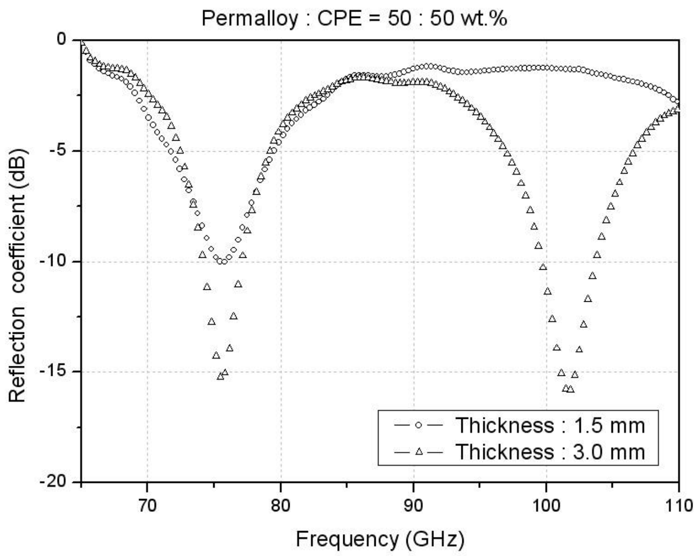

Fig. 6.29 Reflection coefficients of samples containing Permalloy:CPE=50:50 wt.% at several thicknesses.

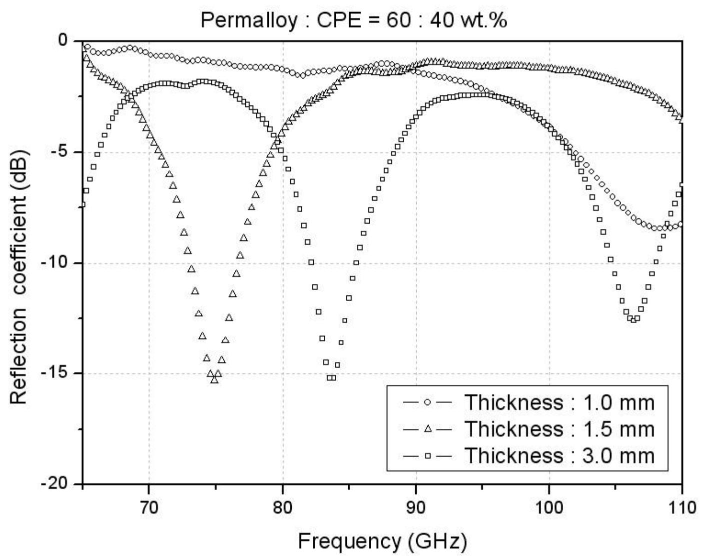

Fig. 6.30 Reflection coefficients of samples containing Permalloy:CPE=60:40 wt.% at several thicknesses.

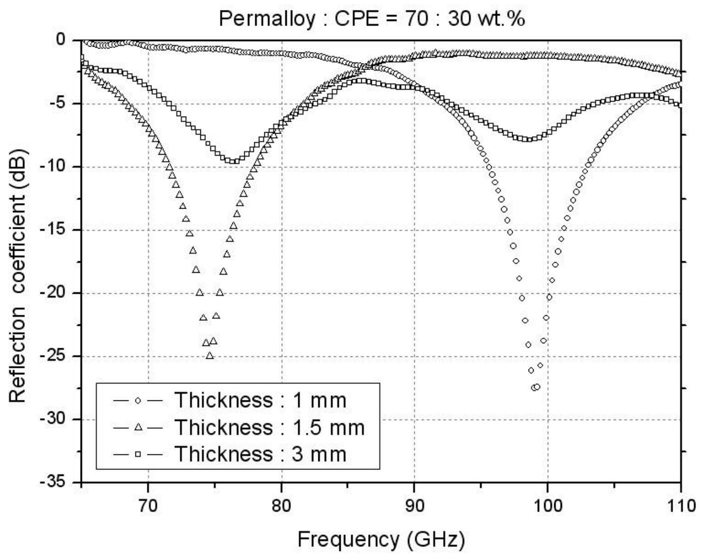

Fig. 6.31 Reflection coefficients of samples containing Permalloy:CPE=70:30 wt.% at several thicknesses.

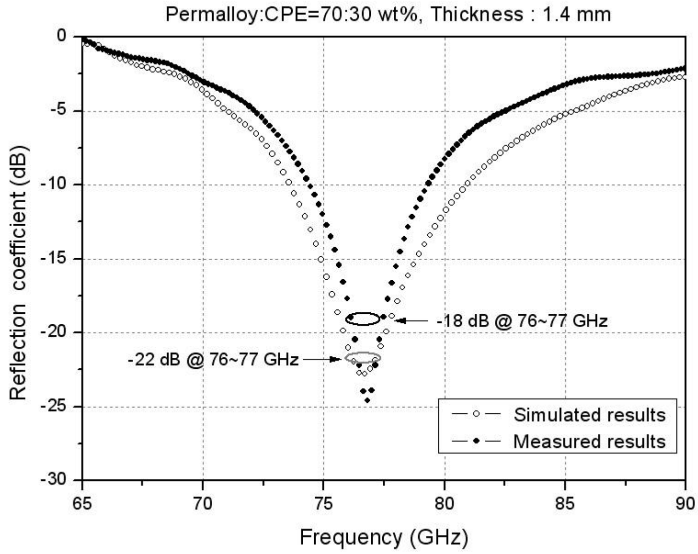

Fig. 6.32 Simulated and measured reflection coefficients of 1.4 mm sample containing Permalloy:CPE=70:30 wt.% in frequency range of 76~77 GHz

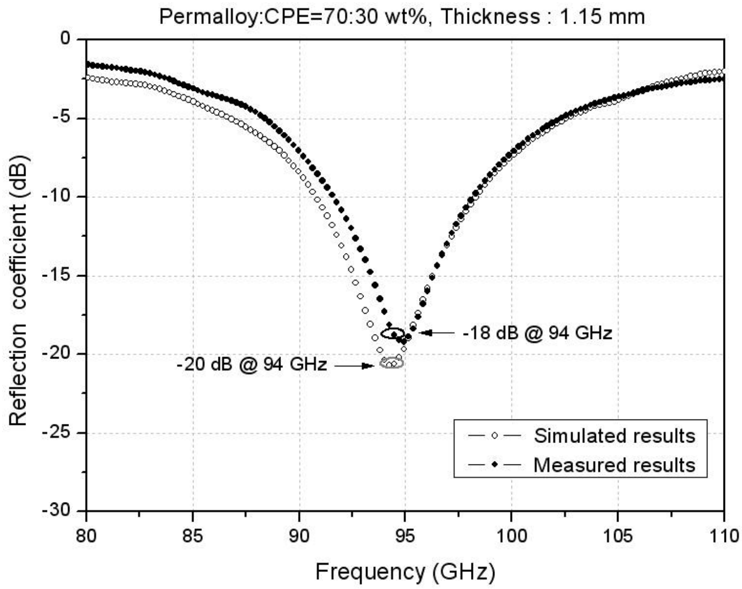

Fig. 6.33 Simulated and measured reflection coefficients of 1.15 mm sample containing Permalloy:CPE=70:30 wt.% at 94 GHz

Chapter 7

CONCLUSIONS

Millimeter wave sensors are superior to microwave and infrared-based radars in most applications because millimeter wave radars offer better range resolution than lower frequency microwave radars, and can penetrate fog, smoke and other obscurants much better than infrared sensors. Therefore, millimeter wave radars are employed in a wide range of commercial, military and scientific applications for remote sensing, safety, and measurements.

However, radar systems suffer from two major problems, such as false images and system-to-system interference. False echoes cause driving hazards. These problems can be eliminated through the use of an EM wave absorber.

In this dissertation, the EM wave absorbers are developed for W-band navigation radars using Carbon as a conductive material, TiO_2 as a dielectric material, and Permalloy as a magnetic material with CPE as a binder.

First of all, the absorption ability of samples containing difference composition ratio of Carbon, TiO_2, and Permalloy with CPE is analyzed in frequency range of 65-110 GHz. It is known that the absorption ability of sample containing Carbon has a tendency to increase from 10 wt.% to 20 wt.% and decrease from 30 wt.% to 50 wt.%, the absorption ability of sample containing TiO_2 has a tendency to increase from 40 wt.% to 70 wt.% and decrease from 70 wt.% to 80 wt.%, and the absorption ability of sample containing Permalloy has a tendency to increase with increasing the composition ratio. As a result, the optimum composition ratios of Carbon, TiO_2, and Permalloy are about 20 wt.%, 70 wt.%, 70 wt.%, respectively.

To design EM wave absorber in W-band, the material properties, such as complex relative permittivity and permeability, of samples are calculated from the S-parameter. Absorption abilities of the EM wave absorbers are simulated using the calculated complex relative permittivity and permeability by changing the thickness without changing the composition.

To verify design results, the EM wave absorbers are fabricated based on the simulated designs. The simulated and measured results agree very well. As a result, the EM wave absorbers for W-band radar are developed as follows:

[1] *The EM wave absorber using Carbon:*

An EM wave absorber has a thickness of 2 mm and absorption ability higher than 20 dB in frequency range of 76-77 GHz for collision-avoidance radar.

An EM wave absorber has a thickness of 0.7 mm and absorption ability higher than 24 dB at 94 GHz for missile guidance radar.

[2] *The EM wave absorber using TiO_2:*

An EM wave absorber has a thickness of 1.85 mm and absorption ability higher than 20 dB in frequency range of 76-77 GHz for collision-avoidance radar.

An EM wave absorber has a thickness of 1.45 mm and absorption ability higher than 17 dB at 94 GHz for missile guidance radar.

[3] *The EM wave absorber using Permalloy:*

An EM wave absorber has a thickness of 1.4 mm and absorption ability higher than 18 dB in frequency range of 76-77 GHz for collision-avoidance radar.

An EM wave absorber has a thickness of 1.15 mm and absorption ability higher than 18 dB at 94 GHz for missile guidance radar.

These results also show that altering the absorber thickness can control the absorption ability peak of composite material in frequency range of 65-110 GHz.

References

[1] Kai Chang, *Encyclopedia of RF and Microwave Engineering, Volume 6*, John Wiley & Sons, Inc., New Jersey, 2005.

[2] Mark E. Russell, Arthur Crain, Anthony Curran, Richard A. Campbell, Clifford A. Drubin, and Willian F. Miccioli, "Millimeter-Wave Radar Sensor for Automotive Intelligent Cruise Control(ICC)," *IEEE Trans. on Microwave Theory and Tech.*, vol.45, no.12, pp. 2444-2453, Dec. 1997.

[3] Graham M. Brooker, David Birch, and Justin Solms, "W-Band Airborne Interrupted Frequency Modulated CW Imaging Radar," *IEEE Trans. on Aerospace and Electronic System*, vol.41, no.3, pp. 955-971, July 2005.

[4] Graham M. Brooker, Steven Scheding, Mark V. Bishop, and Ross C. Hennessy, "Development and Application of Millimeter Wave Radar Sensors for Underground Mining," *IEEE Sensors J.*, vol.5, no.6, pp. 1270-1280, Dec. 2005.

[5] Jay A. Farrell and Matthew Barth, *The Global Positioning System & Inertial Navigation*, McGraw-Hill, New York, 1999.

[6] B. Hofman-Wellenhof, K. Legat, and M. Wiser, *Navigation: Principles of Positioning and Guidance*, Springer-Verlag, Wien, New York, 2003.

[7] C. P. Neo and V. K. Varadan, "Optimization of Carbon Fiber Composite for Microwave Absorber," *IEEE Trans. Electromag. Compat.*, vol.46, no.1, pp. 102-106, Feb. 2004.

[8] Dong Il Kim, Chang-Mook Choi, Rui Li, and Dae Hee Lee, "A Study on Electromagnetic Wave Absorber for W-Band Radars Using Permalloy," *IEICE Trans. Commun.*, vol.E90-B, no.8, pp. 2138-2142 Aug. 2007

[9] Chang Mook Choi, Dong Il Kim, Seung Hun Je, and Yun Seok Choi, “A study on electromagnetic wave absorber for the collision-avoidance radar,” *Current Applied Physics*, vol.7, no.5, pp 586-589, July 2007.

[10] William H. Emerson, “Electromagnetic Wave Absorbers and Anechoic Chambers Through the Years,” *IEEE Trans. Antennas Propagat.*, vol.AP-21, no.4, pp. 484-490, July 1973.

[11] Christopher L. Holloway, Ronald R. DeLyser, Robert F. German, Paul McKenna, and Motohisa Kanda, “Comparison of Electromagnetic Absorber Used in Anechoic and Semi-Anechoic Chambers for Emissions and Immunity Testing of Digital Devices,” *IEEE Trans. Electromag. Compat.*, vol.39, no.1, pp. 33-47, Feb. 1997.

[12] A. Vander Vorst, A. Rosen, and Y. Kotsuka, *RF/Microwave Interaction with Biological Tissues*, John Wiley & Sons, Inc., New Jersey, 2006.

[13] Y. Maeda, K. Takaya, and N. Kuwabara, “Requirements for Controlling Coverage of 2.4-GHz-Band Wireless LANs by Using Partitions with Absorbing Board,” *IEICE Trans. Commun.*, vol.E83-B, no.3, pp. 525-531, Mar. 2000.

[14] M. Amano and Y. Kotsuka, “A Method of Effective Use of Ferrite for Microwave Absorber,” *IEEE Trans. Microwave Theory Tech.*, vol.51, no.1, pp. 238-245, Jan. 2003.

[15] O. Hashimoto, “EM-wave Absorber Technology for Wireless LAN and ITS,” *J. IEICE*, vol.88, no.12, pp. 956-959, Dec. 2005.

[16] Y. Kotsuka, “Advanced EM-wave Absorber Technologies,” *J. IEICE*, vol.88, no.12, pp. 932-936, Dec. 2005.

[17] R. K. Pokharel, M. Toyota, and O. Hashimoto, “Analysis of Effectiveness of Wave Absorbers to Improve DSRC Electromagnetic Environment on Express Highway,” *IEEE Trans. Microwave Theory Tech.*, vol.53, no.9, pp. 2726-2731, Sep. 2005.

[18] H. Kurihara, Y. Hirai, K. Takizawa, T. Iwata, and O. Hashimoto, "An Improvement of Communication Environment for ETC System by Using Transparent EM Wave Absorber," *IEICE Trans. Electron.*, vol.E88-C, no.12, pp. 2350-2357, Dec. 2005.

[19] T. Soh, N. Yoshioka, K. Nakamura, and O. Hashimoto, "An Experimental Study of a 60-GHz-Band Wave Absorber Using Epoxy-Urethane Rubber Mixed with Carbon Particles," *IEICE Trans. Commun.*, vol.J82-B, no.3, pp. 469-475, March 1999.

[20] S. Nitta, "The Future of EMC Technology," *IEEE Trans. Commun.*, vol.E83-B, no.3, pp. 435-443, Mar. 2000.

[21] Y. Naito, *Electromagnetic Wave Absorbers*, New ohm, Tokyo, 1987.

[22] O. Hashimoto, *Introduction to Wave Absorber*, Morikita Shuppan, Tokyo, 1997.

[23] T. Soh and O. Hashimoto, "A Study on Millimeter-Wave Absorber Coating for V Band and W Band," *Trans. IEICE*, vol.J84-B, no.8, pp. 1523-1528, Aug. 2001.

[24] T. Soh and O. Hashimoto, "A Fundamental Study on Millimeter-Wave Absorbers Composed of Epoxy-Modified Urethane Rubber Mixed with Carbon Particles for 76 GHz or 94 GHz Frequency Band," *Trans. IEICE*, vol.J83-B, no.6, pp. 923-925, June 2000.

[25] Y. Naito and K. Suetake, "Application of Ferrite to Electromagnetic Wave Absorber and Its Characteristics," *IEEE Trans. Microwave Theory and Tech.*, vol.MTT-19, no.1, pp. 65-72, Jan. 1971.

[26] J. Y. Shin and J. H. Oh, "The Microwave Absorbing Phenomena of Ferrite Microwave Absorbers," *IEEE Trans. Magnetics*, vol.29, no.6, pp. 3437-3439, Nov. 1993.

[27] Morihiko Matsumoto and Yoshimori Miyata, "Thin Electromagnetic Wave Absorber for Quasi-Microwave Band Containing Aligned Thin Magnetic Metal Particles," *IEEE Trans. Magnetics*, vol.33, no.6, pp. 4459-4464, Nov. 1997.

[28] Y. Kotsuka and H. Yamazaki, “Fundamental Investigation on a Weakly Magnetized Ferrite Absorber,” *IEEE Trans. Electromag. Compat.*, vol.42, no.2, pp. 116-124, May 2000.

[29] E. F. Knott, J. F. Shaeffer, and M. T. Tuley, *Radar Cross Section, Second Edition*, SciTech Publishing, Inc., Raleigh, 2004.

[30] D. R. Frieden and G. P. Bender, *Principles of Naval Weapon System*, Naval Institute Press, 1985.

[31] FCC OET, *Millimeter Wave Propagation: Spectrum Management Implications*, Bulletin, no.70, July 1997.

[32] Quinstar Technology Inc., http://www.quinstar.com

[33] J. Saily and A. V. Raisanen, *Studies on Specular and Non-specular Reflectivities of Radar Absorbing Materials(RAM) at Submillimeter Wavelengths*, Helsinki University of Technology Radio Laboratory Publication, Feb. 2003.

[34] Chen K. L., *Optimization and engineering of microwave absorbers*, Ph.D Dissertation Department of Engineering Science and Mechanics, Pennsylvania State University, 1998.

[35] David M. Pozer, *Microwave Engineering, 3rd ed.*, J. Wiley & Sons, New Jersey, 2005.

[36] Emerson & Cuming Microwave Products, http://www.eccosorb.com

[37] Sony Corporation Product, *Sony's Electromagnetic Wave Absorber Reduces EMC and SAR Problems*, http://www.sony.net

[38] O. Hashimoto and Y. Shimizu, “A Measurement of the Complex Permittivity Tensor by a Standing-Wave Method in a Rectangular Waveguide,” *IEEE Trans. Electromag. Compat.*, vol.29, no.2, pp. 141-149, May 1987.

[39] H. B. Sequeira, *Extracting* μ_r *and* ε_r *of Solids from One-port Phasor Network Analyzer Measurements*, Wiltron Corp., Sep. 1989.

[40] J. Baker-Jarvis, E. J. Vanzura, and W. A. Kissick, “Improved Technique for Determining Complex Permittivity with the Transmission/Reflection Method,” *IEEE Trans. Microwave Theory Tech.*, vol.38, no.8, pp. 1096-1103, Aug. 1990.

[41] Product Note 8510-3, *Materials Measurement*, Hewlett Packard, Aug. 1985.

[42] Sang-Hyun Moon, Seung-Jae Shin, Jae-Man Song, Dong-Il Kim, and Ki-Man Kim, “Development of composite Ba ferrite EM wave absorbers for GHz frequency,” *J. Korea Electromagnetic Engineering Soc.*, vol.14, no.12, pp. 1329-1334, Dec. 2003.

Published papers concerned with this dissertation

- **International Journal**

[1] Dae-Hun Kim, Dong Il Kim, Chang-Mook Choi, and Jun-Young Son, "A Study on Design and Fabrication of Complex Type EM Wave Absorber with Super Wide-band Characteristics," *International Journal of Navigation and Port Research*, vol.30, no.2, pp.161-166, March 2006.

[2] Rui Li, Dong Il Kim, and Chang-Mook Choi, "Semi-Lumped Compact Low-Pass Filter for Harmonics Suppression," *Journal of The Korea Electromagnetic Engineering Society*, vol. 6, no. 3, pp. 171-175, Sep. 2006.

[3] Rui Li, Dong Il Kim, and Chang-Mook Choi, "Compact Low-Pass Filter with Sharp Skirt Characteristics and Broad Stopband," *International Journal of Navigation and Port Research*, vol.30, no.7, pp. 607-610, Sep. 2006.

[4] Chang-Mook Choi, Dong Il Kim, Rui Li and Kwang-Soob Ko, "Development of the Electromagnetic Wave Absorber for 94 GHz Radar Sensors Using Permalloy," *International Journal of KIMICS*, vol. 4, no. 3, pp 14-17, Sep. 2006.

[5] Rui Li, Dong Il Kim and Chang Mook Choi, "Compact Structure With Three Attenuation Poles for Improving Stopband Characteristics," *IEEE Microw. Wireless Compon. Lett.*, vol. 16, no. 12, pp. 663-665, Dec. 2006. **(SCI)**

[6] Chang-Mook Choi, Dong Il Kim, Rui Li, Dong-Han Choi, "Development of Broadband Electromagnetic Wave Absorber for X-band Sensors in Double-layered Type Using Carbon," *International Journal of Navigation and Port Research*, vol.30, no.9, pp. 763-766, Dec. 2006.

[7] Dong-Han Choi, Dong Il Kim, Chang-Mook Choi, Rui Li, "A Study on Multi-Layered EM Wave Absorber Using Natural Lacquer as a Binder," *International Journal of Navigation and Port Research*, vol.30, no.9, pp. 767-772, Dec. 2006.

[8] Chang Mook Choi, Dong Il Kim, and Rui Li, "A Study on the Absorption Properties of EM Wave Absorbers Using Carbon," *J. Korean Phys. Soc.*, vol.41, no.2, pp. 470-473, Feb. 2007. **(SCI)**

[9] Chang Mook Choi, Dong Il Kim, Seung Hun Je, and Yun Seok Choi, "A study on electromagnetic wave absorber for the collision-avoidance radar," *Current Applied Physics*, vol.7, no.5, pp 586-589, July 2007. **(SCI-E)**

[10] Dong Il Lim, Chang-Mook Choi, Rui Li, and Dae Hee Lee, "A Study on Electromagnetic Wave Absorber for W-Band Radars Using Permalloy," *IEICE Trans. Commun.*, vol.E90-B, no.8, pp 2138-2142, Aug. 2007. **(SCI)**

● International Conference

[1] Dong Il Kim, Chang Mook Choi, “A Study on the Electromagnetic Wave Absorbers,” *The 6-th Asia-Pacific Engineering Research Forum on Microwaves and Electromagnetic Theory*, Shanghai, China, pp. 244-248, Aug. 2006.

[2] Dae Hee Lee, Dong Il Kim, Chang Mook Choi, and Rui Li, “A Study on Electromagnetic Wave Absorber for W-Band Radar Using Permalloy,” *2006 Korea-Japan Joint Conference on AP/EMC/EMT*, Ishikawa, Japan, pp. 217-220, Sep. 2006.

[3] Chang-Mook Choi, Dong-Il Kim, Dong-Han Choi, and Rui Li, "Development of Broad-Band Electromagnetic Wave Absorber for X-band Sensors in Double-layered Type Using Carbon," *12th IAIN*

World Congress 2006 International Symposium on GPS/GNSS, ICC Jeju, Korea, pp. 297-300, Oct. 2006.

[4] Dong-Han Choi, Dong-Il Kim, Chang-Mook Choi, and Rui Li, "A Study on Multi-layered EM Wave Absorber Using Natural Lacquer as a Binder," *12th IAIN World Congress 2006 International Symposium on GPS/GNSS*, ICC Jeju, Korea, pp. 157-161, Oct. 2006.

[5] Rui Li, Dong-Il Kim, Chang-Mook Choi, and Young-Man Song, "A Novel Design of Compact Low Pass Filter and Its Equivalent Circuit Model," *Asia Navigation Conference 2006*, ICC Jeju, Korea, pp. 79-84, Oct. 2006.

[6] Rui Li, Dong Il Kim, Chang Mook Choi, “Compact Low-Pass Filter for Harmonics Suppression,” *2006 Asia-Pacific Microwave Conference*, Yokohama, Japan, pp. 1687-1690, Dec. 2006.

[7] Young Man Song, Dong Il Kim, Chang-Mook Choi, and Dae Hee Lee, “Development of the EM Wave Absorber for ETC System Using MnZn-ferrite and Carbon,” *2007 Korea-Japan Microwave Workshop*, Okinawa, Japan, pp. 85-87, Nov. 2007.

[8] Dae Hee Lee, Dong Il Kim, Chang-Mook Choi, and Young Man Song, “A Study on the Improvement of EM Wave Absorption Properties with $Al(OH)_3$,” *2007 Asia-Pacific Microwave Conference*, Bangkok, Thailand, pp. 125-128, Dec. 2007.

- **Domestic Journal**

[1] 김동일, 최창묵, 고광섭, “ITS 의 차량충돌방지 레이더용 전파흡수체 개발”, 대한전자공학회 논문지, 제 43 권 TC 편 제 9 호, pp. 991-995, 2006. 9.

[2] 이서, 김동일, 최창묵, 이대희, 송영만, “Compact Structure with Three Attenuation Poles for Harmonics Suppression," 한국해양대학교 산업기술연구소연구논문집, Vol. 24, pp. 29-35, 2007. 1.

[3] 이대희, 김동일, 최창묵, 송영만, “Sendust-Al$(OH)_3$ 를 이용한 전파흡수체 특성 분석,” 한국전자파학회논문지, 제 18 권, 제 10 호, pp. 1136-1141, 2007. 10.

[4] 송영만, 최창묵, 이대희, 김동일, “ITS 의 ETC 용 전파흡수체 개발,” 한국항해항만학회지, 제 31 권, 제 8 호, pp. 671-674, 2007. 10.

[5] 윤상길, 김동일, 이대희, 최창묵, “실내 무선 LAN 전자파 환경 대책용 전파흡수체에 관한 연구,” 한국전자파학회논문지, 제 18 권, 제 11 호, pp. 1224-1230, 2007. 11.

● **Domestic Conference**

[1] 최창묵, 김동일, 이서, 오경진, “RCS 법에 의한 전파흡수체 측정기법 분석,” 전자파기술 하계 학술대회 논문집, 제 5 권 제 1 호, pp. 159-162, 2005. 6.

[2] 최창묵, 김동일, 최동한, 이대희, “차량충돌방지 레이더용 전파흡수체 개발,” 제 7 회 산업기술연구소 학술강연 논문집, pp. 16-20, 2006. 5.

[3] 최창묵, 김동일, 제승훈, 최윤석, “밀리미터 레이더용 전파흡수체 개발,” 한국해양정보통신학회 춘계종합학술대회, 제 10 권, 제 1 호, pp. 223-227, 2006. 5.

[4] 최윤석, 김동일, 제승훈, 최창묵, “광대역 전파흡수체에 관한 연구,” 마이크로파 및 전파전파학술대회 논문집, 제 29 권, 제 1 호, pp. 511-514, 2006. 5.

[5] 최창묵, 김동일, 곽영신, 이대희, “W-band 대역에서 카본의 전파흡수 특성 분석,” 전자파기술 하계학술대회 논문집, pp. 18-21, 2006. 6.

[6] 제승훈, 김동일, 최윤석, 최창묵, “다층형 전파흡수체에 관한 연구,” 전자파기술 하계학술대회 논문집, pp. 22-25, 2006. 6.

[7] 송영만, 김동일, 최창묵, 이대희, “퍼멀로이를 이용한 94 GHz 레이더용 전파흡수체 개발에 관한 연구,” 한국마린 엔지니어링학회 후기학술대회 논문집, pp. 215-218, 2006. 11.

[8] 이대희, 김동일, 최창묵, 제승훈, “2.4 GHz 무선랜용 전파흡수체 개발,” 한국항해항만학회 추계학술대회 논문집, 제 30 권, 제 2 호, pp. 113-118, 2006. 12.

[9] 이대희, 김동일, 박우근, 최창묵, “MnZn-Ferrite 와 Sendust 를 이용한 2.4 GHz 무선 LAN 용 전파흡수체 개발,” 한국항해항만학회 춘계학술대회 논문집, 제 31 권, 제 1 호, pp. 37-42, 2007. 4.

[10] 이대희, 김동일, 제승훈, 최창묵, “Sendust-Al(OH)3 전파 흡수체 특성에 관한 연구,” 춘계 마이크로파 및 전파전파 학술대회 논문집, 제 30 권, 제 1 호, pp. 541-544, 2007. 5.

[11] 최창묵, 김동일, 김민정, “차량충돌방지 레이더용 전파흡수체 개발에 관한 연구,” 제 8 회 산업기술연구소 학술강연 논문집, pp. 8-13, 2007. 5.

[12] 최창묵, 김동일, 고광섭, “W-대역에서 유전손실재료인 TiO_2 의 전파흡수특성 분석,” 한국해양정보통신학회 2007 춘계종합학술대회, 제 11 권, 제 1 호, pp. 95-98, 2007. 6.

[13] 이대희, 김동일, 최창묵, 윤상길, “실내무선 LAN 환경 대책용 전파흡수체에 관한 연구,” 전자파기술 하계학술대회 논문집, pp. 88-91, 2007. 6.

[14] 송영만, 김동일, 최창묵, 박수훈, “5.8 GHz DSRC 용 전파흡수체 개발에 관한 연구,” 한국마린엔지니어링학회 전기학술대회 논문집, pp. 283-286, 2007. 6.

[15] 최창묵, 김동일, 박우근, 고광섭, “차량충돌방지 레이더의 허상방지 대책용 전파흡수체 개발에 관한 연구,” 대한전자공학회 하계종합학술대회, 제 30 권, 제 1 호, pp. 107-108, 2007. 7.

[16] 박수훈, 김동일, 최창묵, 이대희, “UHF 대역 RFID 시스템용 전파흡수체 개발에 관한 연구,” 추계 마이크로파 및 전파 학술대회 논문집, 제 30 권, 제 2 호, pp. 649-652, 2007. 9.

[17] 윤상길, 김동일, 최창묵, 송영만, “PCB 노이즈 제거용 광대역 전파흡수체 개발,” 추계 마이크로파 및 전파 학술대회 논문집, 제 30 권, 제 2 호, pp. 673-676, 2007. 9.

[18] 박수훈, 최창묵, 송영만, 김동일, “UHF 대역 RFID 리더 간섭방지용 전파흡수체 개발,” 한국항해항만학회 추계 학술대회 논문집, 제 31 권, 제 2 호, pp. 14-16, 2007. 12.

감사의 글

나의 인생에서 대학원생활의 결실인 학위논문을 마무리 하면서 둘러보니, 그 동안 은혜를 베풀어주신 분들이 너무나 많은 것 같습니다.

먼저, 제가 배움의 길에 오를 수 있도록 모든 기회를 마련해준 대한민국 해군에 감사하며, 그 동안 세심한 배려와 지대한 관심으로 지도해 주신 김동일 교수님, 배움의 길 앞에서 망설일 때 한길로 인도해 주신 고광섭 교수님 진심으로 감사를 드립니다. 그리고 학위논문의 결실을 맺기 위한 지식과 사랑을 가르쳐주신 정세모 교수님, 김민석 교수님, 민경식 교수님, 그리고 전파공학과 교수님들께 감사 드립니다.

또한 저의 대학원 생활에 항상 활력을 준 KBS 박우근 박사님, (주) ETL 최동한 박사님, (주) 테스콤 Li Rui 박사님, 전파공학과 철성이와 동식이를 비롯한 후배들, 마이크로파 연구실의 대희, 영만, 수훈, 상길, 미화, 은미, 상미... 모든 분들께 감사의 마음을 전합니다.

그리고 이 작은 결실에 영예로움이 있다면 사랑하는 할머님, 아버님, 어머님과 장인/장모님, 그리고 천국에 계신 할아버님께 바칩니다.

마지막으로 그 동안의 모든 과정을 함께하며, 격려와 도움을 준 사랑하는 아내 이수경에게 이 모든 공을 돌리고자 합니다. 아울러 가장 소중한 딸 선아, 아들 선우와 함께 이 기쁨을 나누고 싶습니다.

여러분들의 도움에 힘입어 제가 있음을 확인하며, 이 논문은 새로운 시작을 위한 밑거름으로 생각하고 지속적인 연구를 하겠습니다.

앞으로도 많은 조언과 질책을 부탁 드리며, 다시 한 번 감사의 마음을 드립니다.

2007. 12. 31.

아치섬에서...